INFORMATION TO USERS

This manuscript has been reproduced from the microfilm master. UMI films the text directly from the original or copy submitted. Thus, some thesis and dissertation copies are in typewriter face, while others may be from any type of computer printer.

The quality of this reproduction is dependent upon the quality of the copy submitted. Broken or indistinct print, colored or poor quality illustrations and photographs, print bleedthrough, substandard margins, and improper alignment can adversely affect reproduction.

In the unlikely event that the author did not send UMI a complete manuscript and there are missing pages, these will be noted. Also, if unauthorized copyright material had to be removed, a note will indicate the deletion.

Oversize materials (e.g., maps, drawings, charts) are reproduced by sectioning the original, beginning at the upper left-hand corner and continuing from left to right in equal sections with small overlaps.

Photographs included in the original manuscript have been reproduced xerographically in this copy. Higher quality 6" x 9" black and white photographic prints are available for any photographs or illustrations appearing in this copy for an additional charge. Contact UMI directly to order.

Bell & Howell Information and Learning
300 North Zeeb Road, Ann Arbor, MI 48106-1346 USA

UMI®
800-521-0600

A QUANTUM CHEMICAL STUDY OF CARBON MONOXIDE ADSORPTION ON MODELS OF THE MgO (001) SURFACE

Bryan Howard Long

A dissertation presented to the
Graduate Faculty of Middle Tennessee State University
in partial fulfillment of the requirements
for the degree Doctor of Arts

December, 1999

A QUANTUM CHEMICAL STUDY OF CARBON MONOXIDE ADSORPTION ON MODELS OF THE MgO (001) SURFACE

APPROVED:

Graduate Committee:

Preston J. MacDougall
Major Professor

James C. Howard
Committee Member

Nancy C. Hess
Committee Member

Earl F. Johnson
Chairman of the Department of Chemistry

Donald L. Avery
Dean of the Graduate School

ABSTRACT

The adsorption of CO molecules on models of the MgO (001) surface was investigated using GAUSSIAN 92. Different sized cluster models and basis sets were used to determine the optimized geometries of the CO molecule, the dipole moment and the adsorption energy, and for some clusters, the surface geometry. Clusters of MgO one layer thick with nine atoms in the layer (3x3x1), one layer thick with twenty-five atoms in the layer (5x5x1), and two layers thick with nine atoms in each layer (3x3x2) were used as cluster models with the STO-3G, LANL1DZ and 3-21G* basis sets to determine the optimized CO position above the surface. These values were compared to values determined experimentally and by other computational models. The 3x3x1 cluster model with Mg or O as the central atom, the presence of an atom (possibly a defect) under the central atom, the charge on the cluster, and the orientation of the CO molecule were investigated for each basis set, and the results on the optimized geometry were compared.

The 3-21G* basis set and the 3x3x1 cluster model were used to determine dipole moments and binding energies for each of the above mentioned conditions. To model catalyst defects, a sulfur atom was placed below the central Mg and the geometry optimizations, dipole moment, and adsorption energy were determined using the 3-21G* basis set.

Finally, the Laplacian of the electron distribution was used to investigate the chemical properties of the interaction of the CO molecule with the MgO (001) surface. The effect of the different cluster conditions and CO orientations are demonstrated using contour plots of the Laplacian of the electron density ($-\nabla^2\rho$).

ACKNOWLEDGEMENTS

There are many people who have helped in the completion of this dissertation and in my attaining the D.A. in Chemistry. I wish to thank the following members of the MTSU Chemistry Department: Dr. Martin Stewart for suggesting the D.A. program to me; Dr. Dan Scott for allowing me to have a summer fellowship; Dr. Ed Woods for his timely suggestions that led to my writing a successful NSF proposal; Dr. Roy Clark, Dr. James Hutchinson, and Dr. Judith Bonnicamp, for the enjoyment of being in their classes and all that they were able to teach me; Dr. James Howard for the time we spent on the NMR and all that I got out of that experience; and Mrs. Ann Smith for her ability to fix anything.

Thanks to Glenda Vandygrift for her patience with all of the extensions and delays, and to Dr. Donald Curry for accepting the dissertation when he did. I appreciate Dr. Howard, and Dr. Nancy Keese for being on my committee and for doing a lot of reading in a short period of time, and for their helpful comments. I also appreciate Dr. Earl Pearson's input and comments.

A special thanks to Dr. Preston MacDougall. For your suggestions at just the right time, patience, and tremendous input into this dissertation, I thank you. I am looking forward to future collaborations.

The biggest thanks is for my wife and daughter for support, encouragement, and love. I truly live with Angels.

Finally, I wish to thank God for all of His many blessings in my life. With Him, all things are possible.

DEDICATION

This dissertation is dedicated to my mother, Sally (Sadie Ray) Long. I love you mom.

TABLE OF CONTENTS

TABLE OF CONTENTS (Continued)

LIST OF TABLES

LIST OF FIGURES

Figure Page

Figure Page

Figure Page

Figure Page

Figure Page

Figure Page

LIST OF APPENDICES

CHAPTER 1

THE DEVELOPMENT OF QUANTUM CHEMISTRY

1.1 Introduction

Chemistry may be defined as the study of the composition, structure, and properties of matter and of the reactions by which one form of matter may be produced from or converted into other forms[1]. Quantum chemistry applies quantum mechanics to problems in chemistry, using the motions and interactions of electrons and nuclei to determine molecular properties. Quantum chemistry is used today in all branches of chemistry and molecular physics. *Ab initio* quantum chemistry is a computational method that has become a useful tool for the study of molecular structure, structural stability, and reaction mechanisms[2]. *Ab initio* is Latin for "from the beginning" which means these are calculations based on fundamental principles and universal constants, and not parametrized to fit existing knowledge. Using a computational approach to the study of chemistry allows the comparison of experimental results to theoretical models. Computational methods can also be used to study problems that may be difficult or impossible to study experimentally. A deeper understanding of molecular processes is obtained that could not be acquired by experimental methods alone. Computational quantum mechanics

can be used to estimate the relative stabilities of molecules or to investigate the mechanisms of chemical reactions. Spectroscopists use quantum mechanics to understand and interpret the frequencies and intensities of lines in a spectrum. Biochemists can use computational methods to study the conformation of biological molecules, enzyme-substrate binding, and solvation of biological molecules. Finally, computational methods can produce results with great accuracy but may be more economical than experimental methods[3]. For example, the costly disposal of hazardous materials is completely avoided.

The *ab initio* method uses a theoretical model within which the structures, energies, and other physical properties can be explored. This is done using variational methods where an approximation to the ground state energy of a system can be obtained by calculating an approximate solution to the Schrödinger equation, not an exact solution. This expectation value will be greater than the energy for the exact wavefunction which reduces the problem to one of finding values that minimize the energy of the theoretical wavefunction. The wavefunction, Ψ, is a mathematical function that contains all the information that can be known about a system.

The importance of *ab initio* quantum chemistry was recognized by the Swedish Academy of Sciences. The 1998 Nobel Prize in Chemistry was awarded to Walter Kohn and John

A. Pople for their contributions in the area of quantum chemistry. The citation reads, "to Walter Kohn for his development of the density-functional theory and to John Pople for his development of computational methods in quantum chemistry."[4]

Kohn demonstrated that it is not necessary to consider the motion of each individual electron in a molecule, but rather the average number of electrons located at any one point in space. This density-functional theory has led to a method that is simpler from a computational perspective. It postulates that the total energy for a system described by the laws of quantum mechanics can be determined theoretically if the spatial distribution (electron density) is known. This is a function that will be explored later in order to characterize chemical interactions, not just the energy of the system. The equation for calculating the energy has been determined accurately enough to allow large-scale studies of molecular systems.

Pople developed the computational methods that made possible the theoretical study of molecules, their properties, and their behavior in chemical reactions. Pople knew that if theoretical methods were to be accepted in chemistry it would be necessary to know the accuracy of the results for any given situation. Also, the methods must be easy to use and not require an excessive amount of computer resources or user programming. GAUSSIAN-70 is a computer

program developed by Pople at the end of the 1960s that satisfied the above requirements. This program has been refined in methodology while building up a well-documented model chemistry. Pople included Kohn's density-functional theory in the beginning of 1990. (GAUSSIAN 92 is the version used in this paper.) Kohn and Pople have provided the tools necessary for studying more complex molecules.

The currency of *ab initio quantum* chemistry is demonstrated by two articles that appeared recently in Physics Today, and Scientific American. The feature article in the September 1999 issue of Physics Today, is titled *Computational Materials Science: The Era of Applied Quantum Mechanics* by Jerzy Bernholc. "The properties of new and artificially structured materials can be predicted and explained entirely by computations, using atomic numbers as the only input"[5]. The article includes a brief description of the methodology of *ab initio* calculations, examples of current applications to materials such as C_{60}, C_{36}, and silicon, new methods in *ab initio* calculations, and the future outlook for materials science using quantum mechanics and *ab initio* methods. *Why Things Break* by Mark E. Eberhart in the October 1999 issue of Scientific American uses the change in charge density as a bond is breaking or forming to predict whether a material fails by brittle (breaking) or ductile (bending) means. The author concludes, "Rather than searching blindly for a base alloy with the ideal set of

intrinsic properties, materials designers will use computers to calculate the charge density of candidate base alloys. From this information they will determine how the charge density must be changed to produce the desired properties and then make predictions as to which alloying elements will produce these changes. For the first time, a new alloy will be designed beginning with its electronic structure."[6] "Having a theory for creating materials that behave just as they are intended could revolutionize, ..., the conventional trial-and-error searches that eat up billions of dollars and years of researchers' time."[6]

1.2 Development of Quantum Mechanics

Quantum mechanics was developed between 1925 and 1927 by two groups, Werner Heisenberg, Max Born, and P. A. M. Dirac, who developed matrix mechanics, and Erwin Schrödinger who developed wave mechanics. Wave mechanics uses differential equations instead of the matrix calculations used by Heisenberg's formulation. Dirac showed that matrix mechanics and wave mechanics, although different in form, are equivalent in content[7]. Quantum mechanics explains how entities such as electrons have both particle-like and wave-like characteristics. The Schrödinger equation

$$\left(\frac{-h^2}{8\pi m}\nabla^2 + V\right)\Psi(\boldsymbol{r}, t) = \frac{ih}{2\pi}\frac{\partial\Psi(\boldsymbol{r}, t)}{\partial t}$$

describes the wavefunction of a particle. Here Ψ is the wavefunction, m is the mass of the particle, h is Planck's constant, and V is the potential field in which the particle is moving[8]. The Schrödinger equation for a collection of particles such as a molecule is similar. In this case, Ψ would be a function of the coordinates of all the particles in the system, in addition to time (t). The solution of Schrödinger's differential equation for Ψ will allow one to determine molecular properties and make quantitative predictions of most chemical phenomena while using only the values of a small number of constants. The constants that are used include Planck's constant, the charges of the electrons and nuclei, and the masses of the electrons and nuclei[2]. These are the only values that need to be experimentally determined. Many different wavefunctions are solutions to Schrödinger's equation which correspond to different stationary states of the system. Molecular orbital (MO) theory is based upon the laws of quantum mechanics but uses approximations and mathematical transformations to solve these fundamental equations.

The Schrödinger equation can be simplified using separation of variables. Writing the wavefunction as a product of a spatial function and a time function,

$$\Psi(\boldsymbol{r}, t) = \psi(\boldsymbol{r})\tau(t)$$

and substituting these functions into the above equation

results in two equations, one which is a function of the position of the particle, independent of the time, and the other which is a function of the time, only. The time-independent Schrödinger equation[2] is given by

$$H\psi = E\psi$$

where H is the Hamiltonian operator which represents the total energy, E is the numerical value of the energy of the state, and ψ is the wavefunction. ψ depends on the cartesian coordinates and the spin coordinates of all particles. ψ^2 is the probability density for the particle(s) represented by the wavefunction, which means ψ must be normalized. That is, integrating over all space the probability must be 1. Multiplying ψ by a constant c such that

$$\int_{-\infty}^{+\infty} |c\psi|^2 dv = 1$$

normalizes the wavefunction. Because the Schrödinger equation is an eigenvalue equation, if ψ is a solution to the equation, then $c\psi$ is also a solution. An eigenvalue equation is an equation in which an operator acting on the function produces a multiple of the function itself as its result, such as $H\psi = E\psi$ where H is the operator, ψ is a function, and E is a constant. The set of functions that are solutions to the equation are known as eigenfunctions. Each eigenfunction has an associated value of E known as its eigenvalue. For the Schrödinger equation the eigenvalues are

the energies corresponding to the different stationary states of the system[7]. Other eigenvalues corresponding to observable properties other than E, have their own operators.

There are conditions that must be placed on the function ψ for molecular systems. ψ must be antisymmetric, meaning when two identical particles are interchanged, the sign of the function must change. That is

$$F(i,j) = -F(j,i)$$

for any antisymmetric function F. The Hamiltonian operator **H** is

$$\mathbf{H} = \mathbf{T} + \mathbf{V}$$

where **T** and **V** are the kinetic and potential energy operators of the particles in the system, respectively. The kinetic energy operator **T** is a sum of differential operators

$$\boldsymbol{T} = -\frac{h^2}{8\pi^2}\sum_i \frac{1}{m_i}\left(\frac{\partial^2}{\partial x_i^2} + \frac{\partial^2}{\partial y_i^2} + \frac{\partial^2}{\partial z_i^2}\right)$$

In the above equation, h is Planck's constant, the sum is over all of the i particles (nuclei and electrons) and m_i is the mass of the i^{th} particle. The potential energy operator **V** is derived from the Coulomb force between each pair of charged particles, where each nucleus is considered a single charged mass. This operator is

$$\boldsymbol{V} = \sum_i \sum_{j<i} \left(\frac{e_i\, e_j}{r_{ij}}\right)$$

Here the sum is over the distinct pairs of particles with

charge e_i, e_j and separation distance r_{ij}. For the electrons, $e_i = -e$, and for the nuclei $e_i = Ze$ where Z is the atomic number for that nucleus. The various solutions to the Schrödinger equation correspond to different stationary states of the system (particle or molecule). The solution with the lowest energy is called the *ground state*. Schrödinger's equation is a non-relativistic description of the system which is not valid when the velocities of the particles approach the speed of light. However, it was also recognized that the solution of the Schrödinger equation was impossible for any but the simplest systems.

If the system under investigation has two or more electrons the Schrödinger equation is too difficult to solve exactly. There have been many approximation techniques developed to simplify the solution to Schrödinger's equation and this chapter will present an introduction to the theories used in the *ab initio* methods.

1.3 The Born-Oppenheimer Approximation

The Born-Oppenheimer approximation[9] assumes the separability of the nuclear and electronic motions. Since the nuclei are much heavier than the electrons, the motion of the nuclei relative to the motion of the electrons, in a given time frame, is negligible. Because of the mass difference, the electrons change their positions rapidly while the nuclei move very slowly. The electron motion can

be approximated as occurring in a field of fixed nuclei. This means the number of terms in the non-relativistic Hamiltonian can be reduced by two. The kinetic energies of the nuclei are set equal to zero and the repulsions between the nuclei are treated as a constant. Then, the Schrödinger equation becomes

$$\mathbf{H}^{elec}\psi^{elec}(\mathbf{r},\mathbf{R}) = \mathbf{E}^{np}(\mathbf{R})\psi^{elec}(\mathbf{r},\mathbf{R})$$

In this equation ψ^{elec} is the electronic wavefunction depending on the coordinates of the electrons, $\mathbf{r}$, and the nuclei, $\mathbf{R}$. $\mathbf{E}^{np}$ is the effective nuclear potential function which represents the energy landscape that determines the motions and minimum energy configurations of the molecule's nuclear framework. $\mathbf{H}^{elec}$ is the electronic Hamiltonian corresponding to the motion of the electrons in the field of the fixed nuclei. Then

$$\mathbf{H}^{elec} = \mathbf{T}^{elec} + \mathbf{V}$$

where $\mathbf{T}^{elec}$ is the kinetic energy operator of the electrons

$$\boldsymbol{T}^{elec} = -\frac{h^2}{8\pi^2}\sum_{i}^{electrons}\frac{1}{m_e}\left(\frac{\partial^2}{\partial x_i^2}+\frac{\partial^2}{\partial y_i^2}+\frac{\partial^2}{\partial z_i^2}\right)$$

and $\mathbf{V}$ is the potential energy operator

$$\boldsymbol{V} = -\sum_{i}^{electrons}\sum_{p}^{nuclei}\frac{Z_p e^2}{r_{ip}} + \sum_{i}^{elec}\sum_{<j}^{trons}\frac{e^2}{r_{ij}} + \sum_{p}^{nuc}\sum_{<q}^{lei}\frac{Z_p Z_q e^2}{r_{pq}}$$

The first term in the above equation corresponds to the electron-nuclear attraction, the second to the electron-electron repulsion and the third to the nuclear-nuclear

repulsion. The last term will be a constant for a particular configuration of the nuclei. An exact solution to the Schrödinger equation is still possible only for the most trivial molecular systems. To make an approximate solution possible for the Schrödinger equation for larger molecules some additional simplifying assumptions must be made.

1.4 Molecular Orbital Models

Molecular orbital (MO) theory is an approximation of the electron distribution and the electron motion where the motions of the electrons are considered separable yielding one-electron eigenfunctions describing their motions in a static distribution of the other electrons. In the simplest version of the theory, a single assignment of electrons to orbitals is made and then these orbitals are brought together to form a suitable many-electron wavefunction ψ, which is the simplest MO approximation to the solution of the Schrödinger equation[2]. If the molecule is diatomic, the electronic wavefunction is a function of one parameter, the internuclear distance. For a polyatomic molecule the electronic wavefunction depends on the bond lengths, bond angles, and dihedral angles. In this case the electronic wavefunction is calculated for a range of each of these parameters. The equilibrium values are those that minimize the electronic energy (including the nuclear repulsion)[10].

In MO methods the one-electron eigenfunctions are called spin orbitals[2] which are formed by taking the product of spatial functions (molecular orbitals) given by $\psi_1(x,y,z)$, $\psi_2(x,y,z)$, $\psi_3(x,y,z)$ . . ., and a spin component of α or ß (see below). The spin orbitals are allowed to spread throughout the molecule where their exact form is determined by the method of variations to minimize the total energy. Then ψ is reconstructed into a combination of molecular orbitals. The molecular orbitals form a normalized, orthogonal set, where

$$\iiint \psi_i \psi_i^* \, dxdydz = 1$$

$$\iiint \psi_i \psi_j \, dxdydz = 0 \quad i \neq j$$

ψ is then written as a combination of the molecular orbitals by writing their Hartree product

$$\psi(\boldsymbol{r}) = \psi_1(\boldsymbol{r}_1)\ \psi_2(\boldsymbol{r}_2)\ \ldots\ \psi_n(\boldsymbol{r}_n)$$

The above function assumes that each molecular orbital holds only one electron. However, most molecules have an even number of electrons in their lowest energy states (ground states) where the orbitals are either doubly occupied or empty (closed-shell)[11]. Also, this function is symmetric not antisymmetric which violates one of the conditions placed on the wavefunction for molecular systems, a problem noted by Vladimir Fock. To solve the problem of symmetry, the spin

coordinates A for the electron must be included. This coordinate has one of two possible values (±½). The two spin functions $\alpha(A)$, and ß(A) are defined as

$$\alpha(+½) = 1 \qquad \alpha(-½) = 0$$

$$ß(+½) = 0 \qquad ß(-½) = 1$$

where +½ represents spin up and -½ spin down. Multiplying the molecular orbital by the spin function produces the complete wavefunction for a single electron, $\psi(r)\alpha(A)$ or $\psi(r)ß(A)$. This product is called a spin orbital, $\chi(r,A)$ and is a function of the electron's location and spin. If two electrons are in the same molecular orbital, they will have different spin values by the Pauli Exclusion principle which states that no two electrons in a particular multielectron atom can be in the same quantum state[12]. By including the spin function a single spin orbital can have two electrons. For an N-electron case, the general form for a given configuration will be given by

$$\psi = \chi_1(1)\chi_2(2)\chi_3(3) \ . \ . \ . \ \chi_N(N)$$

Because the electrons are indistinguishable, there will be N! possible permutations of the above equation which must all be combined to produce the antisymmetric wavefunction. To construct these equations directly would be a formidable task. J. C. Slater simplified the representation of ψ by showing the correct antisymmetric functions could be expressed as a determinant where the various spin orbitals

appear in rows and the various electrons appear in columns. This determinant is given by

$$\psi = (N!)^{-1/2} \begin{vmatrix} \chi_1(1) & \chi_2(1) & \chi_3(1) & \dots & \chi_N(1) \\ \chi_1(2) & \chi_2(2) & \chi_3(2) & \dots & \chi_N(2) \\ \dots & \dots & \dots & \dots & \dots \\ \dots & \dots & \dots & \dots & \dots \\ \dots & \dots & \dots & \dots & \dots \\ \chi_1(N) & \chi_1(N) & \chi_2(N) & \dots & \chi_N(N) \end{vmatrix}$$

The above determinant is referred to as a Slater determinant[13,14], and is the standard method of expressing a Hartree-Fock representation.

An additional approximation, or restriction, is imposed on the molecular orbitals where they are expressed as a linear combination of a set of N known one-electron functions called basis functions, $\phi_1(x,y,z)$, $\phi_2(x,y,z)$, ..., $\phi_N(x,y,z)$. Then

$$\psi_1 = \sum_{m=1}^{N} C_{mi}\phi_m$$

These basis functions are defined in the specifications of the model being used and constitute a basis set; there is, in fact, some optimization of these functions to reproduce known atomic properties, but these functions can then be used for any molecule.

Once the basis set has been selected, the unknown coefficients c_{mi} are determined such that the total

electronic energy calculated using the many-electron wavefunction is minimized and is as close as possible to the energy that would be obtained from the exact solution of the Schrödinger equation. Using these limited basis sets for the molecular orbital expansion and a determinantal wavefunction corresponding to a single electron configuration is called the Hartree-Fock approximation. These Hartree-Fock models are the simplest *ab initio* methods to use for chemical applications and have been carried out in many studies to date[2]. To fully specify the model a unique basis set ϕ_1, ϕ_2, ..., ϕ_N must be defined for the specific nuclear configuration. To do this, one has a standard set of basis functions for each atom, centered at the nuclear position, which depend only on the atomic number for that element. This means there would be a set of functions for each hydrogen atom, a different set for each carbon atom, and continuing for the different types of atoms in the molecule.

The simplest Hartree-Fock models use the smallest number of basis functions possible for each atom. This means the number of basis functions will be just enough to describe all the electrons and still be spherically symmetric. In this case the molecular orbitals defined by

$$\psi_1 = \sum_{m=1}^{N} C_{mi}\phi_m$$

will have limited flexibility. If larger basis sets are

used, the number of adjustable coefficients in the variational procedure increases proportional to N^4 producing a better description of the molecular orbitals at a considerable computational expense. If very large basis sets are used, then there will be almost complete flexibility. The Hartree-Fock limit represents the best approximation that can be achieved using a single-electron configuration.

In the above discussion, the basis functions are assumed to be a set of totally arbitrary functions under the restriction that they are normalized and orthogonal. It is also assumed that there is one function per electron, on each atomic center. However, it should be stated that one could use any number of basis functions per atomic center; in fact, using more functions will provide a more exact series expansion for the wavefunction. If the basis functions are the atomic orbitals for the atoms that make up the molecule then the equation above is called a linear combination of atomic orbitals (LCAO) approximation, and is used in the qualitative description of the electronic structure. The LCAO approximation has several disadvantages. First, atomic orbitals situated on different atomic centers in the molecule are not mutually orthogonal. Second, the form of the atomic orbitals on any isolated atom except for hydrogen, cannot be exactly known. Even if the form is known in the isolated atom, it would be different in the molecule because the presence of other atoms would perturb the

orbitals of the given atom. Finally, many of the integrals that must be calculated become difficult, if not impossible, to calculate[15]. This is because the form of an exact atomic orbital has a cusp at the nucleus, making analytical methods difficult.

A different method of choosing basis sets is to use a set of functions of some convenient mathematical form. The choice of function is made in order to simplify the calculations of certain integrals, especially the electron repulsion integrals. If the integral calculations can be kept simple, than a larger number of basis functions can be used without a huge increase in computational expense. To provide a well-defined basis set for any nuclear configuration one needs to define a set of basis functions for each element that depends only on the charge on its nucleus. These functions may have the symmetry properties of atomic orbitals and may even be classified as s, p, d, f,... types according to their angular properties.

One basis set consists of gaussian-type atomic functions. These are powers of x, y, and z multiplied by $\exp(-\alpha r^2)$, where α is a constant determining the radial extent (size) of the function. In normalized form, one of the second order gaussian-type atomic functions is

$$g_{xy}(\alpha, r) = \left(\frac{2048\alpha^7}{9\pi^3}\right)^{1/4} xy \exp(-\alpha r^2)$$

There are six second order gaussians with the factors x^2,

y^2, z^2, xy, xz, and yz. Five linear combinations (having the factors xy, xz, yz, x^2-y^2, and $2z^2-x^2-y^2$) can be formed to have the same angular behavior as the five real d-type atomic orbitals[10]. The STO-3G basis set consists of expansions of Slater-type atomic orbitals (STOs) in terms of 3 gaussian functions. Chapter 2 will consider STO basis functions in greater detail.

The greatest deficiency of Hartree-Fock theory is that a complete description of the correlation between the motions of the electrons is not possible. In other words, the motions of the electrons can not be completely separated. One way to treat this interdependence is to do a Hartree-Fock calculation on all possible electron configurations with each weighted by their population. The Schrödinger equation cannot be solved in terms of a single electron configuration, even using very large basis sets. One must go beyond the Hartree-Fock level by using wavefunctions that represent more than a single electron configuration. For example, let ψ_0 represent the full Hartree-Fock many electron wavefunction. Then a more accurate wavefunction ψ can be created, which is given by

$$\psi = a_0\psi_0 + a_1\psi_1 + a_2\psi_2 + a_3\psi_3 + \ldots$$

where ψ_1, ψ_2, ψ_3, ... are wavefunctions for other configurations, and a_0, a_1, a_2, ... are linear coefficients that must be determined. If all possible electronic

configurations are included for a given basis set then the complete correlation of the electronic motion will be obtained. This is called the electron interaction method, but there are other ways to treat this electron correlation, including the aforementioned density-functional theory. Generally, computational chemists try to find a practical method which does one of the following:

1. limits the number of configurations;
2. approximates the effect of including a particular configuration into the wave function.

This is done by sequentially placing the configurations into the wavefunction equation in order of increasing sophistication and accuracy. To approach an exact solution of the Schrödinger equation one must either improve the basis sets, *i.e.*, increase the size of the basis sets, thereby increasing the flexibility of the one-electron spin orbitals, or take the sum of an increasing number of many-electron wavefunctions[4]. Either method approaches the exact solution of the nonrelativistic Schrödinger equation.

1.5 Order for the Rest of the Dissertation.

In Chapter 2, three basis sets (STO-3G, LANL1DZ, and 3-21G*) are used in determining the optimized geometry for a CO molecule adsorbing on the surface of a cluster model of a MgO crystal using GAUSSIAN 92[17]. The effects of the basis sets on the optimized bond lengths are compared. Three

different cluster sizes are used for the MgO crystal. Once the best cluster model is determined, the orientation of the atoms within the model is varied between magnesium and oxygen as the central atom. The effect of the charge on the cluster, 0 or ±2, and the presence of an atom in the layer under the central atom are investigated. The CO molecule is allowed to vary its orientation so that it will adsorb through either the carbon atom, or the oxygen atom. Finally, a sulfur atom is placed below the layer, under the central magnesium atom to determine the effect of the sulfur impurity on the optimized geometry. The effects of these parameters on the optimized geometry and other properties such as dipole moment and binding energy are compared.

In Chapter 3, the electron density, ρ, and the Laplacian of the electron density, $\nabla^2\rho$, are defined. Contour maps and relief maps for the free CO molecule are created and the important features are explained. Then, contour maps of $\nabla^2\rho$ are created for the different orientations and conditions mentioned in Chapter 2. These are used to show how electron density affects the geometry and electronic properties of materials.

Chapter 2

Geometry Optimization, Dipole Moment, and Binding Energy for CO Adsorbing on a MgO Surface

2.1 Introduction

The study of adsorbates on metal oxide surfaces has received attention in many areas such as catalysis, solid state physics, materials science, and semiconductor physics. The study of the adsorption of CO on MgO has important implications for heterogeneous catalysis as well as other surface processes[18-23]. In heterogeneous catalysis and surface science, oxides play an important role serving as components, as well as active catalytic agents. Oxide systems provide mechanical and thermal stability for metal particles used in heterogeneous catalysis due to their high melting points and resistance to corrosion[24]. Oxide surfaces are important crust materials in soil chemistry[25,26]. The reduction of atmospheric pollutants such as CO, using magnesium based absorbants, is an important pollution prevention technology[27]. Alkali-doped metal oxides have been successfully employed in the synthesis of ethane and higher hydrocarbons from natural gas[28,29]. Finally, the adsorption of CO on regular sites of MgO(001) has been used as a test for theoretical models of chemisorption on ionic surfaces[30-34].

The interaction of a CO molecule with the MgO(001) surface has been studied in great detail both experimentally and theoretically[18-49]. In this study, the effect of different variables on the geometry optimization of the CO molecule and properties such as dipole moments, adsorption energy, electron density, and the Laplacian of the electron density for the cluster and CO molecule were investigated. The variables probed are:

1. choice of basis set;
2. cluster size used to represent the MgO molecule;
3. choice of magnesium or oxygen in the center;
4. whether there is an atom under the central atom;
5. orientation of the CO molecule;
6. charge on the cluster.

2.2 Atomic Basis Sets

Basis sets are usually analytical functions in three-dimensional space, in which case a basis set is a mathematical description of the orbitals for atomic or molecular systems (which in turn combine to approximate the total electronic wavefunction). The functions serve as input to the theoretical calculation[50]. Using larger basis sets allows a more accurate approximation of the orbitals because fewer restrictions are imposed on the dynamics of the electrons in space. The electrons actually have a finite probability of any symmetry allowed arrangement in space,

including relative positions, but this limit would correspond to an infinite basis set.

Minimal basis sets of nuclear-centered functions are the simplest level of *ab initio* molecular orbital calculations. The STO-3G is an example of a minimal basis set. The series of basis sets known as STO-KG are expansions of Slater-type atomic orbitals (STO) in terms of K gaussian functions, given by

$$\phi_{n1}(\varsigma=1,r) = \sum_{k=1}^{K} d_{n1,k}\exp(-\alpha r^2)$$

where the subscripts n and l represent the principal and angular quantum numbers, *e.g.*, ϕ_{1s}. The values of the linear expansion coefficients, d, and the gaussian exponents, α, are determined by minimizing the error in the gaussian expansion to the exact Slater orbital, using a least squares fit. In normalized form, the first four gaussian-type atomic functions are

1. $$g_s(\alpha,r) = \left(\frac{2\alpha}{\pi}\right)^{3/4} \exp(-\alpha r^2)$$

2. $$g_x(\alpha,r) = \left(\frac{128\alpha^5}{\pi^3}\right)^{1/4} x \exp(-\alpha r^2)$$

3. $$g_y(\alpha,r) = \left(\frac{128\alpha^5}{\pi^3}\right)^{1/4} y \exp(-\alpha r^2)$$

4. $$g_z(\alpha,r) = \left(\frac{128\alpha^5}{\pi^3}\right)^{1/4} z \exp(-\alpha r^2)$$

The gaussian functions g_s, g_x, g_y, and g_z have the angular symmetries of the s-type and three p-type atomic orbitals. The six second order functions, shown below, do not all have the angular symmetry of atomic orbitals.

5. $$g_{xx}(\alpha,r) = \left(\frac{2048\alpha^7}{9\pi^3}\right)^{1/4} x^2 \exp(-\alpha r^2)$$

6. $$g_{yy}(\alpha,r) = \left(\frac{2048\alpha^7}{9\pi^3}\right)^{1/4} y^2 \exp(-\alpha r^2)$$

7. $$g_{zz}(\alpha,r) = \left(\frac{2048\alpha^7}{9\pi^3}\right)^{1/4} z^2 \exp(-\alpha r^2)$$

8. $$g_{xy}(\alpha,r) = \left(\frac{2048\alpha^7}{9\pi^3}\right)^{1/4} xy \exp(-\alpha r^2)$$

9. $$g_{xz}(\alpha,r) = \left(\frac{2048\alpha^7}{9\pi^3}\right)^{1/4} xz \exp(-\alpha r^2)$$

10. $$g_{yz}(\alpha,r) = \left(\frac{2048\alpha^7}{9\pi^3}\right)^{1/4} yz \exp(-\alpha r^2)$$

Five linear combinations, having the factors xy, xz, yz, x^2-y^2, and $2z^2$-x^2-y^2, can be formed having the same angular behavior as the five d-type atomic orbitals. The STO-3G basis set uses a linear combination of three gaussian functions for each STO, which accounts for the 3G designation.

When using the STO-KG minimal basis sets, properties such as optimum geometries, charge distributions, electric dipole moments and energy differences are not strongly

dependent on the value of K but absolute energies of atoms and molecules have a strong dependence on K. Because of the relative computational time, the STO-3G basis set has been chosen as a good compromise for many applications[2].

There are several shortcomings in using the STO-3G minimal basis set. First, the number of atomic basis functions does not depend on electron count. That is, there are the same number of functions (five) whether the atom is lithium (three electrons), boron (five electrons), or oxygen (eight electrons). The descriptions of compounds that contain elements such as oxygen will be less accurate than compounds containing elements with fewer electrons such as lithium or boron. Second, since a minimal basis set contains only one valence function of each symmetry type (*i.e.*, 2s, $2p_x$, $2p_y$, $2p_z$) they do not allow the orbitals to change size. This means there is no radial exponent optimization for each atom in the molecule. The 2s orbital in oxygen, while smaller than the 2s orbital in boron, is the same in all compounds. Third, minimal basis sets cannot adequately describe nonspherical anisotropic aspects of molecular charge distributions. Finally, functions of these types are still not orthogonal when they are centered on different atomic positions in a molecule[2,15].

The first two deficiencies may be overcome by increasing the number of basis functions per atom. Split valence basis sets, such as the 3-21G, use two STOs for each

valence atomic orbital but only one STO for each inner-shell atomic orbital. The two STOs for the valence atomic orbitals differ in their orbital exponents[51,52]. Polarized basis sets are able to describe atoms that have their center of electron charge density shifted off of the nuclear position. These basis sets add orbitals that have angular momentum beyond what is required for the ground state description of each atom[49]. The 3-21G* basis sets are constructed directly from the corresponding 3-21G representation by the addition of a complete set of six second-order gaussian functions[53]. In the 3-21G* basis set there are three gaussian functions for each inner-shell, or core, atomic orbital and two gaussians for the inner part of each valence shell orbital, and one gaussian for the diffuse part of each valence shell orbital. Since these can be optimized separately, the atom can expand or contract in response to its molecular environment. Finally, the 3-21G* uses the unsupplemented 3-21G basis set for hydrogen, helium and the elements through neon. For geometry predictions the relatively small 3-21G and 3-21G* (3-21G* for molecules having elements between sodium and argon) are the basis sets of choice for molecules of moderate size[10].

The LANL1DZ basis set is commonly used for atoms including and beyond potassium in the periodic table. Here, the inner-shell electrons are treated in an approximate way using effective core potentials (ECPs). For the elements

hydrogen to neon the LANL1DZ basis set uses the D95V basis set which is a double zeta basis set. For sodium to bismuth, the LANL1DZ basis set uses ECPs and double zeta basis functions. The double zeta basis sets replace each STO of a minmal basis set by two STOs that differ in their orbital exponent zeta[54,55]. For molecules containing fourth row elements the LANL1DZ basis set may be more economical to use, in terms of computer time.

2.3 Cluster Models

Three different cluster models of the MgO (001) surface were used in the geometry optimization portion of this research.

1) A surface one atom thick with nine atoms in the layer, referred to as a 3x3x1 cluster.
2) A surface two atoms thick with nine atoms in each layer, referred to as a 3x3x2 cluster.
3) A surface one atom thick with 25 atoms in the layer, referred to as a 5x5x1 cluster.

In these cluster models, a number of approximations must be used. It is known from both theory[41,44,56] and experiment[57,58] that the relaxation of a non-defective (001) surface of MgO is small. As can be seen in the figure below, the amplitude of the "rumpling" is approximately 0.05 Å. Hence, the surface used in the cluster models is approximated by a flat

surface. That is, all atoms are considered to be centered in the same surface plane. The distance between adjacent atoms was taken to be 2.1 Å[59], for the undoped MgO crystal. This value was held constant in the geometry optimization, unless otherwise noted.

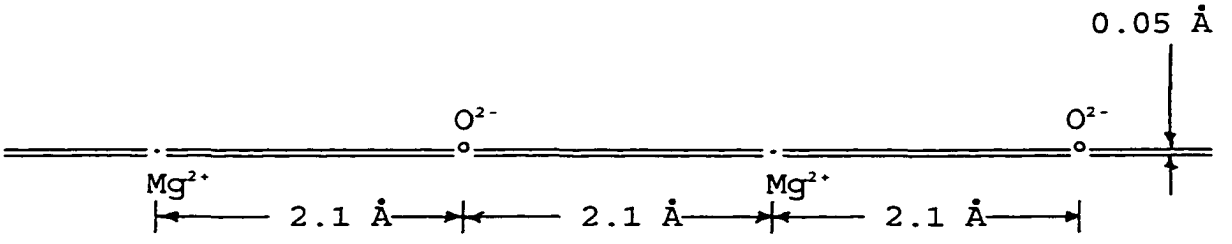

Figure 2-1. The calculated structure of non-defective (001) surface of MgO.

Figure 2-2 shows the different cluster models used for the optimization of the Mg-C and C-O bond lengths. In all instances, magnesium is the center atom (top-center in the 3x3x2 cluster).

Experimental studies have shown that the CO molecules are adsorbed on the surface of MgO in the form of a regular array of single molecules oriented perpendicular to the surface coordinated to the magnesium[60-62]. Because of this, the x and y coordinates of the CO molecule were fixed over the center of the cluster. One trial was done to optimize the C-O, and the X and Y values determined were 2.1 Å, for each. The z coordinates for both carbon and oxygen were

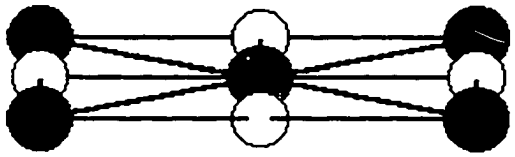

(a)

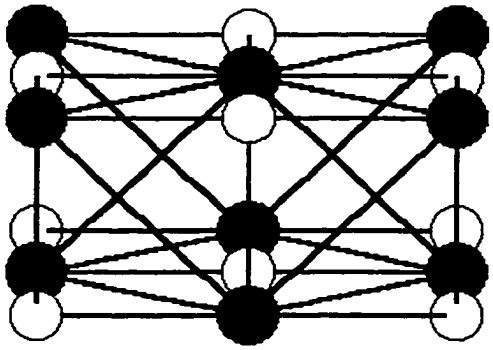

(b)

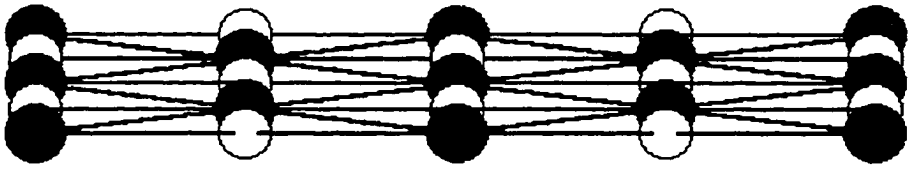

(c)

Figure 2-2. (a) 3x3x1 MgO cluster with Mg in the center.
(b) 3x3x2 MgO cluster with Mg in the center of the top layer.
(c) 5x5x1 MgO cluster with Mg in the center.

determined using GAUSSIAN 92 for the optimized positions. These values were then used to determine the Mg-C and C-O bond lengths. For example, the Z coordinate of the carbon atom was found to be 4.680 Å using the STO-3G basis set and the 3x3x2 cluster model yielding a Mg-C bond length of 2.580 Å.

The optimized C-O position is determined for each of the above cases, and is shown in Table 2-1. The archives for these and all other optimizations and computations are found in Appendix A.

Table 2-1. Table showing the optimized bond lengths, in angstroms, for the different geometries and basis sets.

Geometry	Basis Set	Mg-C bond length	C-O bond length
3x3x1	STO-3G	2.551	1.146
	3-21G*	2.478	1.127
	LANL1DZ	2.678	1.135
3x3x2	STO-3G	2.580	1.145
	3-21G*	2.486	1.126
	LANL1DZ	2.792	1.135
5x5x1	STO-3G	2.534	1.145
	3-21G*	2.429	1.126
	LANL1DZ	2.596	1.134

Table 2-2 shows the values for the Mg-C and C-O bond lengths from various references using different cluster sizes, basis sets, and calculation techniques. The reference number is provided for the reader's convenience. The values shown here were chosen to represent values determined using a diverse set of computational methods.

Table 2-2. Table of data showing Mg-C and C-O bond lengths, in angstroms, from different references.

Reference number	Experimental parameters	Mg-C bond length	C-O bond length
18	$(MgO_5$-PCC)-CO	2.582	1.121
19[a]	Mg_9O_9(9,9)-CO	2.51	1.130
19[b]	$Mg_{21}O_{21}$(21,21)-CO	2.55	1.130
20[c]	Mg^{+2} - CO	2.49	1.13
21	Mg_9O_9PC-CO	2.22	1.124
31[d]	1/2 coverage	2.444	1.124
31[d]	1/4 coverage	2.447	1.127
32	Mg^{+2}-PC	2.46	N/A
34[e]	Mg^{+2}_{5c}	2.70	1.132
38	$Mg_{19}O_{19}$	2.440	1.098
41[f]	$Mg_{50}O_{50}$	2.550	N/A
44	Mg_9O_9-CO	2.22	1.24
48[g]	Mg_5O_5PC-CO	2.48	N/A
63	1/4 coverage	2.78	1.112

[a]BLYP, q = ±1.8, Mg-C distance after BSSE corrections of the potential curve.
[b]BLYP, q = ±1.8
[c]CO bond length fixed at 1.13Å for all cases.
[d]1/2 or 1/4 coverage of the MgO surface with CO at 90°.
[e]BSSE correction.
[f]Using SINDO1.
[g]MgO surface.

It can be seen from the data in Table 2-1 that the choice of cluster has little effect on the optimized Mg-C bond lengths and virtually no effect on C-O bond lengths. Comparing these values with those in Table 2-2 it can also be seen that the 3-21G* basis set produces values in close agreement with values obtained from other modeling schemes.

For the remainder of this dissertation, the 3x3x1 cluster will be used. This choice of using the smaller cluster is based on computational cost. As the number of atoms in the cluster increases, the time required for the calulations to be completed increases dramatically. The 3x3x1 cluster model uses significantly less computer time than the 3x3x2 cluster model. The 5x5x1 cluster model with 25 atoms in the cluster requires a tremendous amount of computational time. For example, finding the optimized position for the CO molecule required more than 11 days for the 5x5x1 cluster, 1 day and 9 hours for the 3x3x2 cluster, and 3 hours 32 minutes for the 3x3x1 cluster, using the 3-21G* basis set. All optimizations were run on Pentium I (133 MHz) processors.

2.4 Effect of Central Atom, Cluster Charge, Presence of an Atom Under the Layer, and CO Orientation on Bond Length

In the 3x3x1 cluster model, the central atom was varied between magnesium and O. In all cases, the CO molecule was adsorbing at the central atom. The central atom is located at the origin for the optimization, with the CO molecule above the surface oriented along the +Z axis. The Z axis is the axis of symmetry for the CO molecule. The orientation of the CO molecule was considered with the carbon or oxygen atom bonding to the central atom, referred to as carbon down or oxygen down, respectively, in this dissertation.

When magnesium was used as the central atom, three conditions were studied: a) no atom under the central magnesium with +2 charge on the cluster (which would be expected for a cluster "cut out" of an ionic lattice); b) no atom under the central magnesium with no charge on the cluster; c) an oxygen atom was placed under the central magnesium with no charge on the cluster. Figure 2-3 shows the various orientations for the 3x3x1 cluster with magnesium as the center atom, without an oxygen atom under the magnesium (a) and with an oxygen atom below the central magnesium (b).

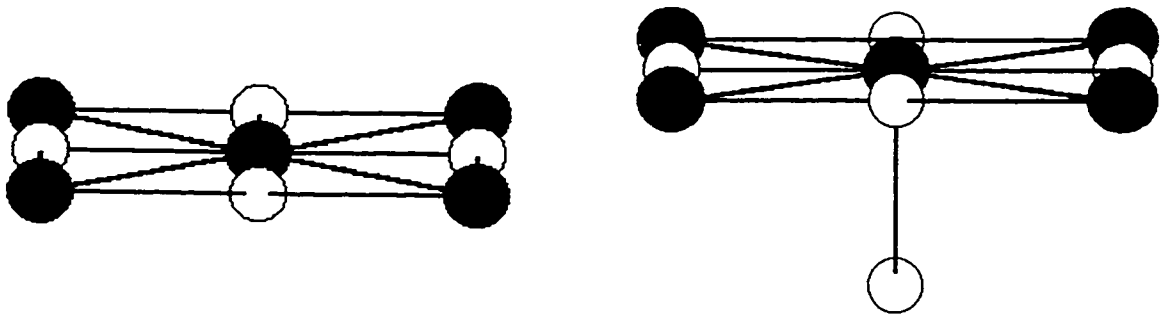

(a) (b)

Figure 2-3. 3x3x1 MgO cluster with Mg in the center without an O under the layer (a), and with an O under the layer (b).

When oxygen was used as the central atom, three conditions were studied: a) no atom under the central oxygen with -2 charge on the cluster (which would be expected for a cluster "cut out" of an ionic lattice); b) no atom under the

central oxygen with no charge on the cluster; c) a magnesium atom was placed under the central oxygen with no charge on the cluster.

In Table 2-3 the Mg-C and C-O bond lengths are listed for the following conditions:

1. STO-3G, 3-21G*, and LANL1DZ basis sets.
2. magnesium in the center with no other atom under the layer, with +2 charge and with 0 charge on the cluster.
3. magnesium in the center with oxygen under the layer and 0 charge on the cluster.

Figure 2-4 shows the 3x3x1 cluster with magnesium in the center for the orientations listed in Table 2-3. The +2 charge on the cluster reflects the net charge on the five Mg^{2+} and four O^{2-} ions that make up the cluster. The 0 charge on the cluster was included to represent the fact that the cluster is a small part of a crystal which would have a net charge of zero. Because the cluster is used as a model of the crystal the zero charge cluster model was included to determine the effect, if any, this would have on the geometry optimization. Since the longest Mg-C bond is to the cluster with no charge, made by imbedding a neutral magnesium atom in the center of a square of ions, there is clearly reduced binding to sites that are less ionic.

The choice of basis set can affect the optimized geometry. Comparing the values in Table 2-3, the LANL1DZ basis set consistently produced the longest Mg-C bonds, and

the 3-21G* basis set, the shortest. Regardless of basis set, the longest Mg-C bonds were to the cluster with with no other atom under the layer and 0 charge on the cluster.

Table 2-3. Table showing the Mg-C and C-O bond lengths (Å).

Condition	Basis Set	Mg-C bond	C-O bond
No O under the layer, +2 charge	STO-3G	2.502	1.143
	3-21G*	2.468	1.126
	LANL1DZ	2.640	1.128
No O under the layer, 0 charge	STO-3G	2.551	1.146
	3-21G*	2.478	1.127
	LANL1DZ	2.678	1.135
O under the layer, 0 charge	STO-3G	2.519	1.146
	3-21G*	2.445	1.128
	LANL1DZ	2.617	1.137

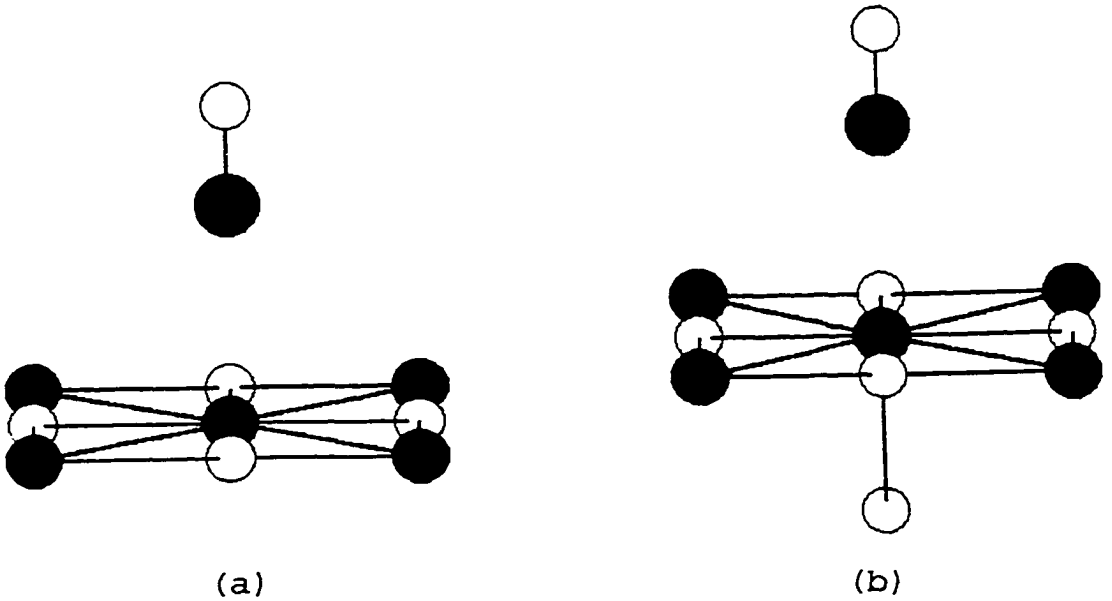

(a) (b)

Figure 2-4. 3x3x1 cluster with Mg in the center, CO with C down, nothing under the layer (a), and O under the layer (b)

There are an additional 2 electrons that must be present to produce the 0 net charge on the cluster. These electrons can be delocalized, but the elongated Mg-C bond shows that they are not completely delocalized to the perimeter. This will be seen later in Chapter 3 where the electron density is examined for these cluster/charge combinations.

Table 2-4 shows the data taken for the same conditions as Table 2-3, except the CO molecule is oriented with the oxygen towards the central magnesium atom.

Table 2-4. Table showing the Mg-O and O-C bond lengths (Å).

Condition	Basis Set	Mg-O bond	O-C bond
No O under the layer, +2 charge	STO-3G	2.174	1.151
	3-21G*	2.365	1.138
	LANL1DZ	2.505	1.141
No O under the layer, 0 charge	STO-3G	2.229	1.147
	3-21G*	2.402	1.132
	LANL1DZ	2.651	1.135
O under the layer, 0 charge	STO-3G	2.242	1.146
	3-21G*	2.412	1.131
	LANL1DZ	3.105	1.135

It is interesting to note that there are significant differences for most of the values of the C-O bond lengths from Table 2-3 and Table 2-4. Hence, the effect of the orientation on the C-O bond length is considerable. There is a large difference in the Mg-C bond length when the LANL1DZ basis set is used. However it should be noted that the

LANL1DZ basis set provides values for the Mg-C bond length that are greater than those using the STO-3G or 3-21G* basis sets in all cases shown in Table 2-4. Also notice that the Mg-C bond lengths are longest for the cluster with oxygen under the center Mg. The cause of this will be explained in greater detail later in this chapter and in Chapter 3, when the distribution of electronic charge in these complexes is investigated.

Next, an oxygen atom is placed at the center of the cluster with the following conditions:

1. STO-3G, 3-21G*, and LANL1DZ basis sets.
2. oxygen in the center with no other atom under the layer, with -2 charge on the cluster, as would be expected for a cluster of ions.
3. oxygen in the center with no other atom under the layer, with 0 charge on the cluster, as would be the case if a neutral oxygen atom was imbedded among ions.
4. oxygen in the center with magnesium under the layer and 0 charge on the cluster, as would be the expected for a cluster of ions.

Two orientations of the CO molecule were considered, carbon down shown in Table 2-5, and oxygen down. It has been shown in previous papers[20,37,63] that the CO molecule oriented with oxygen down does not adsorb at the oxygen position on the surface. One trial was conducted with oxygen in the center of the cluster, CO with oxygen down, STO-3G basis set, and

-2 charge on the cluster. The optimized geometry position resulted in an O-O bond length greater than 19 Å. Obviously, no bond was formed in this case, probably due to a large coulombic barrier, in agreement with the references cited above.

Table 2-5. Table showing the bond lengths (angstroms) with O as the central atom with C down.

Condition	Basis Set	O-C bond	C-O bond
No Mg under the layer, -2 charge	STO-3G	2.174	1.151
	3-21G*	3.211	1.134
	LANL1DZ	3.804	1.143
No Mg under the layer, 0 charge	STO-3G	3.659	1.145
	3-21G*	3.4133	1.127
	LANL1DZ	3.955	1.135
Mg under the layer, 0 charge	STO-3G	3.341	1.145
	3-21G*	3.341	1.127
	LANL1DZ	3.835	1.136

It can be seen from the results in Table 2-5 that the length of the CO bond for the CO molecule has approximately the same value as it has for every other basis set and orientation configuration when appropriate comparisons are made concerning cluster type and basis set. It should also be noted that the O-C bond length, from the oxygen in the surface to the carbon of the CO molecule is longer than the CO bond for the molecule, and longer than the Mg-C and Mg-O bond lengths from the surface to the molecule. The reason

for this is Mg^{2+} is a Lewis acid and can form an acid-base adduct with CO, a Lewis base. When O^{2-} is in the center, the interaction with CO is largely via weak van der Waals' forces. A better comparison can be made when the charge distributions are examined for the respective cases. Also note the value for the O-C bond length with the STO-3G basis set for the -2 charge condition. The 2.174 Å bond length is an example of the anomalous results that can occur when using a minimal basis set in surface chemistry simulations.

2.5 Effect of Central Atom and CO Orientation on Dipole Moment

Aside from electron diffraction, or x-ray diffraction (which can increase the electron charge distribution in gaseous molecules and crystals, respectively) the electric dipole moment is the principal experimental quantity that is related to charge where comparisons with theory can be made[2]. When two electric charges of equal magnitude but opposite in sign, +Q and -Q, are separated by a small distance d, then these two charges form an electric dipole. The electric dipole moment μ is defined as the vector of magnitude Qd which points from -Q to +Q.

For example, if a sodium chloride molecule was 100% ionic, then there would be a Na^{1+} ion and a Cl^{1-} ion spaced 236.1 pm apart. Then

$$\mu = Qd$$

$$\mu = (1.6022 \times 10^{-19}\ C) \cdot (236.1 \times 10^{-12}\ m)$$

$$\mu = 3.7828 \times 10^{-29}\ C \cdot m = 11.34\ D$$

where D is the unit debye named after Peter Debye (1D = 3.336×10^{-30} C·m)[65]. The value for μ for sodium chloride is actually less than this because there is slightly less than 100% charge transfer between the ions and, more importantly, the resulting ions are themselves polarized (possessing "atomic first moments"[66]) in the direction opposite to the Na → Cl charge transfer. Since the dipole moment is a vector quantity, not only the magnitude of the different dipole moments must be considered, but also their direction. The figure below shows the dipole moment vectors for the sodium chloride ion pair as well as the atomic first moments for each ion.

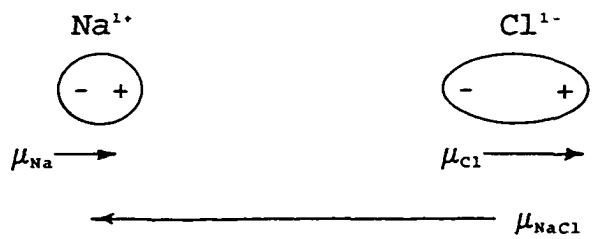

Figure 2-5. The dipole moments for NaCl.

Note in the above figure for the ion pair that the dipole moment for the molecule points from the negative charge towards the positive charge (it is treated as an algebraic vector). This is also the convention used in the GAUSSIAN 92

program used in this dissertation, although the reverse convention is often used in freshman chemistry texts.

The dipole moment is the first derivative of energy with respect to an applied electric field and is a measure of the asymmetry in the molecular charge distribution with respect to an inversion through a central point. Dipole moments may provide an indication of the overall charge distribution in molecules. In addition, by comparing the results of calculated and measured dipole moments the performance of the theoretical model in describing charge distributions may be assessed.

Molecular dipole moments have symmetry imposed restrictions. A symmetry operation produces a configuration that is indistinguishable physically from the original configuration. Hence, the direction of the dipole moment vector must remain unchanged after a symmetry operation. If a molecular system has an axis of symmetry, then the dipole moment must lie along this axis. If the molecule has two or more noncoincident axes of symmetry then it cannot have a dipole moment. If there is a plane of symmetry, then the dipole moment vector must lie in this plane. If there are two or more planes of symmetry, then the dipole moment vector will lie along the line of intersection of these planes. A molecule with center of inversion symmetry cannot have a dipole moment since an inversion reverses the direction of the vector.

The dipole moment vector is described by X, Y, and Z components. The dipole moment vector is directed from the negative charge towards the positive charge. For all of the cluster models in this study, the X and Y components of the dipole moment were zero. The Z axis is the axis of symmetry for the models used in this study, hence the dipole moment vector is along the Z axis.

The accuracy of *ab initio* SCF STO-3G and 3-21G dipole moments is only fair. The 3-21G* basis set gives improved results[8]. A sample of 21 small molecules, such as CO, ClF, NH_3, and CH_3F produced an average error of 0.65 D using STO-3G, 0.49 D using 3-21G, and 0.34 D using 3-21G*[2]. Compounds containing either very electropositive or very electronegative elements such as lithium and/or fluorine (eg. lithium fluoride) produce the poorest agreement between theory and experiment when using the STO-3G basis set. There is an improvement in accuracy using the 3-21G* basis set for compounds containing elements between sodium and argon in the periodic table. These errors will not be a factor in this study as the dipole moment data will be used to show how the dipole moment changes, and therefore how the charge distribution changes, as the CO molecule adsorbs on the surface.

Table 2-6 shows the optimized bond length and the dipole moment for the CO molecule calculated using the STO-3G, 3-21G*, and LANL1DZ basis sets. For each case, the

carbon atom was placed at the origin and the oxygen atom was placed on the Z axis. Experimentally determined values are also included for comparison.

Table 2-6. Table showing the bond length and the dipole moment, μ, in the Z direction for CO with O above C in the +Z direction.

Basis Set	STO-3G	3-21G*	LANL1DZ	Expt.
Bond length (Å)	1.145	1.129	1.138	1.13[20]
μ (debye)	0.1243	-0.3973	-0.4776	0.11[2]

The LANL1DZ and 3-21G* basis sets show the dipole moment pointing from the oxygen (negative end of the molecule) to the carbon (positive end of the molecule). The STO-3G basis set has the carbon atom as the negative end of the molecule, the oxygen as the positive indicating that large atomic first moments must be present. The experimental value[2] for the dipole moment for the CO molecule is 0.11 D, and opposite to the direction expected on the basis of charge, so the STO-3G basis set comes closest to the experimental value for CO, but the 3-21G* basis set will be used for the determination of the dipole moments for the various cluster models and CO orientations because it is the best basis set overall, of the three used here.

Figure 2-6 shows the MgO surface with a CO molecule with nothing under the layer (a) and another atom under the layer (b), and the orientation of the X, Y and Z axes. Because of symmetry, the dipole moment in the X and Y

directions is zero for all configurations. The dipole moment in the Z direction exists when there is an atom under the layer, or when there is a CO molecule adsorbed on the surface.

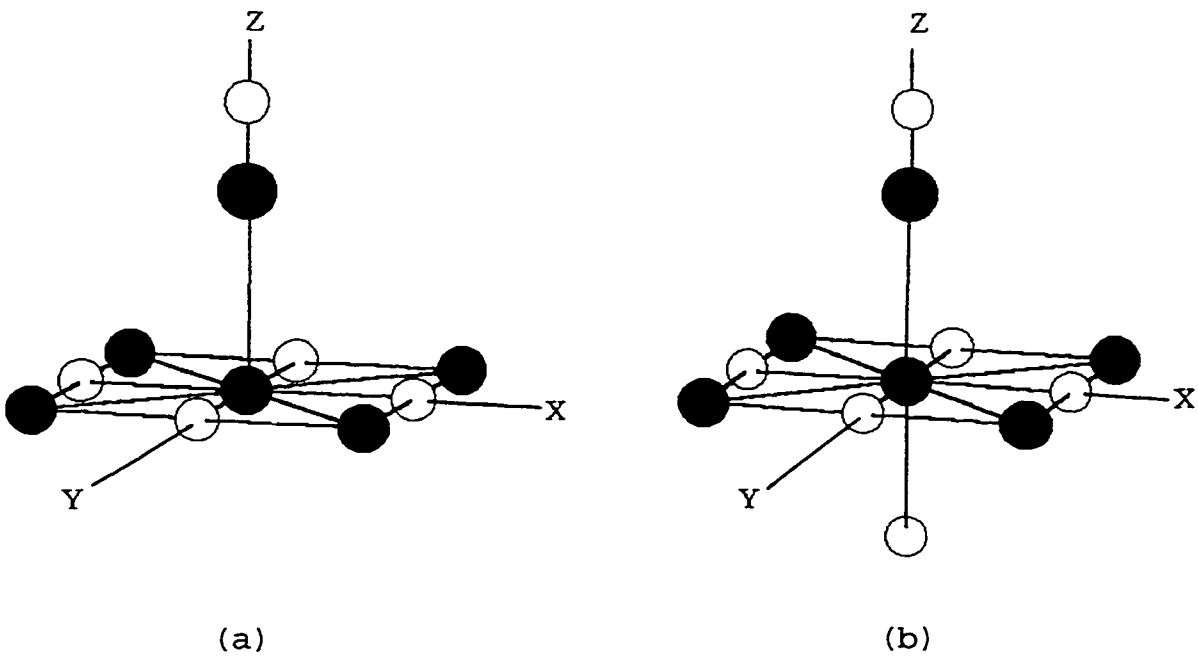

Figure 2-6. Figure showing the MgO surface and the X, Y, and Z axes. In (a) there is a CO molecule and nothing under the layer. In (b) there is an atom under the layer.

Table 2-7 shows the dipole moment for the different orientations of the CO molecule, and the different 3x3x1 cluster models. The 3-21G* basis set was used for all cases. For the values in the table, the MgO surface is on the XY plane with the CO molecule along the positive Z axis. Any atom under the layer is on the negative Z axis.

Table 2-7. Table showing the dipole moments, μ, in the Z direction with Mg and O as the central atom, for the different configurations of CO.

Central Atom	Atom under the layer	Cluster charge	C or oxygen down	μ(z) (debye)
Mg	none	0	none	0.0
Mg	none	0	C	-0.0884
Mg	none	0	O	1.025
Mg	none	+2	none	0.0
Mg	none	+2	C	-3.498[a]
Mg	none	+2	O	-1.968[a]
Mg	O	0	none	8.122
Mg	O	0	C	1.039
Mg	O	0	O	9.143
O	none	0	none	0.0
O	none	0	C	0.0543
O	none	-2	none	0.0
O	none	-2	C	4.319[a]
O	Mg	0	none	-7.884
O	Mg	0	C	-7.997

[a]For charged clusters the dipole moment is origin-dependent (unless dictated by symmetry to be zero).

When magnesium or oxygen are the central atoms with nothing under the layer and no CO molecule, the dipole moment is zero, regardless of charge on the cluster. This is due to the symmetry of the cluster model of the surface. The oxygen atom under the layer greatly accentuates the change in μ as the CO is flipped in its orientation. This seems to indicate more reorganization of charge during bond formation

at the surface. Again, this will be graphically explored when the electron density is examined.

When magnesium is the central atom with nothing under the layer and the CO molecule is oriented with carbon towards the layer the dipole moment has a negative value, meaning the dipole moment points down toward the surface. Since the oxygen atom is above carbon on the Z axis, the negative value for this orientation is supported. Oxygen is the negative end of the CO molecule, and with the surface being either neutral or having +2 charge, the dipole must point from the negative (oxygen) towards the positive (carbon or surface) provided there is not significant opposing charge in any atom's polarizations as a result of bond formation. It was stated earlier that the dipole moment for CO is 0.11 D from the carbon to oxygen due to the polarization of the carbon and oxygen atoms. This would be in the +Z direction when carbon is towards the surface. This means there may be some charge reorganization within the CO molecule, or there is some charge transfer between the CO molecule and the surface. The magnitude of the dipole moment is different for the 0 charge and +2 charge cases. When the surface has a +2 charge, the values of both Q (charge) and d (distance between charges) are greater than when the surface has a zero charge. For the case where the surface has a zero charge, the positive end of the dipole is on the carbon atom. Therefore the dipole moment has a larger absolute

value for the +2 cluster charge condition. Note that since the dipole moment is not uniquely defined for a charged system (it is origin dependent), the absolute values of μ are not physically significant, it is the change in μ that is significant when the CO molecule is flipped. Here, the behavior is as expected. As the oxygen is moved closer to the surface (O down), the magnitude of the cluster's dipole moment is reduced.

There is a difference in the sign of the dipole moment when the oxygen end of the CO molecule is oriented towards the surface when the cluster has zero charge. The dipole is oriented up, pointing from the oxygen towards the carbon, from negative to positive. When the cluster has a +2 charge, the orientation is negative. Here the dipole points towards the cluster, which has a greater positive charge than the carbon atom in the CO molecule. This change is due to two factors. First, there is a difference in the total charge on the cluster which will cause a difference in μ. Second, there is a change in the center of charge. The coordinate system, called the standard orientation, used by GAUSSIAN 92 places the origin at the center of nuclear charge for the molecule. The origin is different for the two cluster charge conditions mentioned above. By changing the origin, the value of the dipole moment is changed.

If there is an oxygen atom below the central magnesium atom in the surface, there exists a dipole moment without

the presence of the CO molecule. The dipole moment for this case has a positive value, 8.122 D. The positive sign is due to the negative oxygen ion below the surface and the positive magnesium ion in the surface at the center. The other O^{-2} and Mg^{+2} ions are symmetrically distributed about the central magnesium ion, therefore there is no dipole moment in the X and Y directions, as stated previously. When there is a CO molecule on the surface, and an oxygen below the surface, the dipole moment is positive for both the carbon down and oxygen down orientations. However, the magnitude of the dipole moment is significantly different for these two orientations, especially when compared with the change in μ for CO flipping when there was no oxygen beneath the layer. When the carbon atom is down, there is a dipole moment between the carbon and oxygen in the CO molecule pointing down. There is also a dipole moment from the oxygen beneath the surface pointing upwards towards the central Mg. The sum of these two direction-oriented values (vectors) is positive, indicating the magnitude of the dipole moment from oxygen to magnesium (surface) is larger in magnitude than the one from oxygen to carbon (molecule). The value of the dipole moment for the free CO molecule is small (Table 2-6) and points from carbon to oxygen. However here there must be some reorganization of charge in the molecule, or between the molecule and the surface because

the value of μ changes from 8.122 D to 1.039 D with the presence of the CO.

For the carbon atom down, when the oxygen atom is the central atom in the surface and the charge on the cluster is zero, the dipole moment is relatively small, 0.0543 D. Because the carbon atom is between two oxygen atoms, there is a net dipole moment of almost zero. The fact that the dipole moment has a positive value implies that the contribution from the surface oxygen to carbon is larger in magnitude than the dipole moment from the oxygen to carbon in the CO molecule. In other words, there is less charge transfer from CO to the cluster than there is within the CO molecule. When the cluster has a -2 charge, the dipole moment is positive (upwards) and has a larger value than the 0 charge case. However, this is an origin dependent quantity, so no direct comparison can be made that is physically significant. This is justified since the surface has a -2 net charge. When there is a magnesium atom under the layer, the dipole moment is negative for both no CO molecule, and the CO molecule with carbon down. Notice that the values are almost the same for both conditions. The major contribution for the dipole moment is between the central oxygen and the magnesium under the layer. The presence of the CO molecule has a negligible effect on the total dipole moment. This was to be expected, as the dipole

moment was almost zero when there was no magnesium under the central oxygen, zero charge, and CO was present.

2.6 Effect of Central Atom and CO Orientation on Binding Energy.

The binding energy, or adsorption energy, was calculated by determining the energy of the cluster, and the energy of the CO molecule separately, then subtracting these values from the energy of the cluster and CO combined. The basis set superposition errors will be small[67], and in any case it is the effect of cluster type and CO orientation and not the absolute value of the binding energy that is of interest. Table 2-8 shows the adsorption energy for the different conditions on the 3x3x1 cluster and CO orientations using the 3-21G* basis set. Note the absence of the CO with oxygen down orientation and an oxygen atom at the adsorption site. The binding energy in this case was a positive value (repulsion energy) indicating no adsorption occurs between the oxygen in the surface and the oxygen end of the CO molecule, as was previously stated. Table 2-9 shows values obtained for adsorption energy using different computational schemes or experimental methods. The reference number is provided for the reader's convenience.

Table 2-8. Table showing the adsorption energy for the different configurations and CO orientations. The energies are in kcal/mole.

Central Atom	Atom under the layer	Cluster charge	C or oxygen down	Adsorption energy
Mg	none	0	C	-7.91
Mg	none	0	O	-7.21
Mg	none	+2	C	-9.79
Mg	none	+2	O	-11.9
Mg	O	0	C	-51.8
Mg	O	0	O	-6.39
O	none	0	C	-10.29
O	none	-2	C	-4.68
O	Mg	0	C	-5.23

Table 2-9. Table showing the adsorption energy for CO on an MgO surface using different computational methods and geometries, or from experimental methods.

Reference	Adsorption energy (kcal/mole)
18	-5.53 for Mg-C, 6.22 for Mg-O
20	-9.0 for Mg-C, 6.0 for Mg-O
21	-8.06 to -27.6 for Mg-C, -11.7 to -16.4 for Mg-O
22	-8.6 for Mg-C, -10.6 for Mg-O
30	-8.5 for Mg-C
31	-9.0 for Mg-C, -6.3 for Mg-O
33	-6.82 for Mg-C, -6.32 for Mg-O
34	-11.1 for Mg-C
36	-9.0 for Mg-C
38	-7.2 to -11.1 for Mg_{3c}, -2.8 to -4.2 for Mg_{4c}

Table 2-9. Continued	
41	-8.1 for Mg-C, -5.0 for Mg-O
46	-6.63 for Mg-C, -5.43 for Mg-O
69	-6.9 to -9.0 for Mg-C (experimental)
70	-3.45 to -10.6 for Mg-C (experimental)
71	-3.00 to -3.22 for Mg-C (experimental)
72, 73	-3.3 for Mg-C

The values in Table 2-8 compare favorably with values determined using other computational and experimental methods with one notable exception. With magnesium in the center, and oxygen under the layer, the value is much larger for the C-down orientation than any experimental or computational value listed in Table 2-9. However, Neyman and Rösch produced binding energy values as high as 30 kcal/mol for Mg-C bonding, and 18.9 kcal/mol for Mg-O bonding[44,45]. The influence of the oxygen atom under the layer, without the surrounding lattice of magnesium and oxygen atoms in the second layer cause the oxygen to have a disproportionate effect on the binding energy and this is instructive. Perhaps the sublayer oxygen stabilizes a greater positive charge on the central magnesium ion, producing a greater attraction for the nonbonding electrons from the carbon than would otherwise be the case. The normal charge transfer is about $0.1e$[19,20] from the CO molecule to the surface. In this instance, the charge transfer would necessarily be greater,

causing the larger adsorption energy value. However, the values produced using the 3-21G* basis set, for any of the charge, cluster, and CO orientations are comparable to experimental values, and values determined using other computational methods.

2.7 Effect of a Sulfur Impurity Below the Central Magnesium Atom.

A final condition investigated in this dissertation places a sulfur atom under the central magnesium atom to see the effect this impurity will have on bond lengths, dipole moment, and binding energy, for the C-down and O-down orientation of the CO molecule.

First, the optimized position for the central magnesium atom was determined. Due to the size of the sulfur atom, it was necessary to determine if the central magnesium atom would be forced above the surface. The 3-21G* basis set was used for this optimization, as well as all other optimizations and calculations in this section. The magnesium optimized position was 0.2875 Å above the surface layer, due to the effect of the sulfur atom beneath the layer. This value was used for the magnesium position for the calculations of bond lengths for the adsorbed CO molecule, dipole moments and adsorption energy. Figure 2-7 shows the MgO surface with the sulfur atom below the surface and the magnesium raised above the surface. Table 2-10 shows

the bond lengths for the adsorbed CO molecule with the C-down and O-down orientations, as well as the dipole moment and adsorption energies.

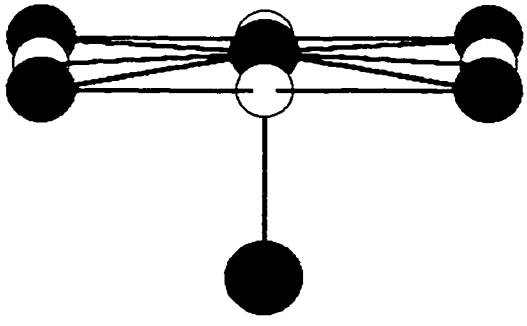

Figure 2-7. 3x3x1 cluster with Mg in the center at the optimized position due to the sulfur atom beneath the layer.

Table 2-10. Table showing the bond lengths, dipole moment and adsorption energy for the 3x3x1 cluster with sulfur under the layer and Mg at the optimized position. Adsorption energy is in kcal/mole.

CO with C-down	CO with O-down
Mg-C bond length = 2.404 Å	Mg-O bond length = 2.239 Å
C-O bond length = 1.122 Å	O-C bond length = 1.135 Å
Dipole moment μ_z = 7.66 D	Dipole moment μ_z = 5.96 D
Adsorption energy = 5.34	Adsorption energy = 10.4

Looking at the values for the bond lengths in the above table, it can be seen that the presence of the sulfur has little effect on the CO bond length, and minimal effect on the Mg-C and Mg-O bond lengths. However, the Mg-C and Mg-O bond lengths are slightly shorter than the values from

Tables 2-3 and 2-4, respectively. This may be due to the polarizability of the sulfur atom stabilizing the positive charge on the central magnesium ion to an even greater extent than an underlying oxygen atom.

The dipole moment for the cluster with magnesium at the optimized position, sulfur under the layer and no CO molecule was 4.54 D. This is the dipole moment between the sulfur atom and the displaced magnesium atom with contributions from the polarized surrounding atoms that are no longer in a plane of symmetry. This effect will be seen in detail in Chapter 3 when the electron charge distribution is investigated. The direction of the dipole is in the +Z direction, from the sulfur (negative) to the magnesium (positive). When the CO molecule is included, there are two orientations to consider. When the carbon atom is down, the dipole moment increases to 7.66 D (same direction). Since the dipole moment is the vector sum of the dipole moments between the various constituents and contributions from the polarized ions (or atoms in a covalent compound), the effect of the negatively oriented dipole moment for the CO molecule is more than compensated by the charge drawn to the surface from the CO molecule. In addition, the surrounding atoms in the cluster and the sulfur under the layer have their electron density distorted due to the presence of the CO molecule, relative to its absence, again seen in detail in Chapter 3. The cumulative effect of these charge

redistributions is to increase the total dipole moment. When the CO molecule is oriented with oxygen down, the increase is not as great. This is primarily due to the orientation of the CO molecule's dipole moment in the +Z direction.

The values for the binding energy, -5.34 kcal/mole for CO with carbon down, and -10.4 kcal/mole for CO with oxygen down are in line with the values reported in Tables 2-8 and 2-9. The effect of the sulfur under the layer has a minimal effect on the binding energy.

2.8 Summary of Chapter 2 Results.

It has been shown that the cluster size and choice of basis set has little effect on the optimized geometry for the CO adsorption on the MgO surface. In addition, changes in cluster condition such as charge (0 or ±2), presence of an atom under the layer, and CO orientation have little effect on the bond lengths. These conditions also have little effect on binding energy, with the exception of magnesium in the center with oxygen under the layer. Only the dipole moment appears to be influenced by the cluster conditions, which is to be expected, as changes in charge magnitude and charge separation are the two components of the dipole moment.

In Chapter 3, the electron density and the Laplacian of the electron density are used to show how the electron structure is altered by changes in the cluster condition.

Chapter 3

Topological Analysis of the Electronic Charge Distribution

3.1 Introduction

The quantum theory of atoms in molecules has been developed by R. F. W. Bader and his associates at McMaster University[76]. This theory provides the tools necessary to interpret the electron density in a molecule in terms of the bonds between atoms and fragments of molecules that are identical to atoms themselves, using the electronic wavefunctions produced from *ab initio* calculations. The topology of the total electronic density $\rho(\mathbf{r})$ and the Laplacian of $\rho(\mathbf{r})$, given by $\nabla^2\rho(\mathbf{r})$, are used extensively in the interpretation of quantum chemical results. Professor Bader and associates have derived a definition of the chemical bonds between atoms in molecules using the topological properties of $\rho(\mathbf{r})$[76-80]. The topology of the Laplacian of the electron charge density has provided a physical basis for the Lewis model and the valence-shell electron pair repulsion (VSEPR) model[81-85]. Using these topological methods means that electronic structure, chemical bonds, and molecular reactivity can be interpreted in terms of $\rho(\mathbf{r})$, which has physical meaning, compared to other interpretive methods such as the Mulliken population or details of a specific set of molecular orbitals[86].

The electron charge density has been used in the study of the electronic structure of molecules[87-90], and the Laplacian of the electron charge density has been used to study the shell structure in atoms and the reactivity of molecules[91-95]. The advantage of using electron charge density for the determination of the structure of molecules and the Laplacian of the charge density for the reactivity of molecules recently has been realized with the development of experimental techniques that parallel the computational methods, an impossibility for orbital-based schemes[96]. The gradient vector field of the electron density provides a definition of the structure in a molecule or crystal by associating a chemical bond with those pairs of atoms whose nuclei are linked by a line of maximum electron density, a bond path[82]. In a given system the set of all bond paths determines and characterizes all of the atomic interactions. A bond path has also proven useful in analyzing the physical properties of metals, alloys, and insulators[95,97]. The electron density can be determined theoretically or experimentally[96,98]. Using single-crystal x-ray diffraction, data collected in less than a day (electron density) were used to determine the structure of d,l-proline monohydrate. This compares with other techniques that took longer than six weeks to collect the necessary data[96].

The reactivity of molecules is reflected in the topology of the Laplacian of the charge density[76,79,81,99]. The

topology of the electron density and its Laplacian have been used to study the structure of surfaces and the reactivity of the surface toward molecules such as CO and NO[99]. There is a correlation between the active sites in a molecule and the critical points (maxima and minima) of $-\nabla^2\rho$ in the valence shell[86]. The function $-\nabla^2\rho$ is used so that maxima in charge concentrations will appear as peaks in relief maps.

3.2 The Electronic Charge Distribution and its Interpretation.

The charge density, or electronic density, $\rho(\mathbf{r})$, is the probability of finding an electron at a given point in space. For a system having N electrons in a stationary state, the charge density is given by

$$\rho(\mathbf{r}) = N\int \psi^*\psi \, d\tau'$$

where τ' denotes the spin coordinates of all the electrons and the Cartesian coordinates of all electrons but one[82]. ψ is the state function of the space and spin coordinates of all the electrons and is an antisymmetric solution to the Schrödinger equation.

The Laplacian of a scalar field f is defined to be the divergence of the gradient of the field, represented as $\nabla^2 f$. For example, if f is a scalar field, then $\nabla^2 f(x,y,z)$ denotes the value of $\nabla^2 f$ at the point (x,y,z). It provides a measure

of the difference between the average value of the field in the immediate neighborhood of the point and the precise value of the field at the point[100].

The properties of a molecular charge distribution can be summarized in terms of the critical points where the gradient of the vector field, $\nabla\rho(\mathbf{r})$, or first derivative, vanishes. Here, the first derivative is given by

$$\nabla\rho = (\partial\rho/\partial x)\mathbf{i} + (\partial\rho/\partial y)\mathbf{j} + (\partial\rho/\partial z)\mathbf{k}$$

i, **j**, and **k** are unit vectors (vectors with a magnitude of 1 unit) pointing in the positive X, Y, and Z directions, respectively. The critical points are either a maximum, a minimum, or a saddle point. To determine the nature of the critical point, the matrix of second derivatives is used. The second derivative along a chosen axis is negative when the critical point is a maximum and positive when the critical point is a minimum, in the corresponding direction.

There are nine second derivatives of the form $\partial^2\rho/\partial x\partial y$, in general, for an arbitrary choice of coordinate axes. The ordered 3x3 array of these second derivatives is called the Hessian matrix of the charge density, or the Hessian of ρ[101]. Because the Hessian of ρ is a real, symmetric matrix, it can be diagonalized. This is an eigenvalue problem solved by finding a rotation of the coordinate axes to a new set such that all of the mixed second derivatives of ρ, the off-

diagonal elements, vanish. This new set of coordinate axes is called the principal axes of curvature because the magnitude of the three second derivatives of ρ which are calculated with respect to those axes are extremized[82]. If the critical point is at the origin of the principal axes, then these axes will correspond to symmetry axes. In the case of symmetrically equivalent axes, the corresponding curvatures are equal and any linear combination of the degenerate set of axes will serve as a principal axis of curvature. The sum of the diagonal elements of the Hessian matrix, called the trace, is invariant to a rotation of the coordinate system[100]. Therefore, the value of the quantity $\nabla^2\rho$, the Laplacian of ρ,

$$\nabla^2\rho = \nabla\cdot\nabla\rho = \partial^2\rho/\partial x^2 + \partial^2\rho/\partial y^2 + \partial^2\rho/\partial z^2$$

is invariant to the choice of coordinate axes. The principal axes and the corresponding curvatures at a critical point in ρ are obtained as eigenvectors and corresponding eigenvalues in the diagonalization of the Hessian of ρ[82,97].

All of the eigenvalues of the Hessian matrix of ρ at a critical point are real, but they may equal zero, which would correspond to an inflection point. The rank of the critical point, denoted by ω, is equal to the non-zero eigenvalues or non-zero curvatures of ρ at the critical point. The signature or index, denoted by σ, is the

algebraic sum of the signs of the curvature of ρ at the critical point[82,101]. These critical points are classified by the curvatures of $\rho(\mathbf{r})$, or the three eigenvalues λ_i (i=1, 2, 3) of the Hessian matrix

$$H_{ij} = \partial^2\rho(\mathbf{r})/\partial x_i \partial x_j$$

In molecules and crystals there are four types of these extremes. Using their rank and signature, these four extremes are the maxima (3,-3), minima (3,+3), and two types of saddle points, (3,+1) and (3,-1). The maxima, or (3,-3) points occur generally at the nuclear position. This means the nucleus is a three-dimensional point attractor in the vector field spanned by $\nabla\rho(\mathbf{r})$[100]. A (3,-1) saddle point, called a bond critical point, is found between every pair of bonded atoms and is a local maximum in the two dimensional surface partitioning the atoms as well as a local minimum along a path linking the nuclei. The set of surfaces formed by all (3,-1) critical points partitions the molecule, or crystal, into a set of chemically identifiable regions called atomic basins[82].

The other two critical points of rank three define the remaining elements of molecular structure, rings and cages. If the bond paths are linked and form a ring of bonded atoms then a (3,+1) or ring critical point is found in the interior of the ring. If the interior of a molecule is

enclosed with ring surfaces, then a (3,+3) or cage critical point is found in the interior of the resulting cage[78].

3.3 The Laplacian of the Charge Density and the VSEPR Model of Molecular Geometry.

The topology of the Laplacian of the charge distribution provides a physical basis to the electron pairs of Lewis and to the associated models of geometry, such as the valence-shell electron pair repulsion (VSEPR) model[78]. The VSEPR model is a natural extension of Lewis' localized electron pair model[77].

As taught to all chemistry students, Lewis symbols consist of the symbol for the element and one dot for each valence electron present, as in Figure 3-1. When two dots are written adjacent to one another, they represent a pair of electrons sharing the same localized domain in physical space, seen in Figure 3-1 (c) and (d).

Figure 3-1. The Lewis symbols for sodium (a), carbon (b), phosphorus (c), and oxygen (d).

Note that although the ground state electron configuration of carbon is described within the orbital model as $1s^2 2s^2 2p^2$, with 2 paired electrons in the 2s orbital and 2 unpaired electrons in the 2p orbital, this state would

correspond to a Lewis structure of ·C·. The Lewis dot diagrams, however, are a representation of an electronic state (without regard to orbitals, which were proposed after Lewis' device) that is "prepared" to form four covalent bonds. The valence bond model utilizes Lewis symbols to show the distribution of electrons in covalently bonded molecules and polyatomic ions in a so-called Lewis structure for the molecule. The Lewis structure for Cl_2 is shown in Figure 3-2. It can be seen that each Cl atom has three pairs of electrons that are not used in bonding (lone pairs or unshared pairs) and one shared pair of electrons, those between the atoms. A dash may be used to represent a shared pair.

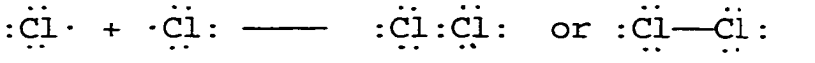

Figure 3-2. The Lewis structure for the Cl_2 molecule.

The VSEPR model allows the prediction of approximate bond angles around a central atom in a molecule from the number of bonds and unshared electron pairs in its Lewis structure. The fundamental basis for this model is the Pauli exclusion principle. The VSEPR model has two fundamental assumptions: (1) the valence shell electrons of a central atom in a molecule form domains either as bonding pairs of electrons which are located primarily between bonded atoms, or by unshared pairs occupying regions of space shaped

similar to that occupied by the bonding pairs, and (2) the electrostatic repulsion of these electrons is a minimum when the domains are as far from each other as possible[1]. This means the geometrical arrangement of the ligands about the central atom maximizes the separation between the pairs, assuming the pairs to be on the surface of a sphere centered on the nucleus of the central atom. Generally, not all pairs of electrons are equivalent, so three additional postulates are required to determine the relative size of the electron pair domains: (1) nonbonding pairs have larger domains than bonding pairs; (2) bonding pair domains decrease in size near the central atom with increasing electronegativity of the ligand, and increase in size with increasing electronegativity of the central atom relative to the ligand; (3) double and triple bond domains are larger than single bond electron domains[77].

The Laplacian of a scalar function, such as the charge density $\rho(r)$, determines where the function is locally concentrated, where $\nabla^2\rho(r) < 0$, and where it is locally depleted, where $\nabla^2\rho(r) > 0$. There is an electronic charge concentration in those regions of space where the Laplacian of the charge density has a negative value. The expression "local charge concentrations" and "local charge depletions" refer to maxima and minima in the function $-\nabla^2\rho(r)$. These extrema are to be distinguished from local maxima and minima in the charge density itself[78].

The Laplacian of the electron charge density, $\nabla^2\rho$, indicates the presence of localized concentrations of electron charge in the valence shell of an atom or molecule. These local charge concentrations duplicate the number, location, and size of the spatially localized electron pairs of the VSEPR model[76,102]. Although the electrons are not highly localized into pairs as stated in the VSEPR model, there are an equal number of valence-shell charge concentrations (VSCC's) that exhibit all the properties attributed to the VSEPR model electron domains. The Lewis and VSEPR models overestimate the extent of localization of electron pairs in a molecule, but there is a partial localization of electrons into pairs that produce small local charge concentrations that have the exact properties postulated for the electron pairs by the VSEPR model[85].

The Laplacian of the charge distribution also recovers the electronic shell model of an atom by producing a corresponding number of pairs of shells of charge concentration and charge depletion[92,93,103].

Generally, a Lewis acid-base reaction corresponds to aligning a local charge concentration of the valence shell on the base (a maximum on $-\nabla^2\rho$) with a local charge depletion on the acid (a minimum on $-\nabla^2\rho$). This phenomenon is observed in many different kinds of interactions[82], such as the formation of hydrogen bonds[104], the adsorption of

molecules on a surface[74,75,105,106], and the alignment of chlorine molecules in a solid[95].

3.4 Application of the Electron Density ρ and the Laplacian of the Electron Density $-\nabla^2\rho$ to the CO Molecule.

The electron density and the Laplacian of the electron density were analyzed using the AIM98PC series of programs[107] using the wavefunction files generated by GAUSSIAN 92. A sample of the wavefunction file for the CO molecule is shown in Appendix B. The wavefunction file shows the assignments for the CO molecule. These numbers refer to the gaussian functions on pages 23 and 24. The gaussians numbered 5-10 are d-type, and so aren't seen in the assignments in this wavefunction file. The exponents are the α's in the gaussian functions. The wavefunction file also lists the gaussian expansion coefficients of the seven orbitals of the molecule and takes about three and a half pages to list the data. By comparison, the wavefunction file for the 3x3x1 MgO cluster with nothing under the layer and no CO, the simplest cluster considered in this paper, has 45 orbitals and runs for eighty-one pages! The wavefunction of these systems is a much lengthier determinantal expansion using these orbitals. Obviously the pictorial representations shown by the contour and relief plots of ρ and $-\nabla^2\rho$ are easier to interpret.

Figure 3-3 shows the relief diagram (a) and the contour diagram (b) of the charge density for the CO molecule. These

plots, and all subsequent relief and contour plots were derived from a 3-21G* RHF calculation. RHF (restricted Hartree-Fock) means the α orbitals = ß orbitals in spatial form. Examining the figure, there is no obvious localization of charge which would correspond to bonding pairs or lone pairs. A bond is only apparent as the ridge of maximum density between the peaks of charge surrounding each nucleus. This ridge is called a bond path[79]. Figures 3-4 and 3-5 show the contour and relief plots of $-\nabla^2\rho$ for the CO molecule, respectively. The local charge concentration in the valence shell between the atoms corresponds to the three bonding pairs of electrons between them. There are also charge concentrations at either end of the molecule corresponding to the nonbonding pairs for oxygen and C. Comparing the diagrams of the Laplacian of the electron density with the possible Lewis structures for the CO molecule, it is seen that there is only one structure suggested by the topology of $-\nabla^2\rho$. Figure 3-6 shows the possible Lewis structures and formal charges for the CO molecule. It is obvious that the structure shown in (c) matches the diagrams in Figures 3-4 and 3-5, where the nonbonded pairs are at the ends of the molecule, with the charge concentration between the atoms. In structures (a) or (b) there would be more than one unbonded pair on the oxygen atom. These same interpretive methods will be applied to cluster models of the MgO lattice, and its reactions

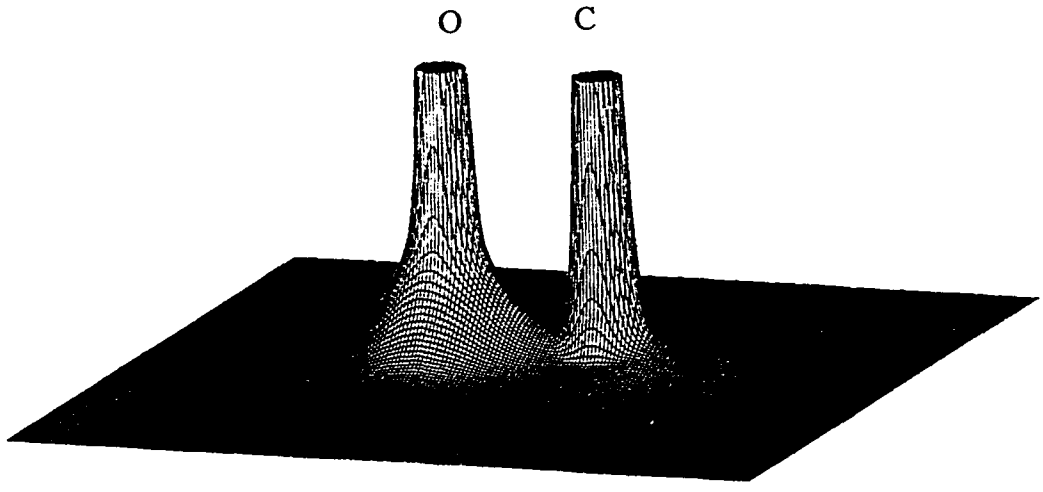

(a)

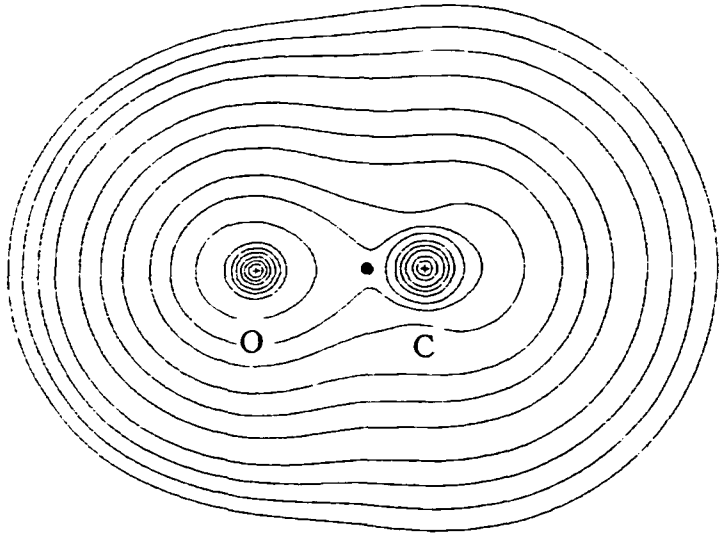

(b)

Figure 3-3. Relief plot (a) and contour plot (b) of the electron density for the CO molecule. The localization of charge corresponding to bonding or nonbonding pairs is not seen in these diagrams.

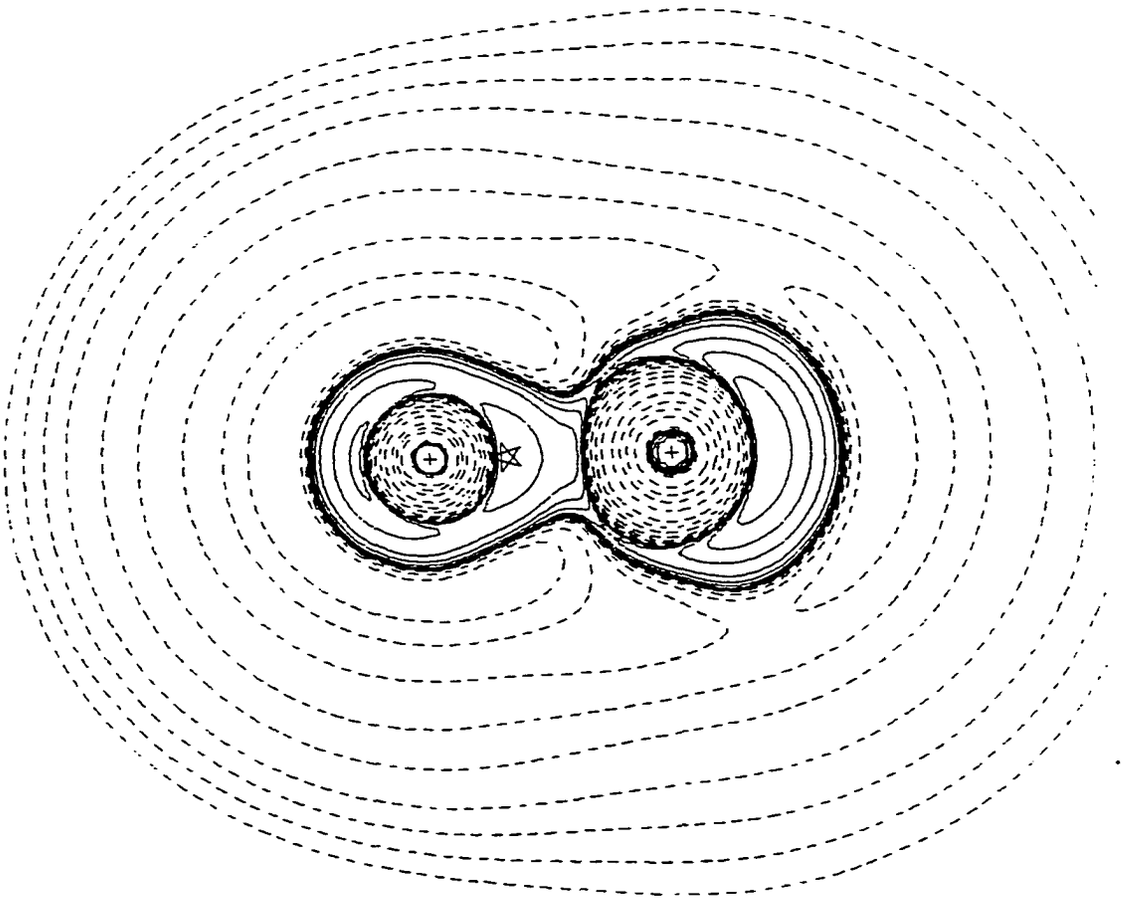

Figure 3-4. Contour plot of the Laplacian of the electron density for the CO molecule, with O on the left, C on the right. The charge concentrations are seen betweeen the atoms (bonding pairs) and at the ends of the atoms (nonbonding pairs).

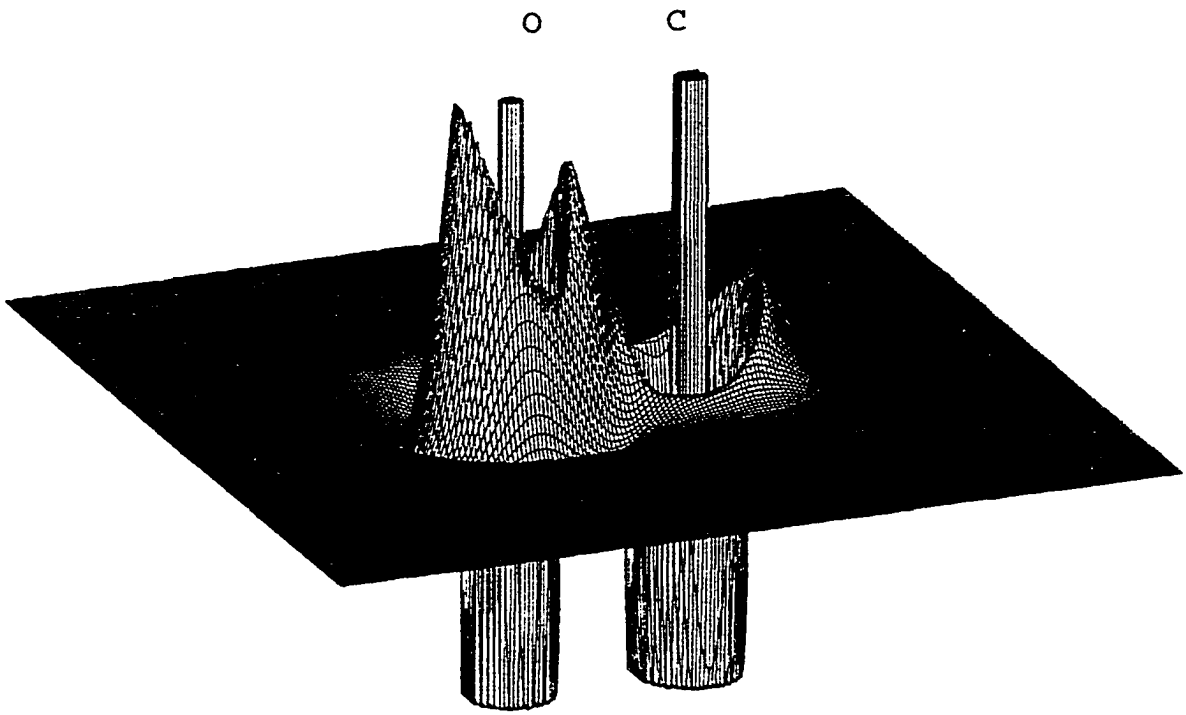

Figure 3-5. Relief plots of the Laplacian of the electron density for the CO molecule from two perspectives. In the relief plot the VSCC is more fully displayed behind and between the atoms. The steep slope and charge depletion seen on the oxygen atom, and the gentle slope on the carbon atom are not seen in the contour plot in Figure 3-4.

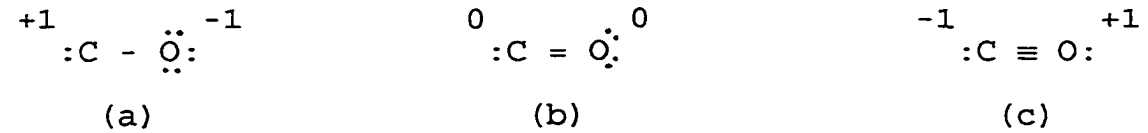

(a) (b) (c)

Figure 3-6. The possible Lewis structures and formal charges for the CO molecule.

with CO. This will represent the first time such techniques have been applied to clusters of this type. It is hoped that new insight into the chemistry of these systems will be gained.

3.5 Interpretation of the Bonding and Reactivity of CO Adsorption on the Model of the MgO Surface using $-\nabla^2\rho$

Contour plots of $-\nabla^2\rho$ will be used in the analysis of the changes in the electron structure caused by different conditions imposed on the 3x3x1 MgO cluster, such as central atom (magnesium or oxygen), charge on the cluster (0, or ±2), and presence of an atom under the central atom. Then the effect of the CO molecule on the electron density of the surface will be investigated using these interpretive tools. Finally, the presence of a sulfur atom under the layer for the cases of no CO, CO with carbon down, and CO with oxygen down will be included. All of the contour plots were generated using wavefunction data from GAUSSIAN 92 and 3-21G* RHF calculations, by means of the AIM98PC series of programs. All cluster models are 3x3x1 with the above conditions imposed on them.

3.5.1 Cluster with magnesium in the center, no CO molecule.

Figures 3-7 and 3-8 show the MgO surface with magnesium in the center, nothing under the layer and 0 charge on the cluster. Figure 3-7 is in the plane of the surface, Figure

3-8 is perpendicular to the surface through an O-Mg-O cross-section. Figures 3-9 and 3-10 show the same orientations but here there is a +2 charge on the cluster. There are several interesting features between these series of contour plots. First is their similarity. Although there are two additional electrons in the surface represented in Figures 3-7 and 3-8, there is virtually no difference between these plots and those in 3-9 and 3-10. This is due to the delocalization of the two additional electrons. The wavefunction for the +2 charge cluster can be expanded from 45 molecular orbitals, and for the 0 charge cluster there are 46 such MO's. The occupation numbers for all of the orbitals is 2 which means the two additional electrons are a small fraction of the total population, and it appears in this case that they are evenly distributed throughout the cluster, since no topological changes are apparent. Another feature seen in Figures 3-7 and 3-9 is the quadrupolar polarization of the surface oxygen atoms. This polarization is like a doughnut, with the "dents" in the oxygen's valence shell oriented toward the corner Mg^{+2} ions, as seen in Figures 3-7 and 3-9. Thus, the bonding and the nonbonding charge concentrations on the oxygen atoms are easily distinguished in the surface plot, but not in the plot perpendicular to the surface.

Figures 3-11 and 3-12 have the same surface with an oxygen atom under the central magnesium with 0 charge on the cluster. Figure 3-11 is in the plane of the surface, 3-12 is

perpendicular to the surface through the central O-Mg-O and showing the oxygen atom under the surface. The most obvious difference is a change in the relative shape of the contours for the bonding and the nonbonding charge concentrations in the surface oxygen atoms compared with those in Figures 3-7 and 3-9. There is an increase in the charge concentration in the bonding region and a decrease for the nonbonding region. This is also seen in Figure 3-12 where the electron density of the surface oxygens is pulled towards the oxygen atom under the layer, towards the center and downwards, while the sublayer oxygen charge concentration is shifted away from the surface, straight down. There seems to be little effect on the electron density of the magnesium atoms in the surface due to the presence of the oxygen under the surface. This is to be expected since the Mg^{+2} ion consists mostly of core electrons. There is also little effect on the plot of the surface oxygen atoms except for the above mentioned change in the bonding and nonbonding charge concentrations.

Note in Figure 3-8 that this is the expected form of $\nabla^2\rho$, a collection of roughly spherical ions, with ± 2 charges on them.

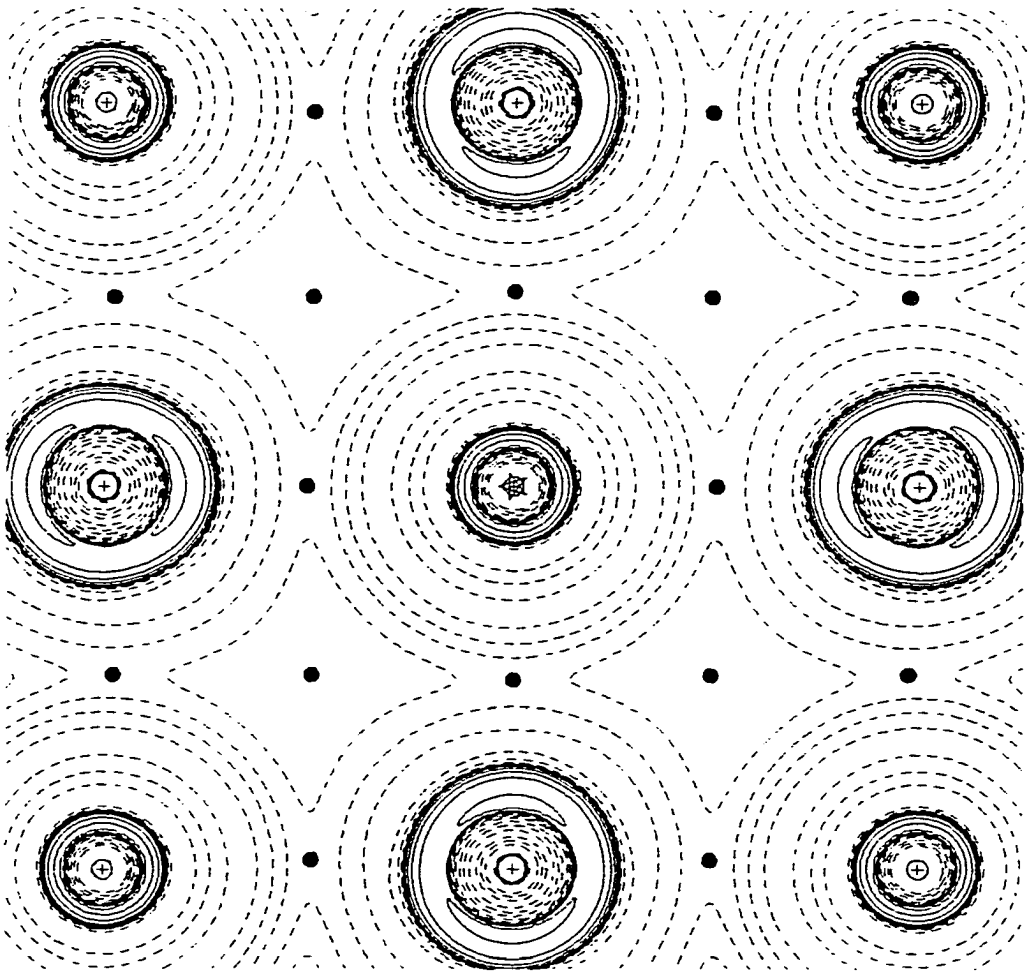

Figure 3-7. MgO surface with Mg in the center, nothing under the surface, no CO, 0 charge on the cluster. The plot is in the surface plane. Solid contours denote negative values in $\nabla^2\rho$ which are concentrations of electronic charge, dashed contours represent regions of charge depletion. The form of the distribution is important, rather than the values of the contours.

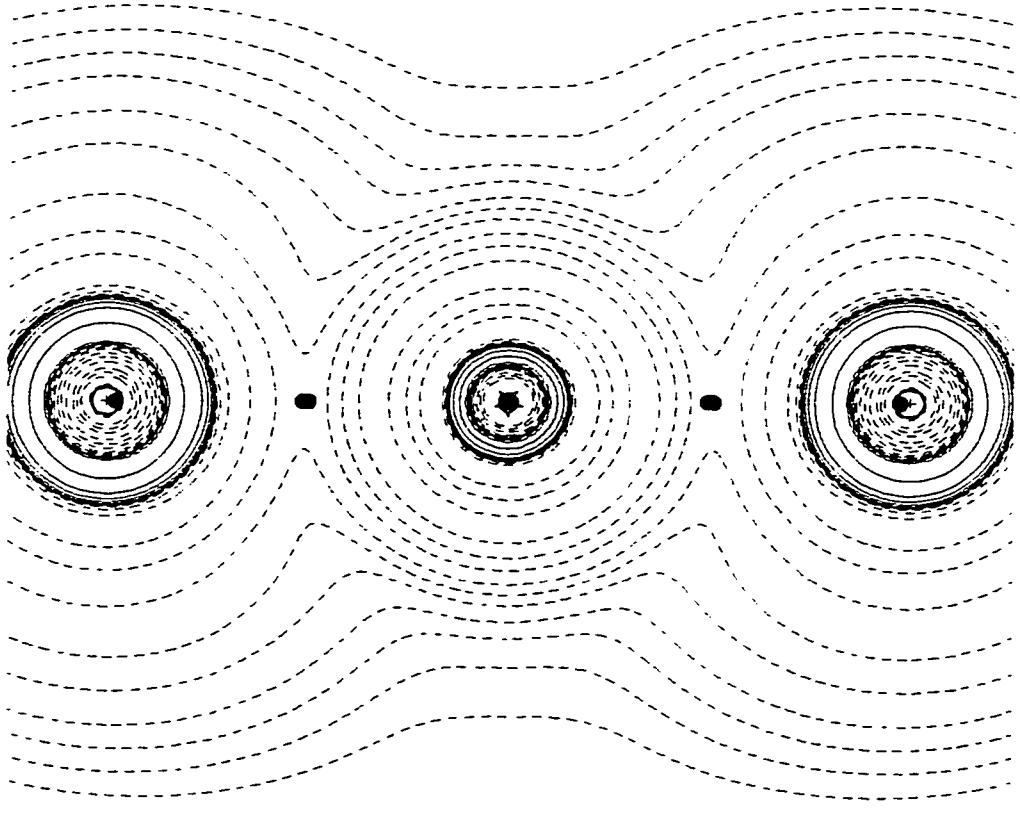

Figure 3-8. MgO surface with Mg in the center, nothing under the surface, no CO, 0 charge on the cluster. The plot is perpendicular to the surface plane.

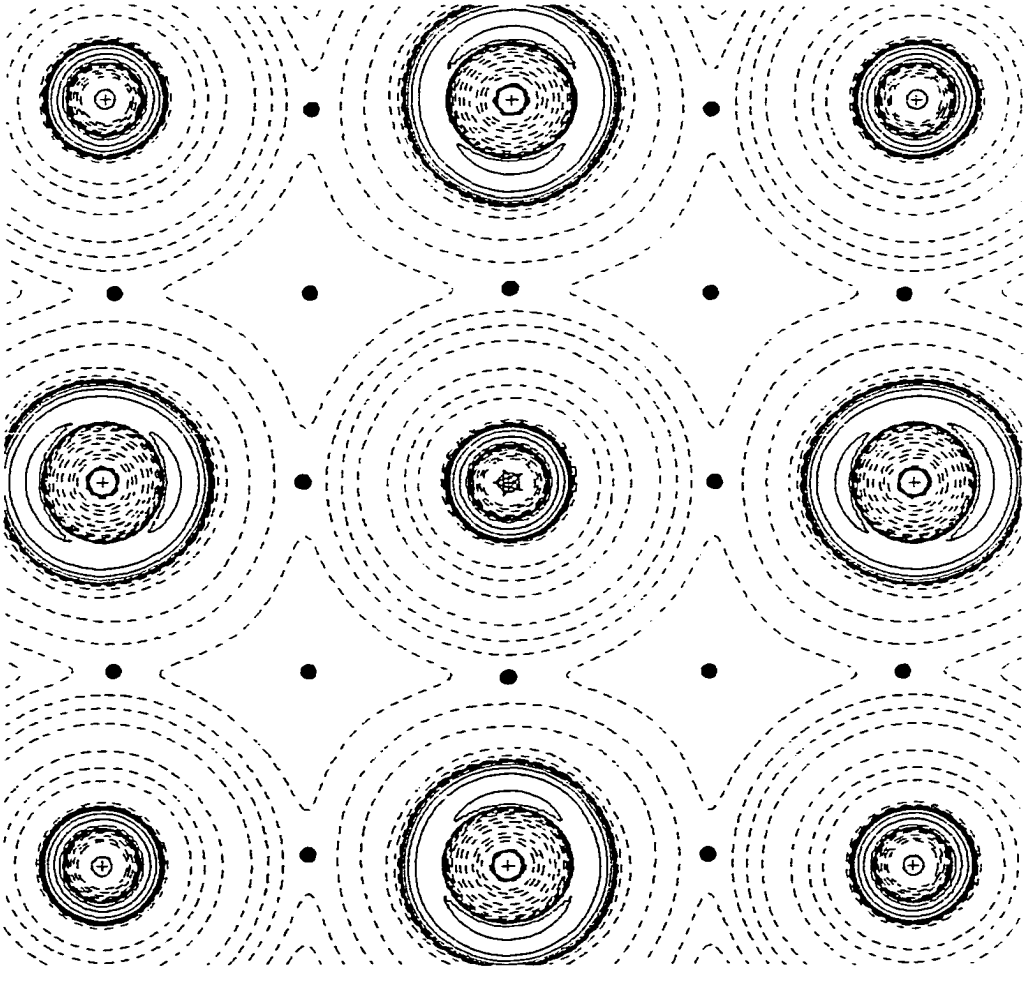

Figure 3-9. MgO surface with Mg in the center, nothing under the surface, no CO, +2 charge on the cluster. The plot is in the surface plane.

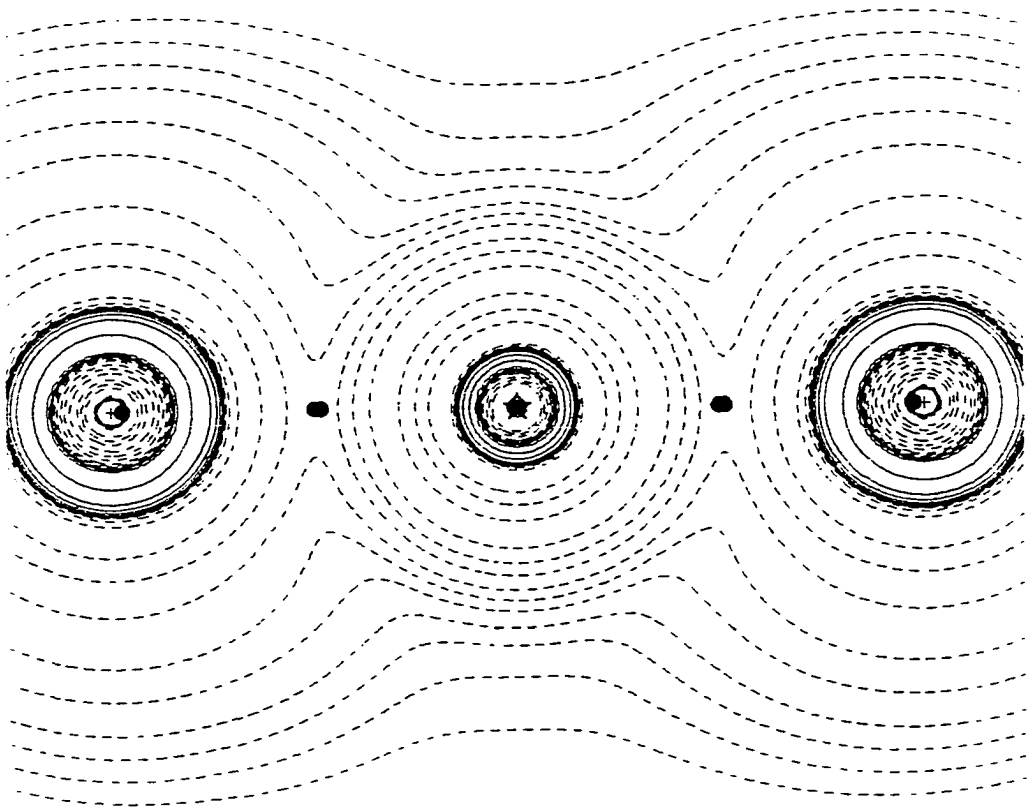

Figure 3-10. MgO surface with Mg in the center, nothing under the surface, no CO, +2 charge on the cluster. The plot is perpendicular to the surface plane.

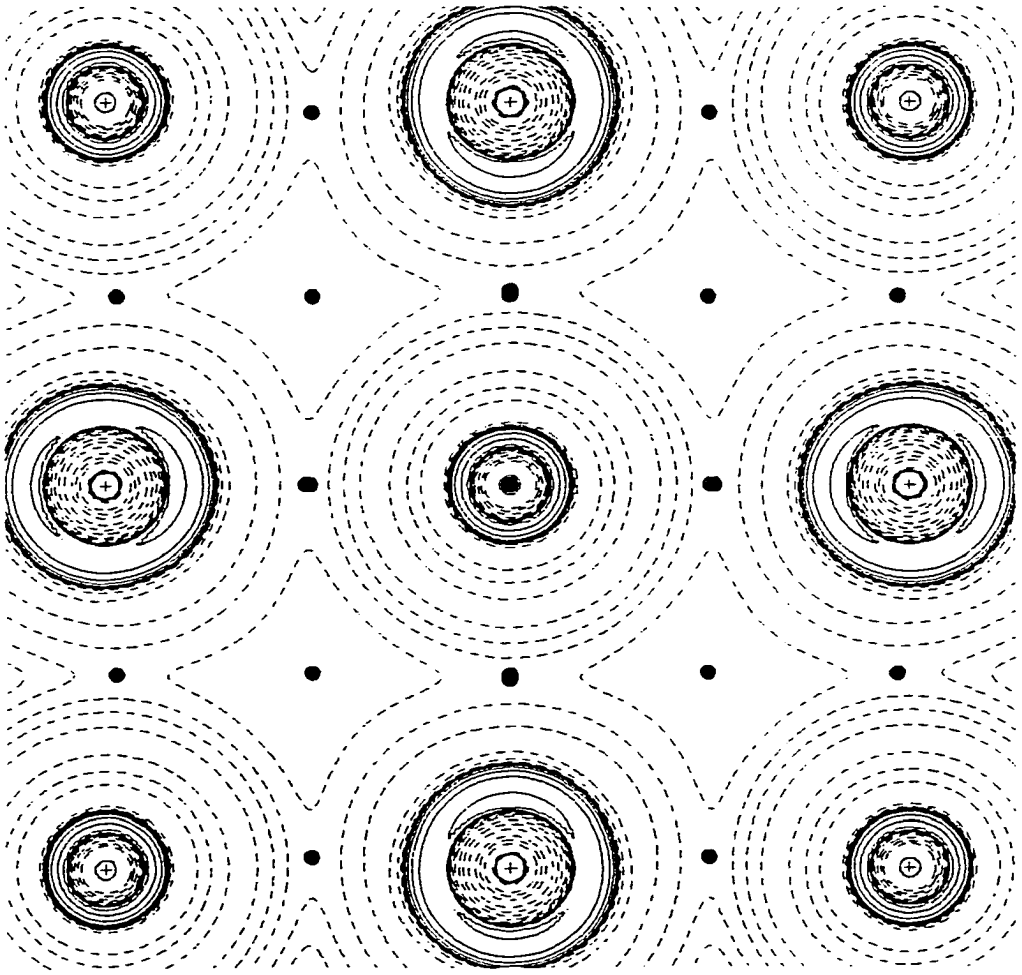

Figure 3-11. MgO surface with Mg in the center, oxygen under the surface, no CO, 0 charge on the cluster. The plot is in the surface plane.

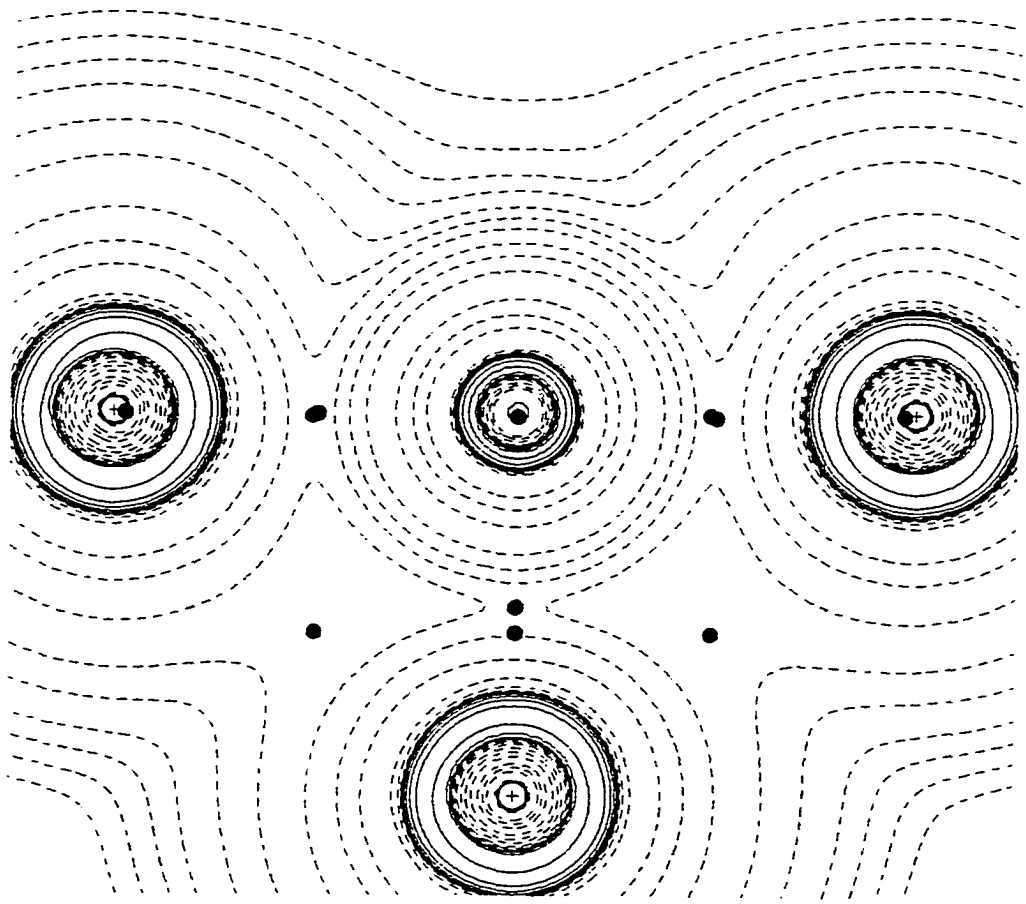

Figure 3-12. MgO surface with Mg in the center, oxygen under the surface, no CO, 0 charge on the cluster. The plot is perpendicular to the surface plane.

3.5.2 Cluster with magnesium in the center, CO adsorbed with Carbon down.

The next series of contour plots and their associated RHF calculations places a CO molecule above the surface with the carbon end towards the central magnesium atom. The same three cluster conditions are present as the previous series; namely, 0 charge on the cluster, +2 charge on the cluster, and 0 charge on the cluster with an oxygen atom under the layer. The figures are as follows:

Figure 3-13; 0 charge on the cluster, surface plane.

Figure 3-14; 0 charge perpendicular to the surface.

Figure 3-15; +2 charge on the cluster, surface plane.

Figure 3-16; +2 charge perpendicular to the surface.

Figure 3-17; 0 charge, oxygen under the layer, surface plane.

Figure 3-18; 0 charge, oxygen under the layer, perpendicular to the surface, showing the Mg-C-O atoms.

Figure 3-19; 0 charge, oxygen under the layer, perpendicular to the surface, showing the O-Mg-C atoms.

Comparing Figures 3-13 with 3-15, and 3-14 with 3-16, it can be seen there is little difference in these contour plots. There is also little difference between these plots and those with no CO molecule on the surface, Figures 3-7 and 3-9. This is because the adsorption of the CO molecule is due mainly to electrostatic interaction and other weak van der Waals' forces and not a transfer of charge, which is

estimated by others to be only 0.1e[20,22,31,45]. This small amount of charge transfer results in electron density donated to, rather than from, the surface[20].

Figures 3-17, 3-18, and 3-19 are for the MgO surface with an oxygen atom below the surface, and the CO molecule oriented with carbon down. Comparing 3-17 and 3-18 with the plots for the two cases with no oxygen, it can be seen that there is little difference in the surface plot and the plot showing the CO molecule. The reason is that there is little charge transfer in the CO adsorption, as stated previously. The difference appears in Figure 3-19 compared with Figure 3-12. The oxygen below the MgO surface has a valence shell concentration that is a torus. The hole in the torus corresponds to an empty p(z) orbital, caused by removing two electrons from this oxygen, which is the least coordinated in the cluster. The surface oxygens have three nearby Mg^{+2} ions, so they bind the electrons more strongly. This effect is not seen in the cluster with no oxygen below the surface because all of the oxide ions there are in the surface, and hence have the three Mg^{+2} ions around them. The effect of having a low-coordinated oxygen ion below the layer provides the two electrons which are distributed to the surface. This effect is not seen in Figure 3-12. The presence of the CO molecule with the carbon end towards the surface must be involved with this reorganization of charge concentrations. This may be the cause of the 51.8 kcal/mole binding energy

for this case shown in Table 2-8. This is not seen when the oxygen end of the CO molecule is towards the surface. Further calculations are required to determine if this is a general effect, or an artifact of some kind. This is a topic worthy of future study.

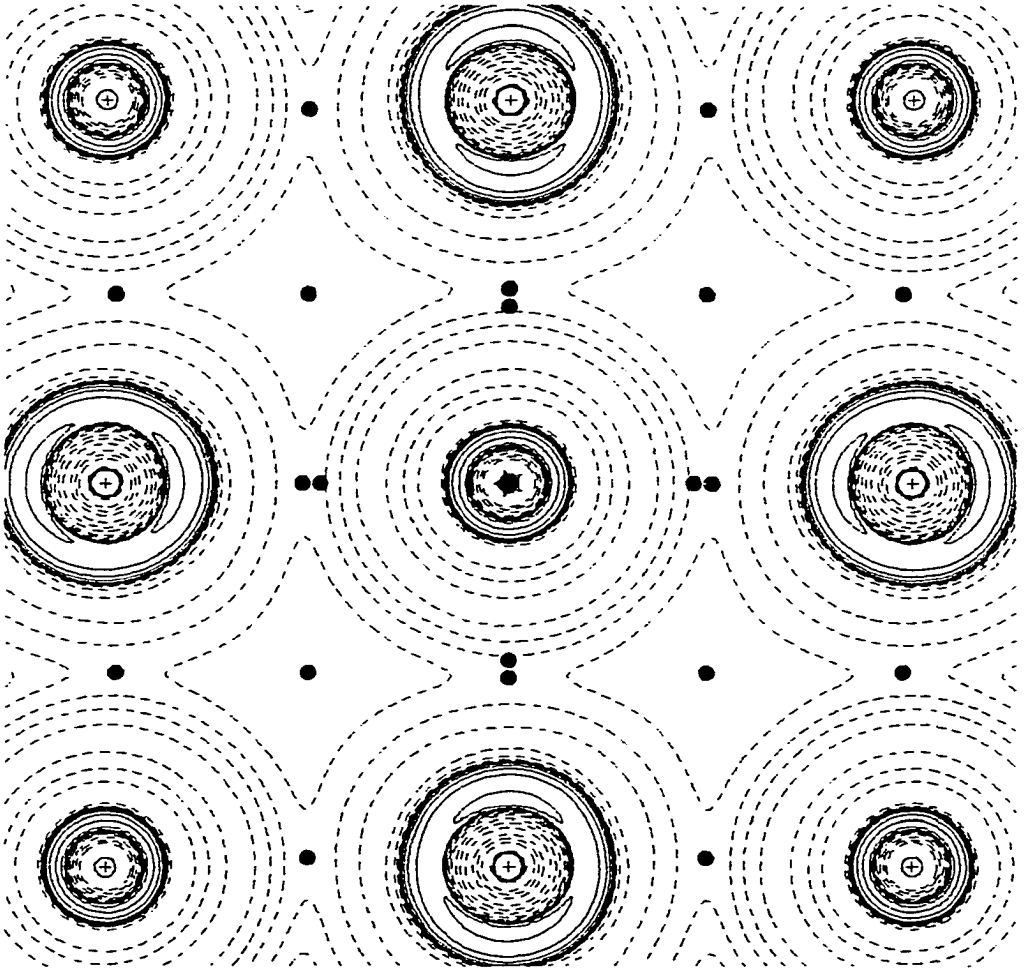

Figure 3-13. MgO surface with Mg in the center, nothing under the layer, 0 charge on the cluster, CO with C down. The plot is in the surface plane.

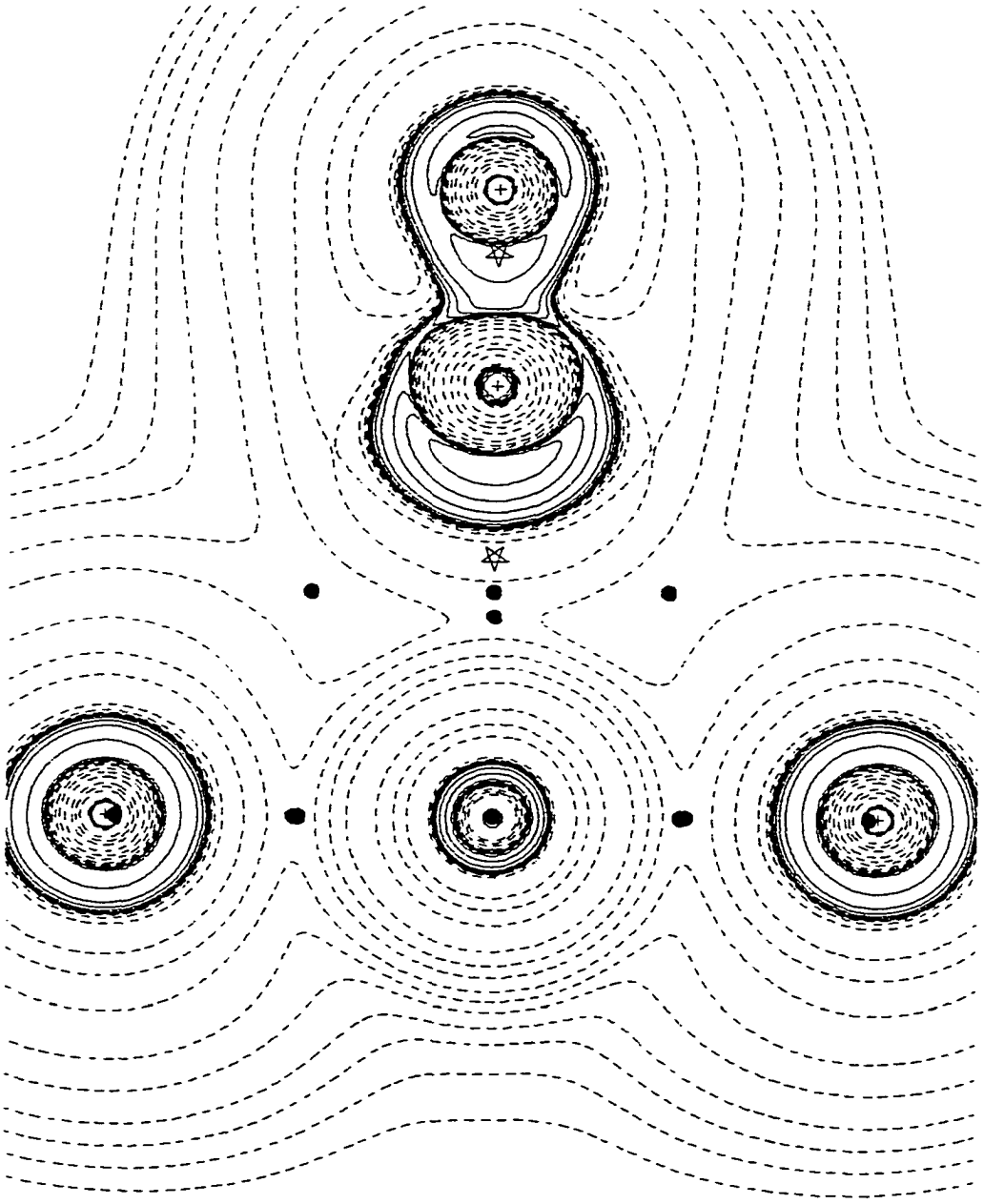

Figure 3-14. MgO surface with Mg in the center, nothing under the layer, 0 charge on the cluster, CO with C down. The plot is perpendicular to the surface plane.

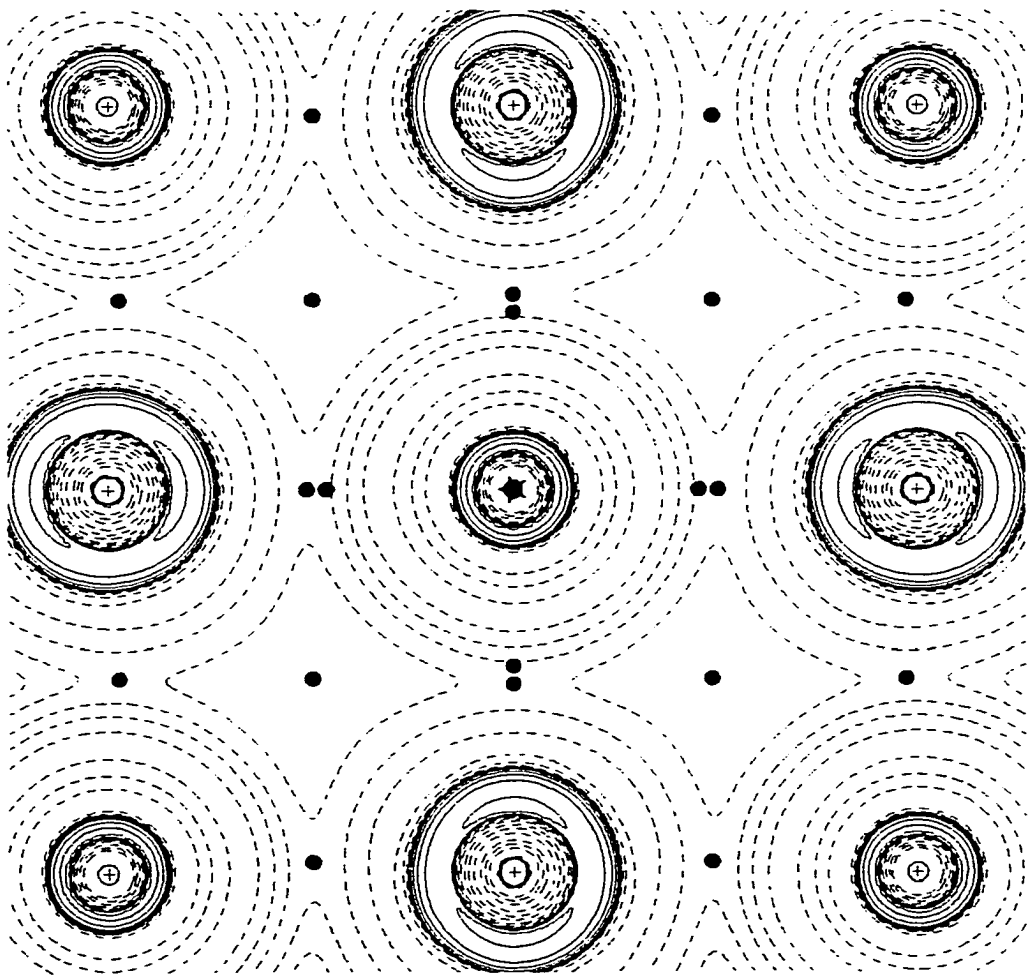

Figure 3-15. MgO surface with Mg in the center, nothing under the layer, +2 charge on the cluster, CO with C down. The plot is in the surface plane.

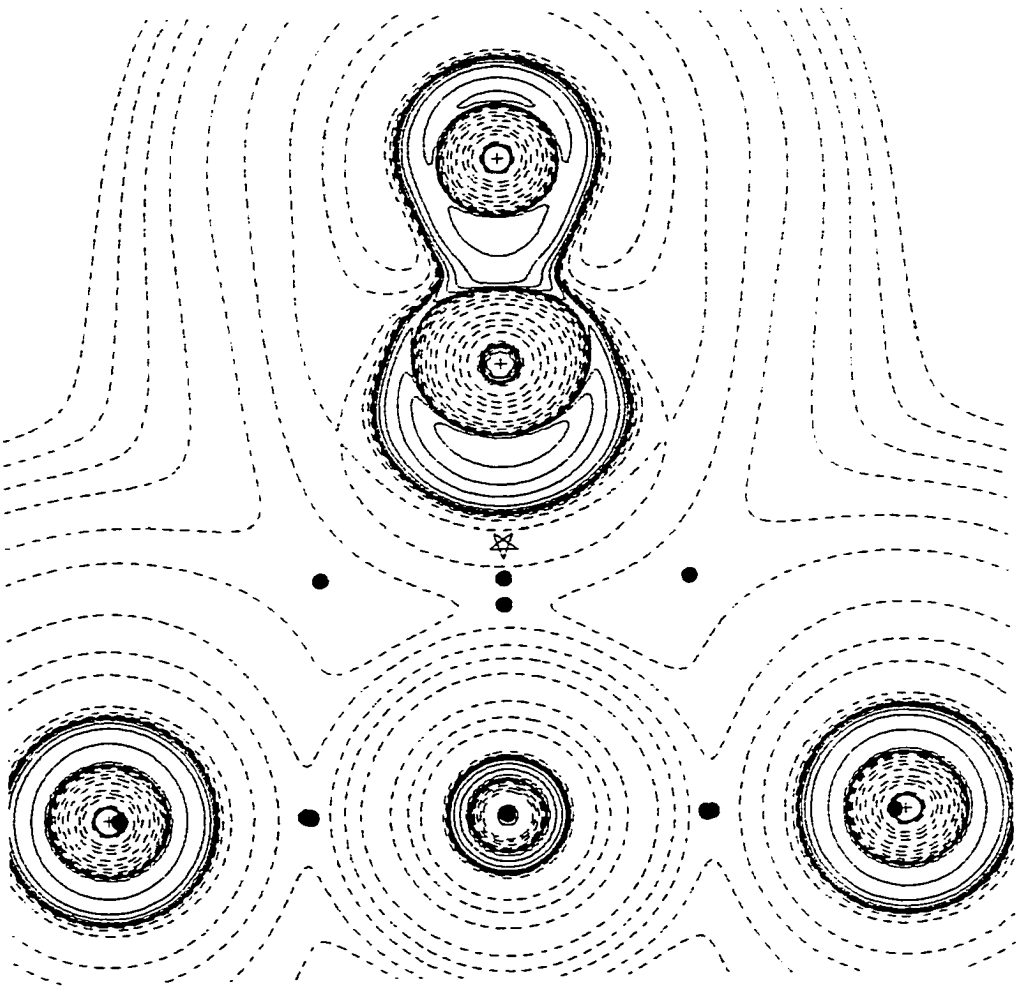

Figure 3-16. MgO surface with Mg in the center, nothing under the layer, +2 charge on the cluster, CO with C down. The plot is perpendicular to the surface plane.

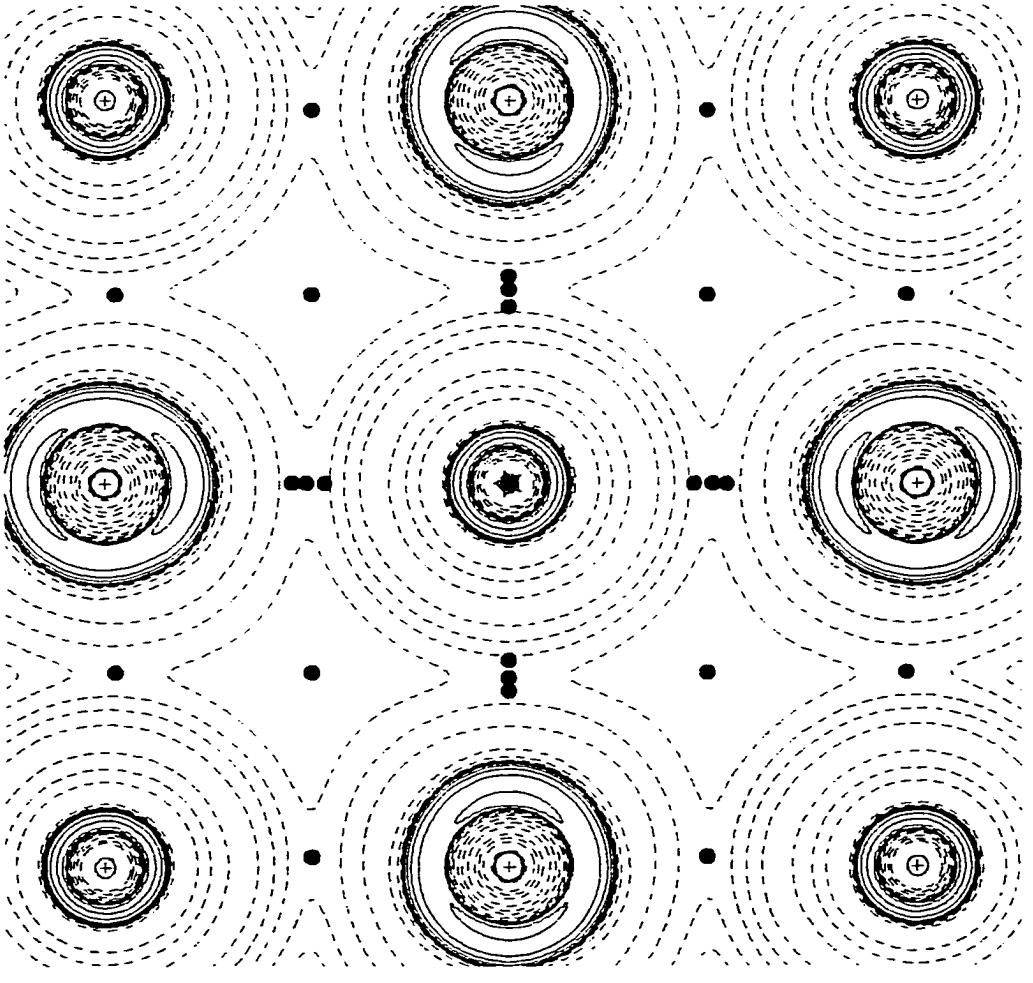

Figure 3-17. MgO surface with Mg in the center, O under the layer, 0 charge on the cluster, CO with C down. The plot is in the surface plane.

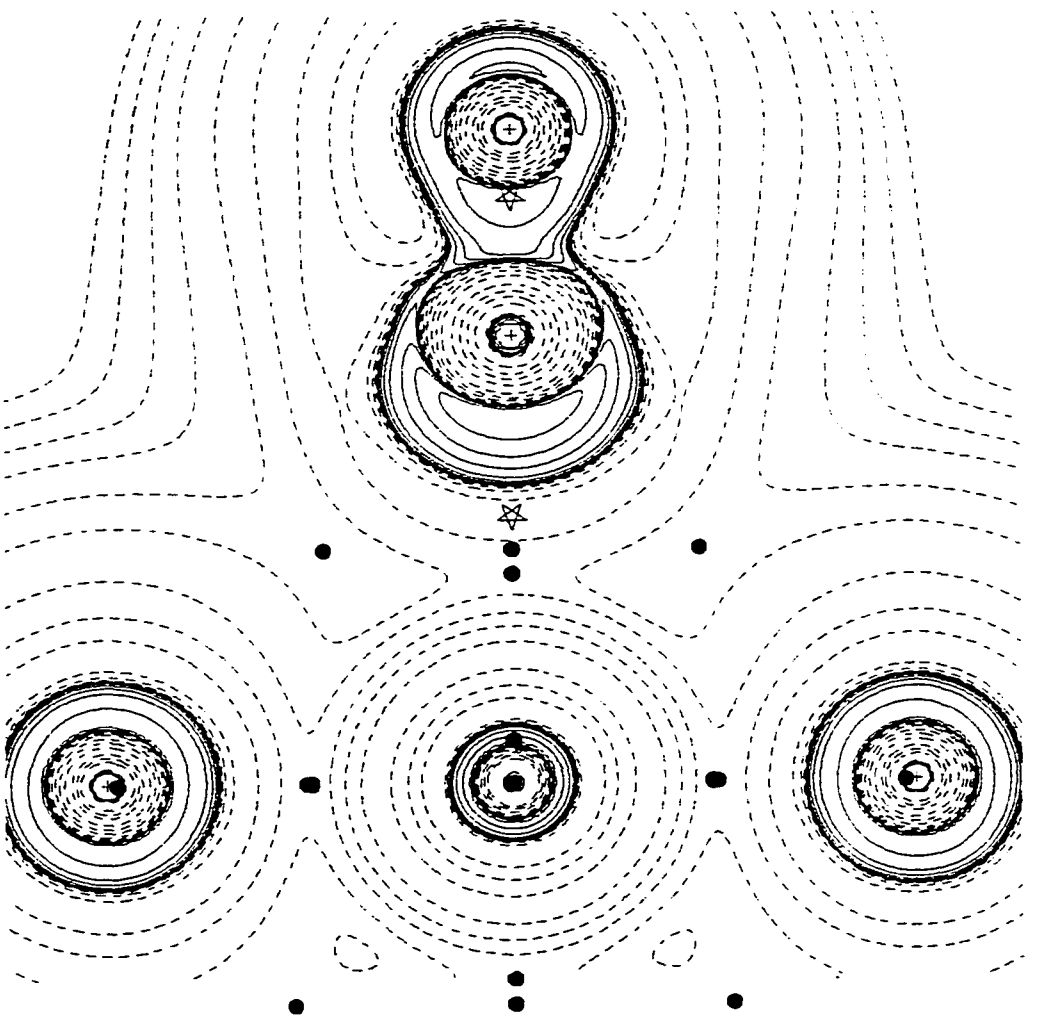

Figure 3-18. MgO surface with Mg in the center, O under the layer, 0 charge on the cluster, CO with C down, showing the Mg-C-O atoms. The plot is perpendicular to the surface plane.

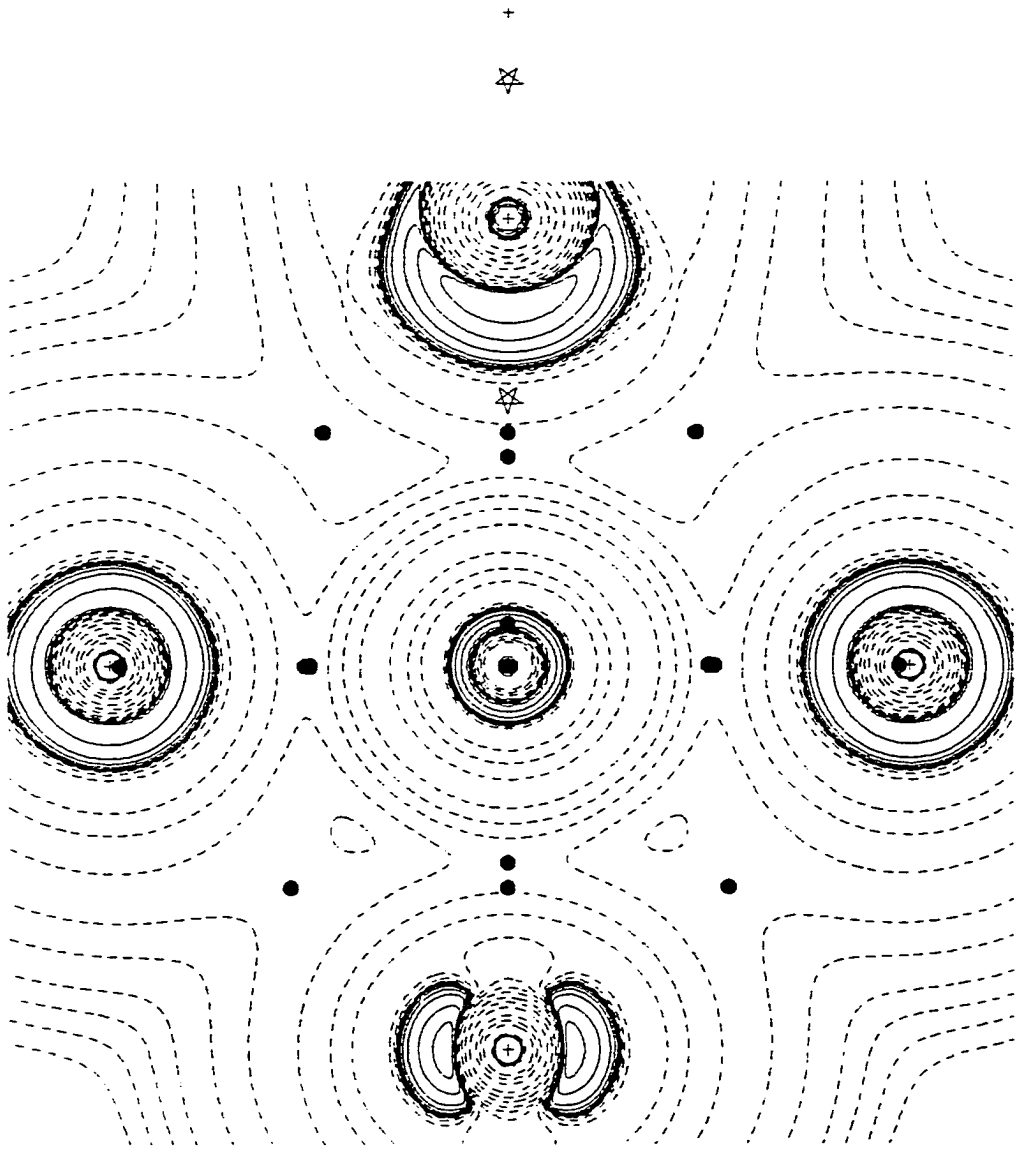

Figure 3-19. MgO surface with Mg in the center, O under the layer, 0 charge on the cluster, CO with C down, showing the O-Mg-C atoms. The plot is perpendicular to the surface plane.

3.5.3 Cluster with magnesium in the center, CO adsorbed with oxygen down.

For the cluster condition where the CO molecule is oriented with the oxygen towards the surface, oxygen down, the same cluster conditions are studied; 0 charge on the cluster, +2 charge on the cluster, and 0 charge on the cluster with oxygen under the central Mg. The contour plots for the various cluster conditions are as follows:

Figure 3-20; 0 charge on the cluster, surface plane.

Figure 3-21; 0 charge perpendicular to the surface.

Figure 3-22; +2 charge on the cluster, surface plane.

Figure 3-23; +2 charge perpendicular to the surface.

Figure 3-24; 0 charge, oxygen under the layer, surface plane.

Figure 3-25; 0 charge, oxygen under the layer, perpendicular to the surface.

The results here are similar to those for the C-down condition. This is because the O-down adsorption is also electrostatic in nature, having even less charge transfer between the CO molecule and the surface[44] (since the oxygen end is less basic than the carbon end). The 0 and +2 contour plots for the surface, Figures 3-20 and 3-22, and the contour plots perpendicular to the surface, Figures 3-21 and 3-23, are almost identical to one another, and even moreso than the corresponding set of plots for the C-down orientation. This is to be expected since the CO orientation

has little effect on the surface due to the electrostatic nature of the adsorption. This can be seen in the comparison of these figures with those in which there is no CO molecule present. Comparing Figure 3-24 with 3-20 or 3-22 the same change in the bonding and nonbonding regions appear as appeared in the C-down orientation. There is one marked difference between the oxygen down and carbon down orientations. Compare Figure 3-25 with Figure 3-19. For the oxygen down orientation the oxygen atom beneath the layer dosen't show the torus shaped valence shell charge concentration. Here, the VSCC appears similar to the condition with oxygen under the layer with no CO present, Figure 3-12. Although there is almost no charge transfer between the CO molecule and the surface for any orientation of the CO molecule, the presence of the low-coordinated oxygen under the layer with the carbon end of the CO molecule towards the surface seems to have caused a shift in the charge distribution of the cluster, leaving a hole in the VSCC of the sub-surface oxygen. As stated before, confirmation of this effect will be a topic of further investigation.

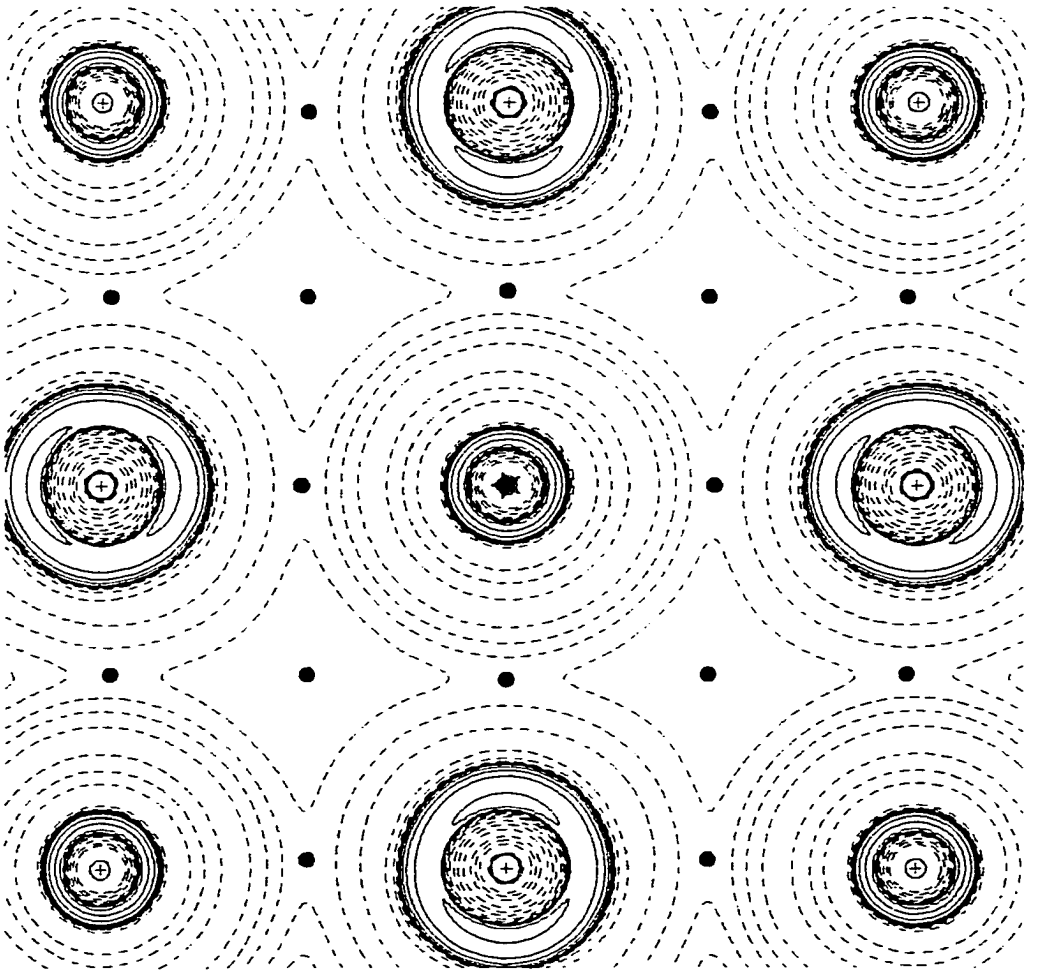

Figure 3-20. MgO surface with Mg in the center, nothing under the layer, 0 charge on the cluster, CO with O down. The plot is in the plane of the surface.

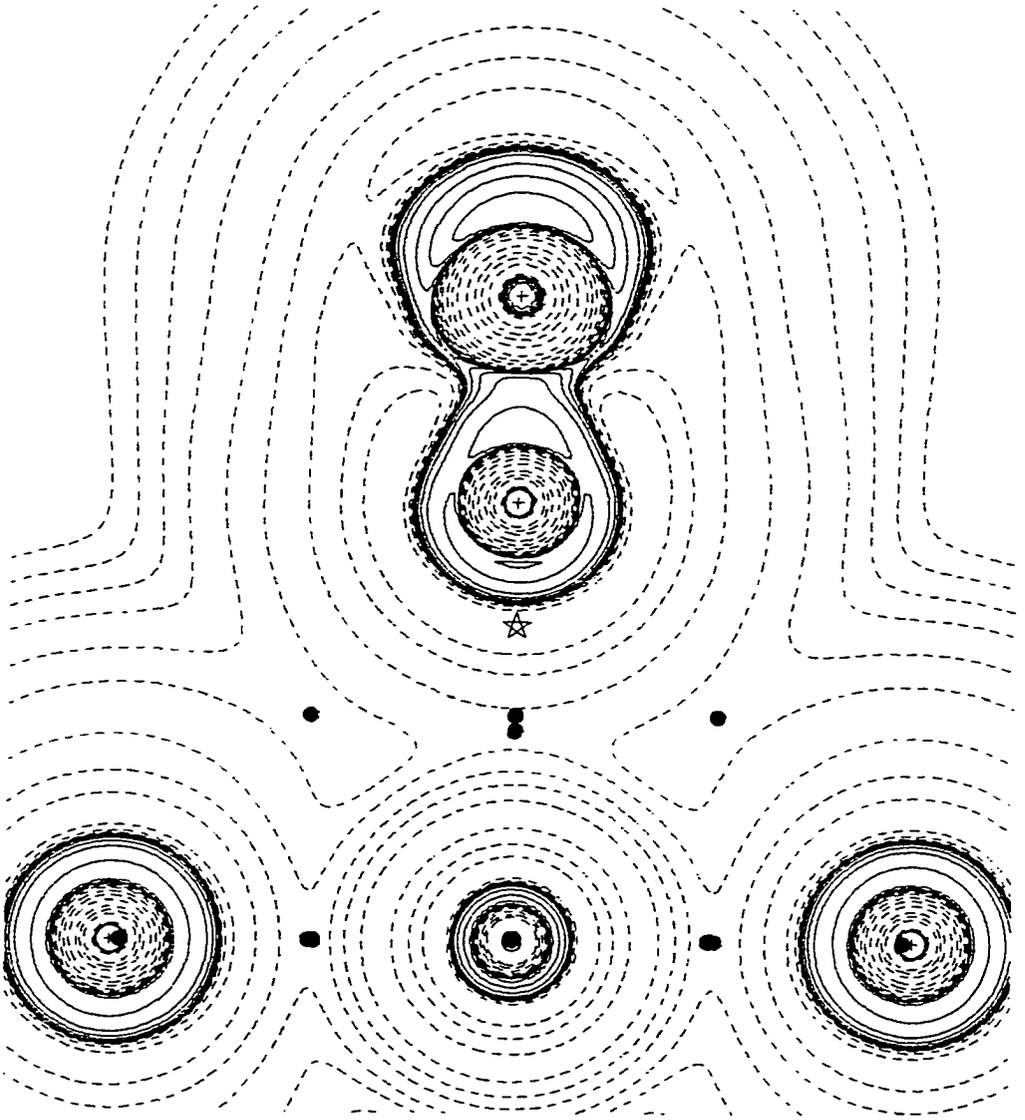

Figure 3-21. MgO surface with Mg in the center, nothing under the layer, 0 charge on the cluster, CO with O down. The plot is perpendicular to the plane of the surface.

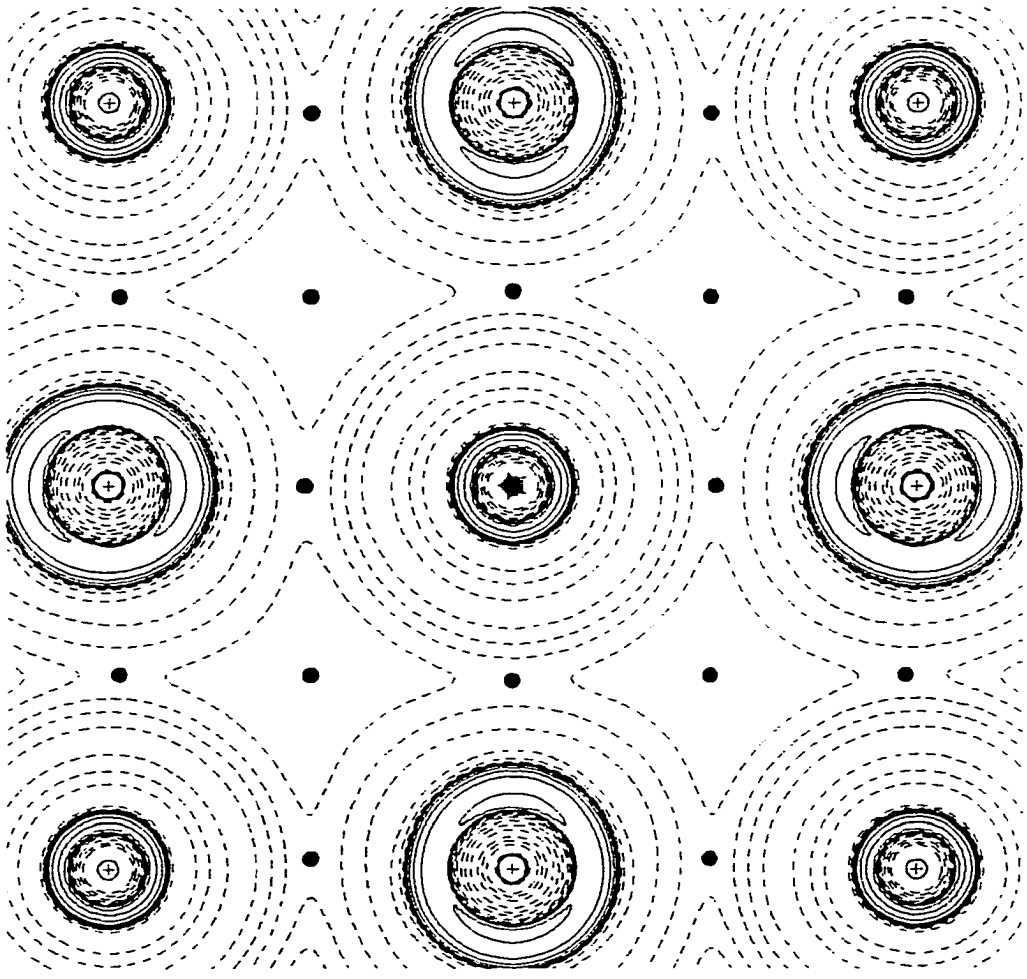

Figure 3-22. MgO surface with Mg in the center, nothing under the layer, +2 charge on the cluster, CO with O down. The plot is in the plane of the surface.

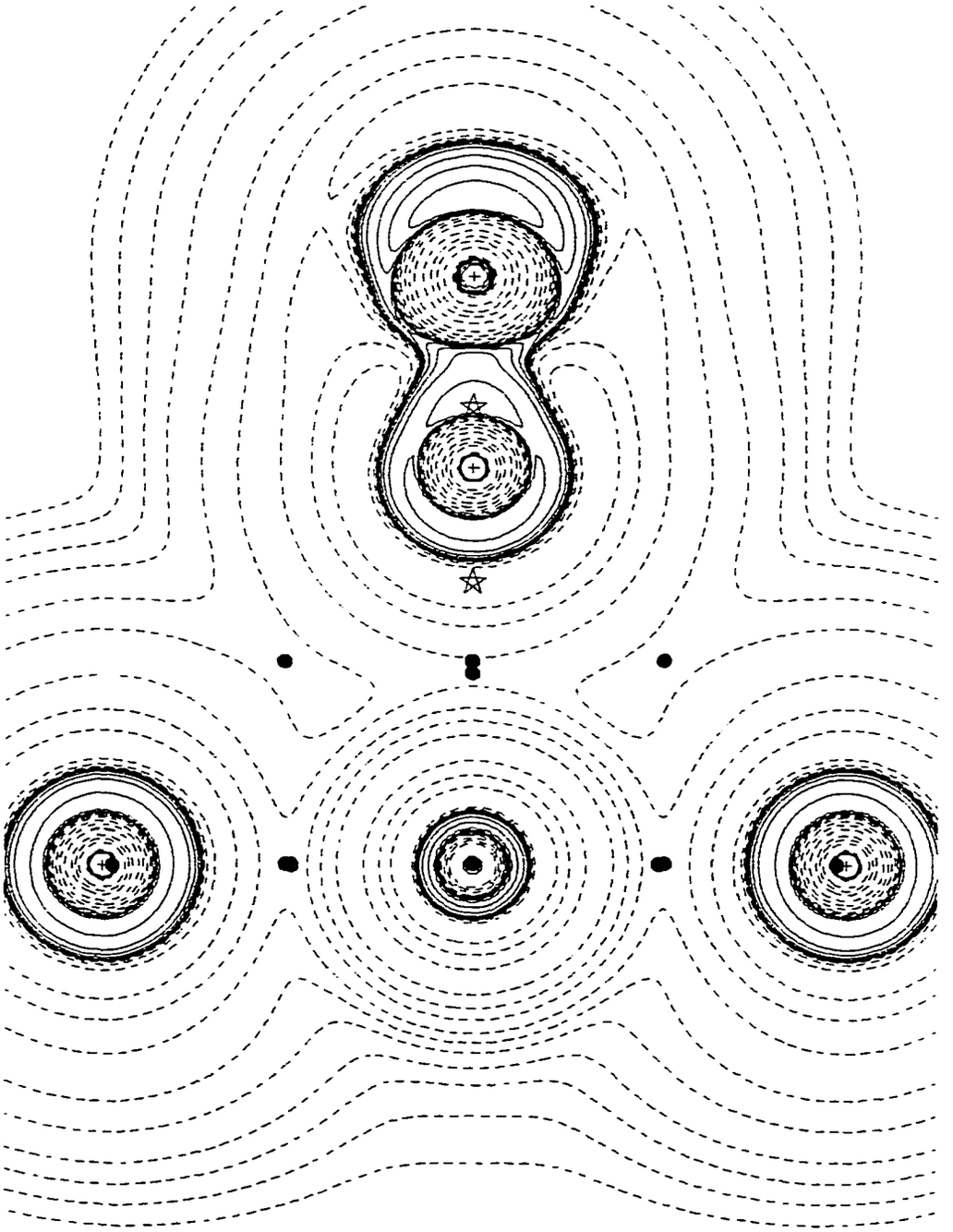

Figure 3-23. MgO surface with Mg in the center, nothing under the layer, +2 charge on the cluster, CO with O down. The plot is perpendicular to the plane of the surface.

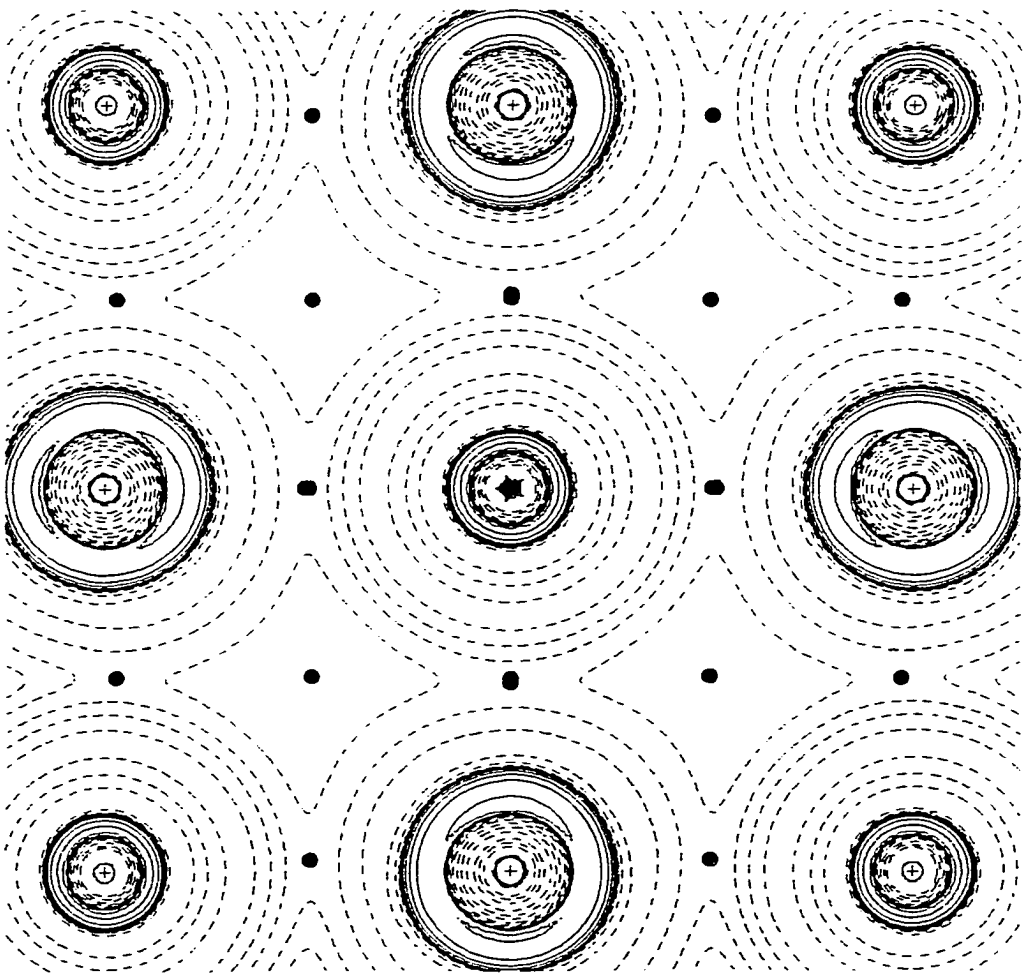

Figure 3-24. MgO surface with Mg in the center, O under the layer, 0 charge on the cluster, CO with O down. The plot is in the plane of the surface.

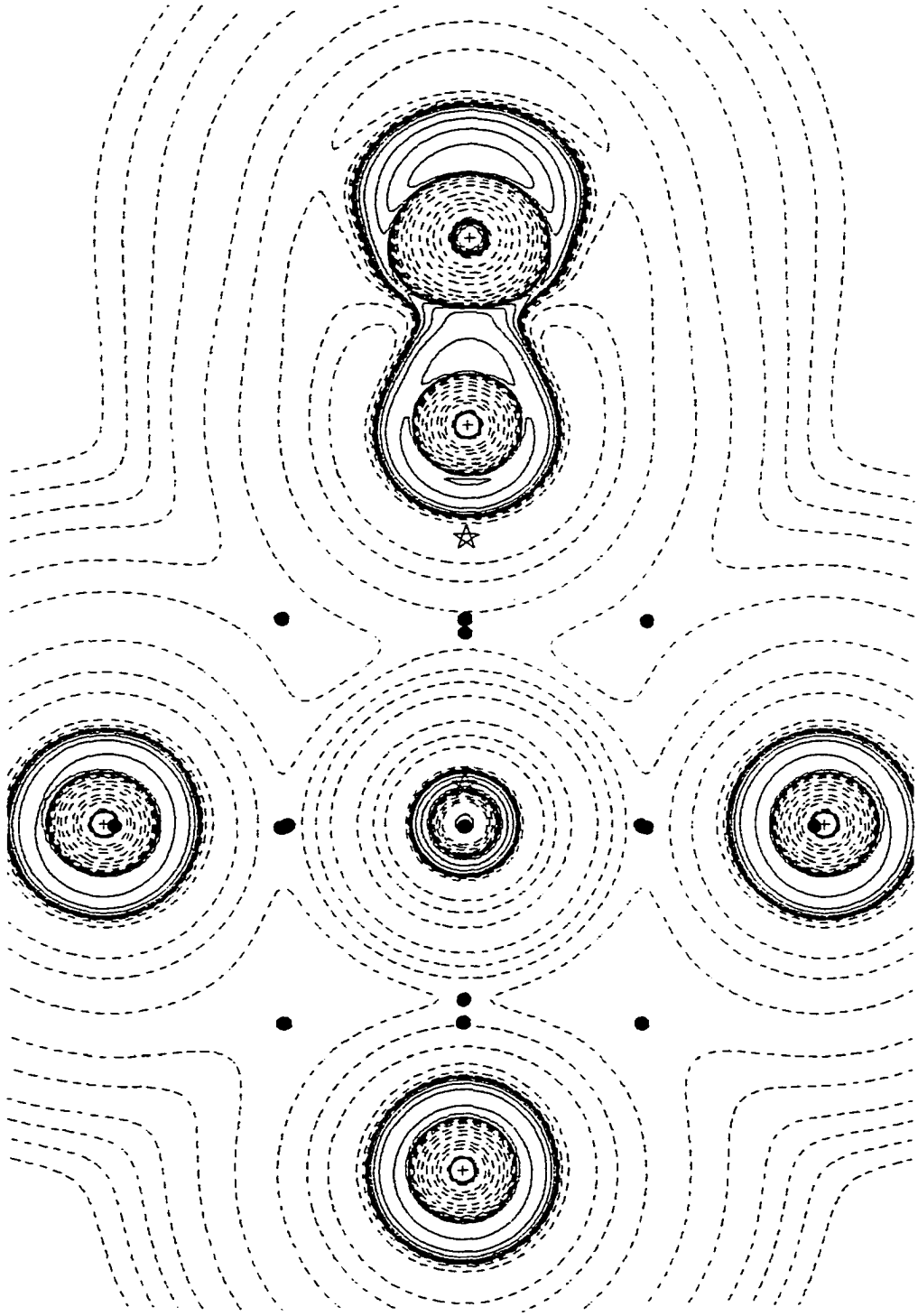

Figure 3-25. MgO surface with Mg in the center, O under the layer, O charge on the cluster, CO with O down. The plot is perpendicular to the plane of the surface.

3.5.4 Cluster with oxygen in the center, no CO molecule.

In this series of contour plots, oxygen is the central atom, with similar conditions imposed as when magnesium was the central atom, namely 0 charge and -2 charge on the cluster, both with no atom under the layer, and 0 charge on the cluster with magnesium under the central oxygen atom. The figures for this series are as follows:

Figure 3-26; 0 charge on the cluster, surface plane.

Figure 3-27; 0 charge perpendicular to the surface.

Figure 3-28; -2 charge on the cluster, surface plane.

Figure 3-29; -2 charge perpendicular to the surface.

Figure 3-30; 0 charge, sub-layer magnesium, surface plane.

Figure 3-31; 0 charge, sub-layer magnesium, perpendicular to the surface.

Here there are very noticeable differences between the neutral cluster and the -2 charge cluster. To achieve a net charge of zero on the cluster with five O^{-2} and four Mg^{+2} ions requires the addition of two "holes", positive charges, to be added to the cluster. Comparing Figures 3-26 with 3-28 and 3-30 it is apparent that holes deform the electron density more than the added electrons did in the previous series of calculations with a central magnesium ion. The outer oxygen atoms' charge concentrations are also greatly affected. The orientation of the charge in 3-28 has the bonding electrons toward the center of the cluster and the nonbonding electrons away from the center, with greater

charge concentration in the nonbonding region. In Figure 3-26 the charge concentration is shifted approximately 90° for the four oxygens at the corner of the cluster, relative to the corresponding oxygens in Figure 3-28. The central oxygen has a similar shape as the corner oxygens, but has its orientation along a diagonal axis of the cluster. To accomodate the two additional positive charges requires a rearrangement of the electron structure of all of the oxygen ions, but has no effect on the structure of the magnesium ions, which again, are core-like. The extra +2 charge has left a hole, and is apparently localized on the central atom. This is in contrast with the delocalized nature of the additional -2 charge placed on the cluster with magnesium in the center, seen in Figure 3-7. This is also readily seen in the comparison of Figures 3-27, 3-29, and 3-31, in the plane perpendicular to the surface. The magnesium ions appear unaffected by the charge differences, or by the presence of the sublayer Mg. If Figures 3-28 and 3-30 are compared with 3-29 and 3-31, the effect of the sublayer magnesium is apparent. When there is no magnesium under the layer, the central oxygen shows a symmetric electron density in both planes, while the outer oxygens show bonded and nonbonded charge concentrations, with the nonbonded ones occupying more space, supporting the VSEPR model. In Figures 3-30 and 3-31 the sublayer magnesium causes a greater concentration in nonbonding electrons for the central and outer oxygens.

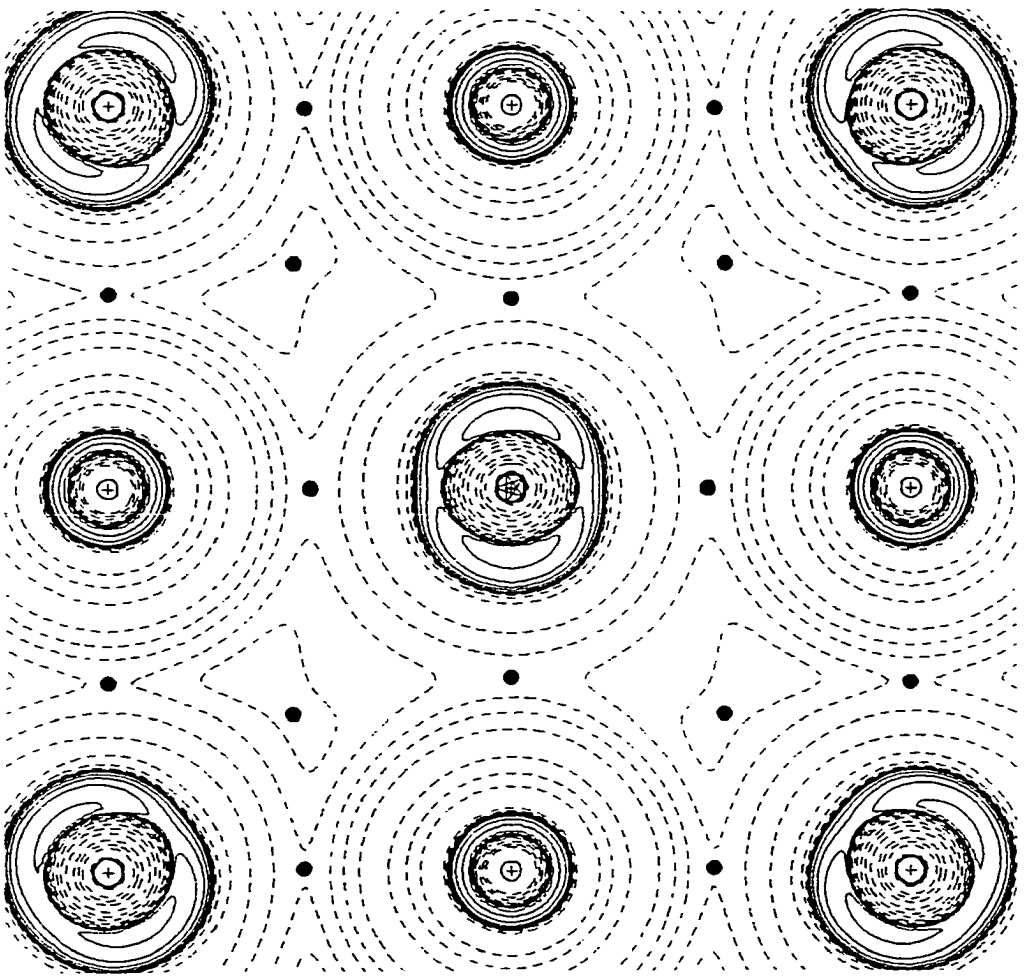

Figure 3-26. MgO surface with O in the center, nothing under the layer, 0 charge on the cluster, no CO. The plot is in the plane of the surface.

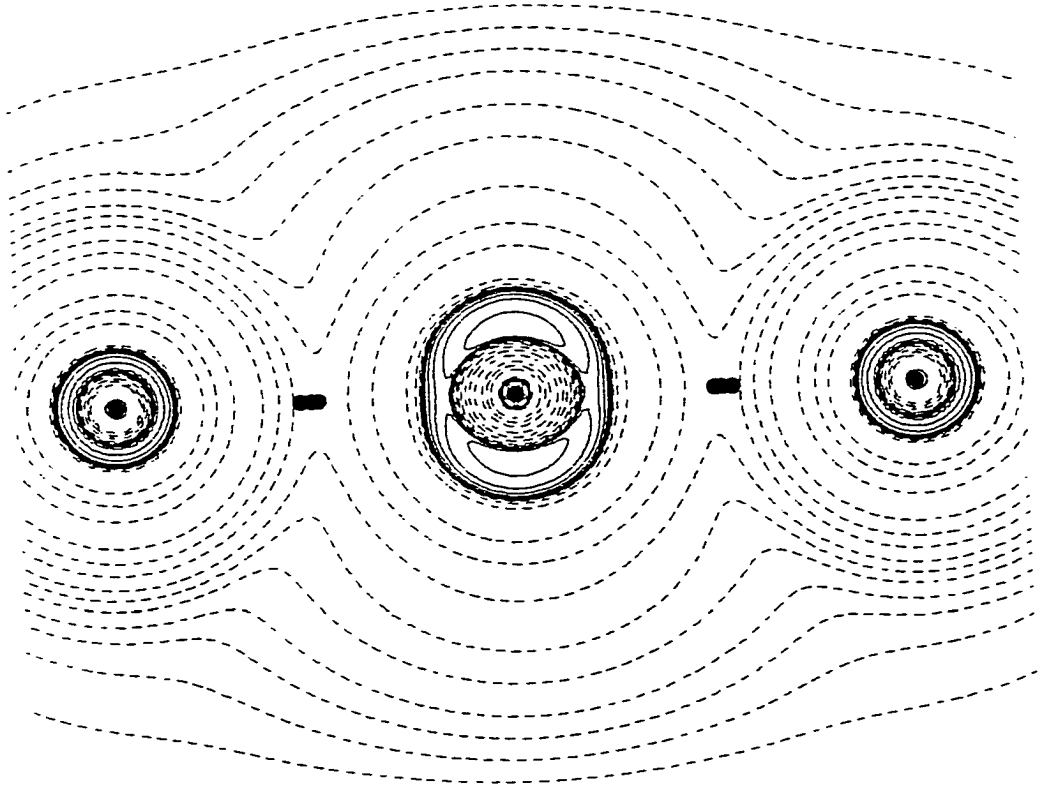

Figure 3-27. MgO surface with O in the center, nothing under the layer, 0 charge on the cluster, no CO. The plot is perpendicular to the plane of the surface.

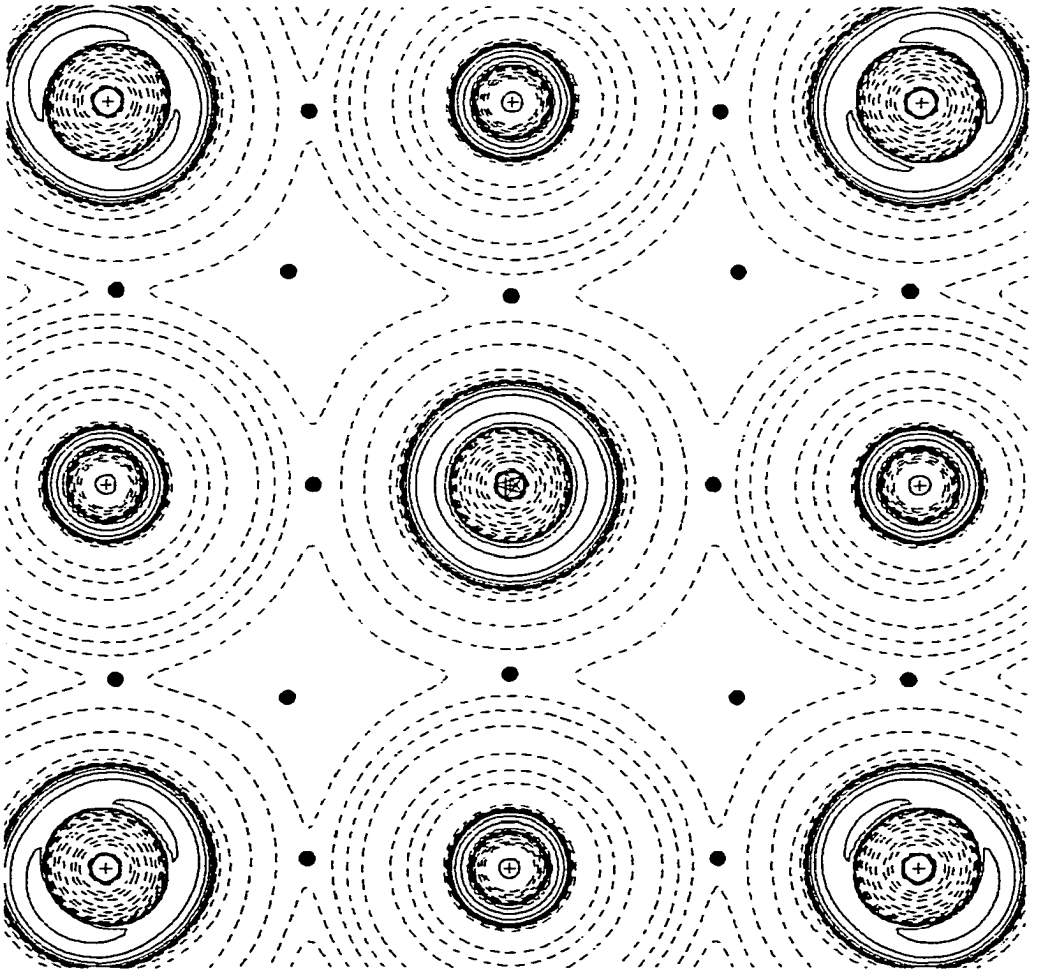

Figure 3-28. MgO surface with O in the center, nothing under the layer, -2 charge on the cluster, no CO. The plot is in the plane of the surface.

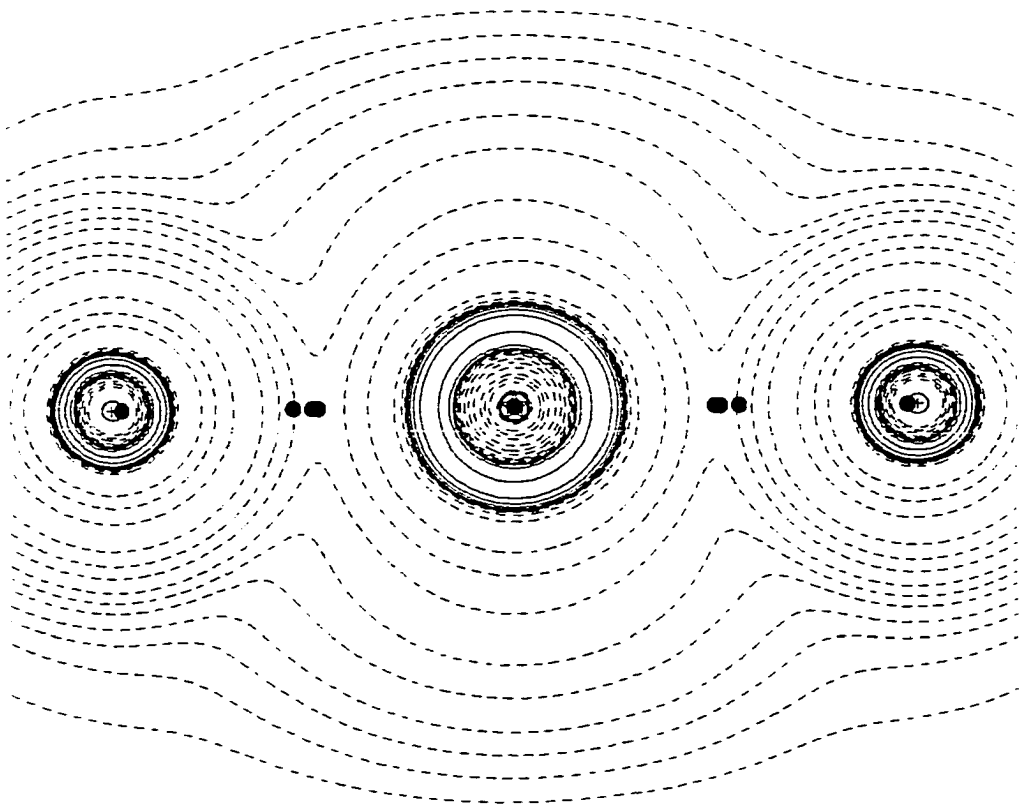

Figure 3-29. MgO surface with O in the center, nothing under the layer, -2 charge on the cluster, no CO. The plot is perpendicular to the plane of the surface.

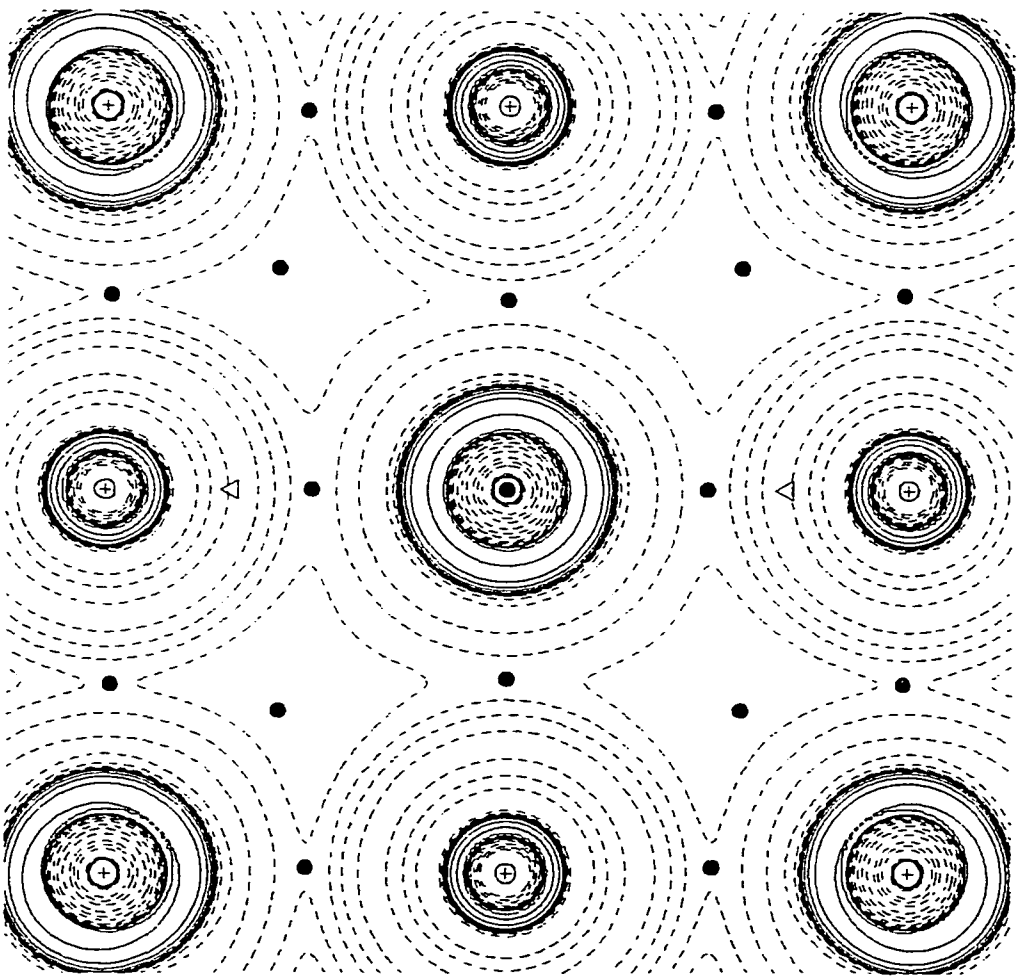

Figure 3-30. MgO surface with O in the center, Mg under the layer, 0 charge on the cluster, no CO. The plot is in the plane of the surface.

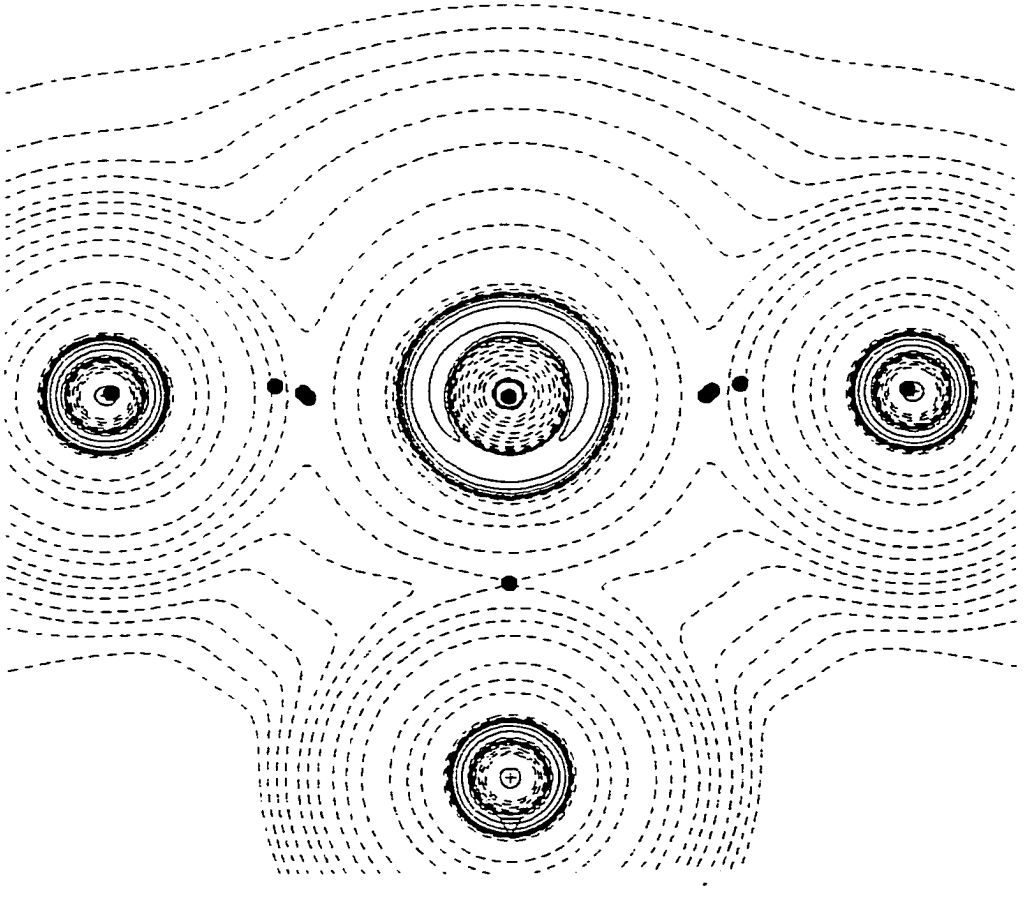

Figure 3-31. MgO surface with O in the center, Mg under the layer, 0 charge on the cluster, no CO. The plot is perpendicular to the plane of the surface.

3.5.5 Cluster with oxygen in the center, CO adsorbed with carbon down.

The final series involving magnesium and oxygen places oxygen in the center of the cluster and the CO molecule oriented with carbon down for the same cluster conditions described in the previous section. The figures are as follows:

Figure 3-32; 0 charge on the cluster, surface plane.
Figure 3-33; 0 charge perpendicular to the surface.
Figure 3-34; -2 charge on the cluster, surface plane.
Figure 3-35; -2 charge perpendicular to the surface.
Figure 3-36; 0 charge, sublayer magnesium, surface plane.
Figure 3-37; 0 charge, sublayer magnesium, perpendicular to the surface.

In Figures 3-32, 3-34, and 3-36 the central oxygen and the surrounding magnesium ions are identical to one another. The differences occur in the exterior oxygens. In Figure 3-32 the oxygens are slightly polarized along the axis connecting them to the central oxygen. The nonbonding charge concentrations are pronounced, but the bonding charge concentrations are less so. This cluster has zero charge, meaning there are two additional holes (positive charges) on the cluster. These holes appear to have reduced the extent of charge concentration in bonding regions of the exterior oxygens. In Figure 3-34 the oxygens are also polarized along the same axis as in Figure 3-32, but both the bonding and

nonbonding charge concentrations are apparent. Here the cluster charge is -2, so the effect of the holes is not operative. In Figure 3-36 the presence of the magnesium ion under the layer has a similar effect to the presence of the two holes in Figure 3-32, however in this case the holes are introduced "naturally" by a +2 ion. The bonding charge concentrations do not appear in the surface plot, but the nonbonded ones are large and pronounced on the corner oxygen atoms. Comparing Figures 3-33 and 3-35 with Figures 3-29, it is evident that the CO molecule has little or no effect on the charge distribution on the cluster. Again, this is because there is little charge transfer between the molecule and the surface.

In Figure 3-37, the nonbonding charge concentrations appear to be much larger than in the previous surface plots. The difference is the presence of the magnesium atom with its +2 charge contribution to the cluster. Although the charge on the cluster is zero, as in Figure 3-32, the effect is different on the corner oxygens. The presence of the sublayer magnesium will draw the electrons from the corners towards itself. This is apparent by comparing Figures 3-35 and 3-37. In Figure 3-37 the central oxygen shows increased nonbonding charge concentrations, but no bonding ones. In Figures 3-33 and 3-35 the central oxygen shows symmetric charge concentration in the plane perpendicular to the surface. Figures 3-33, 3-35, and 3-37 show there is little

effect on the electron density for the CO molecule for any of the cluster conditions. This is due to the adsorption of the CO molecule on the surface being mostly a result of electrostatics and other van der Waals' forces, not due to charge transfer between the molecule and the surface, as stated previously.

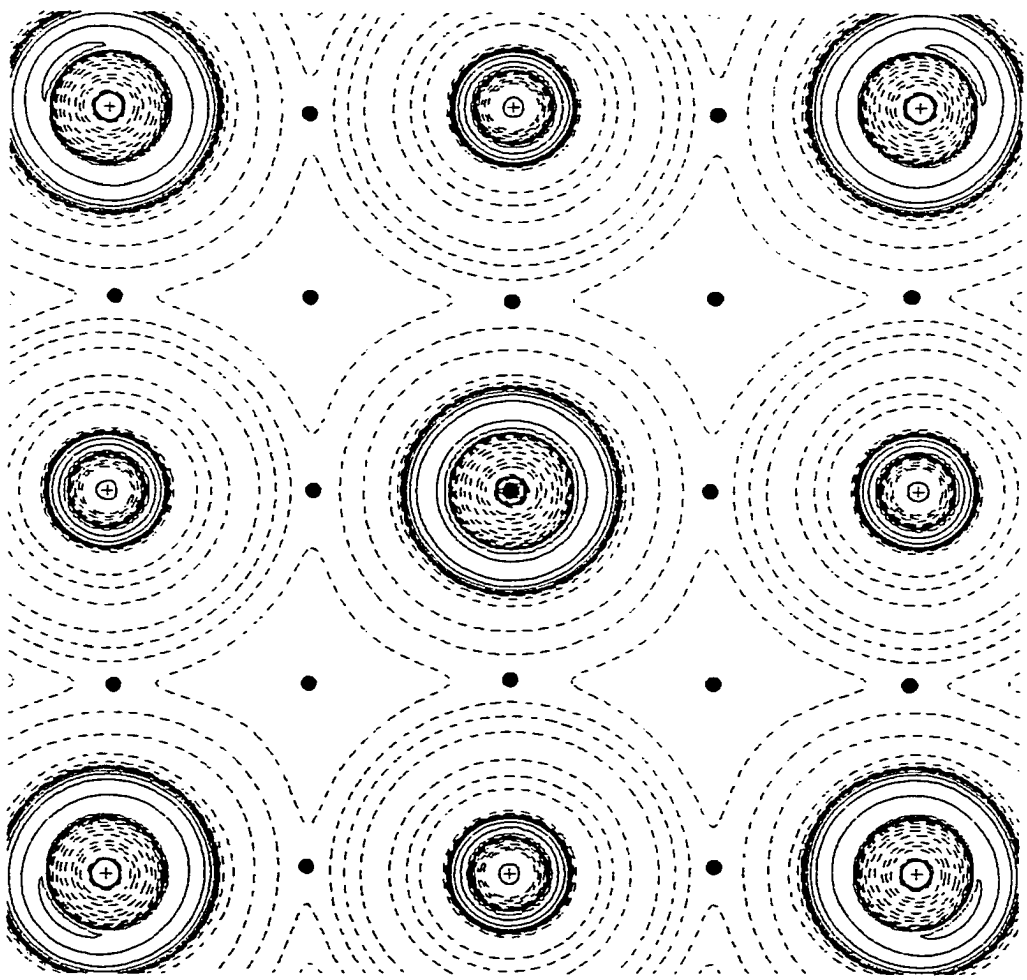

Figure 3-32. MgO surface with O in the center, nothing under the layer, 0 charge on the cluster, CO with C down. The plot is in the plane of the surface.

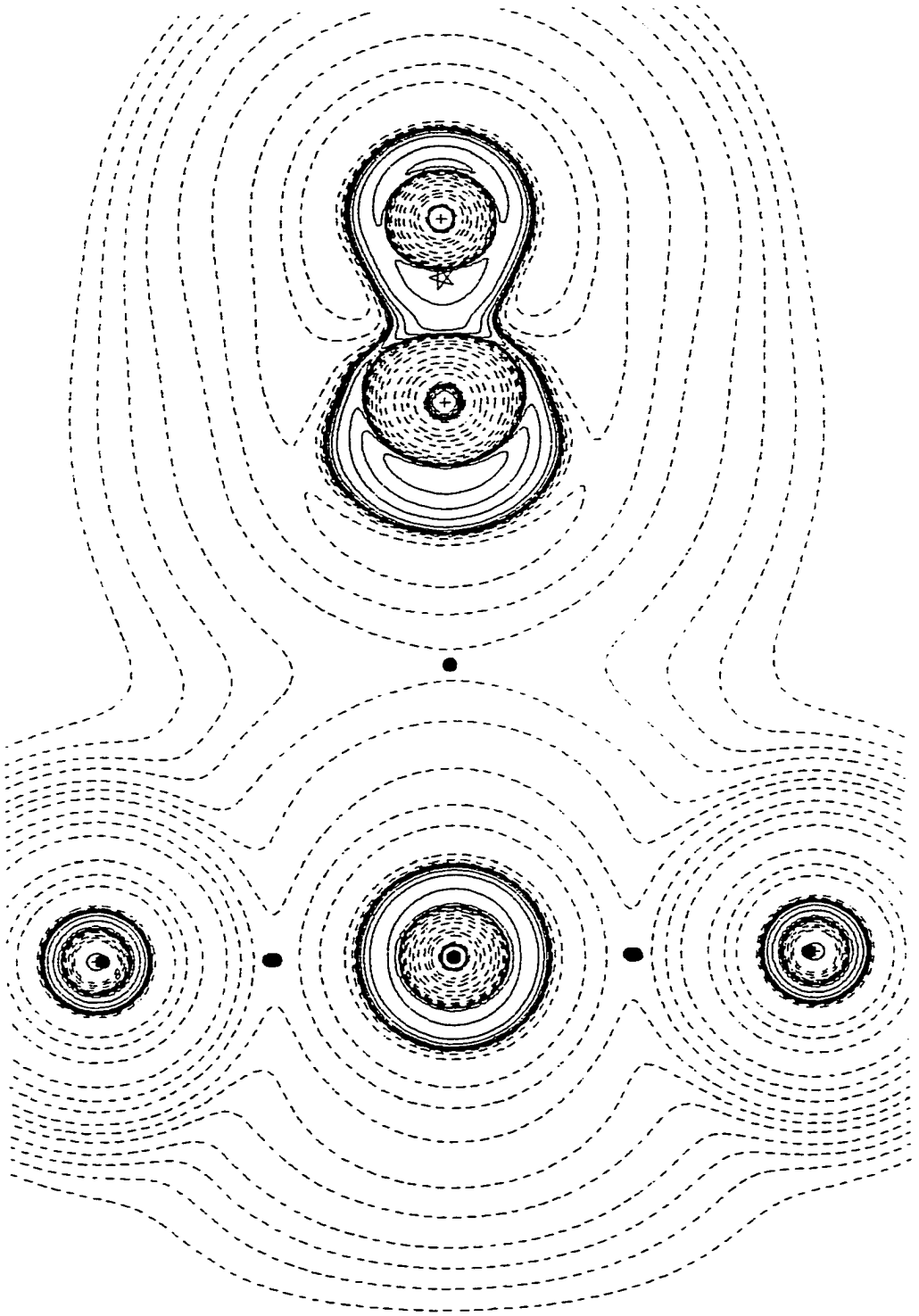

Figure 3-33. MgO surface with O in the center, nothing under the layer, 0 charge on the cluster, CO with C down. The plot is perpendicular to the plane of the surface.

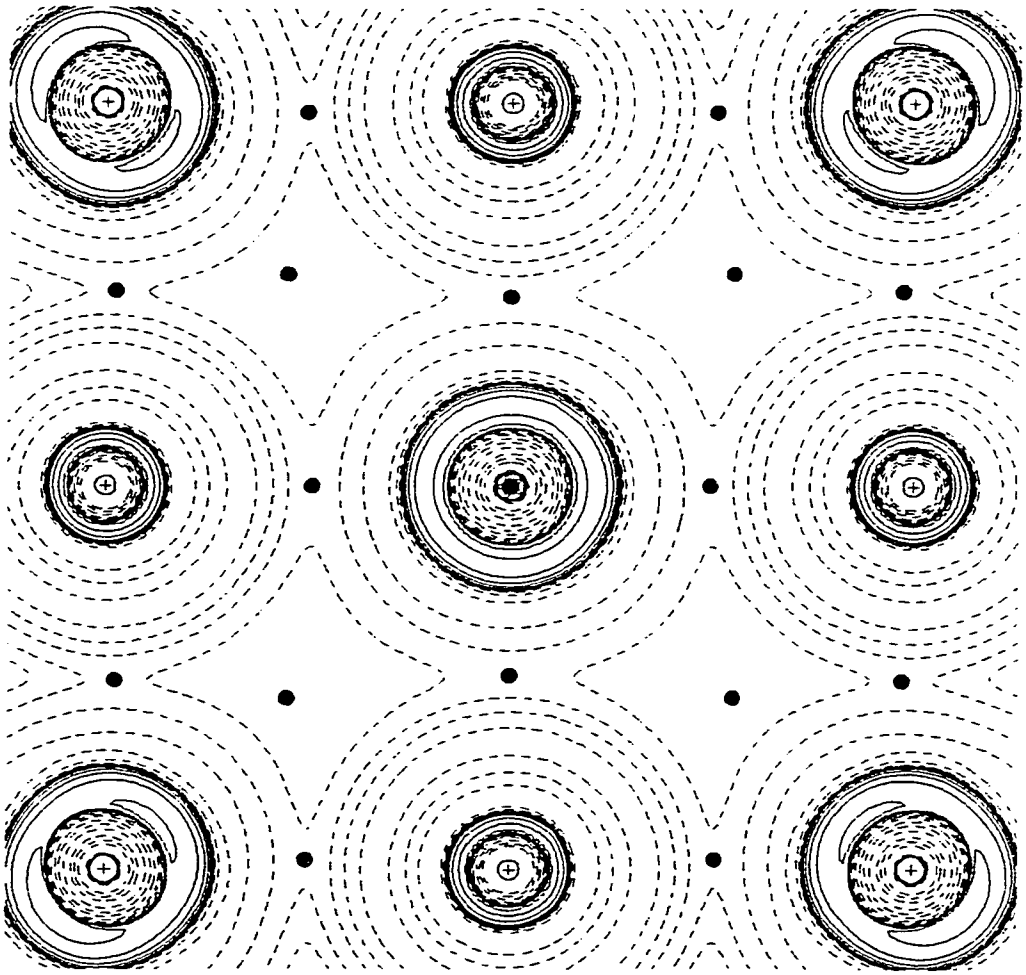

Figure 3-34. MgO surface with O in the center, nothing under the layer, -2 charge on the cluster, CO with C down. The plot is in the plane of the surface.

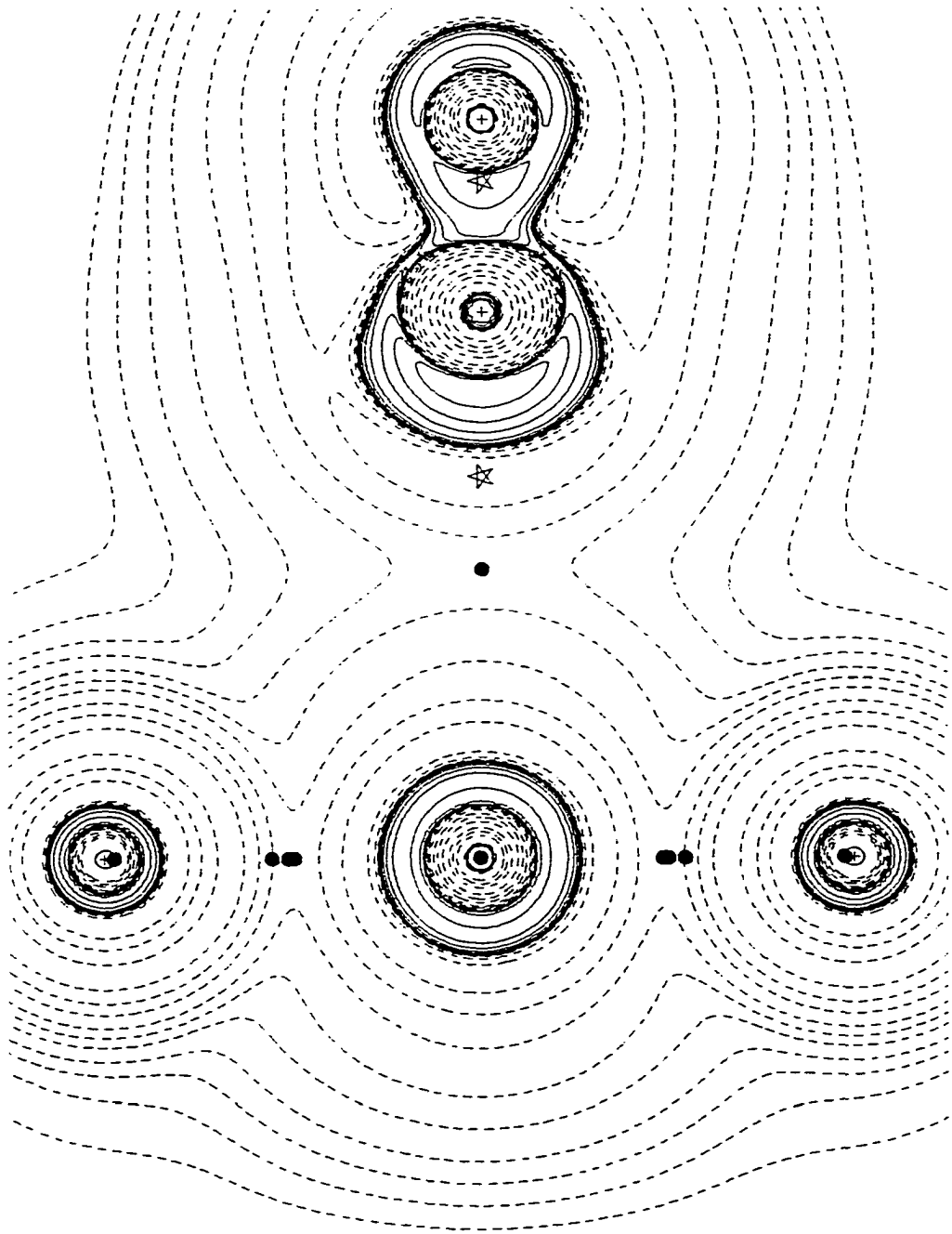

Figure 3-35. MgO surface with O in the center, nothing under the layer, -2 charge on the cluster, CO with C down. The plot is perpendicular to the plane of the surface.

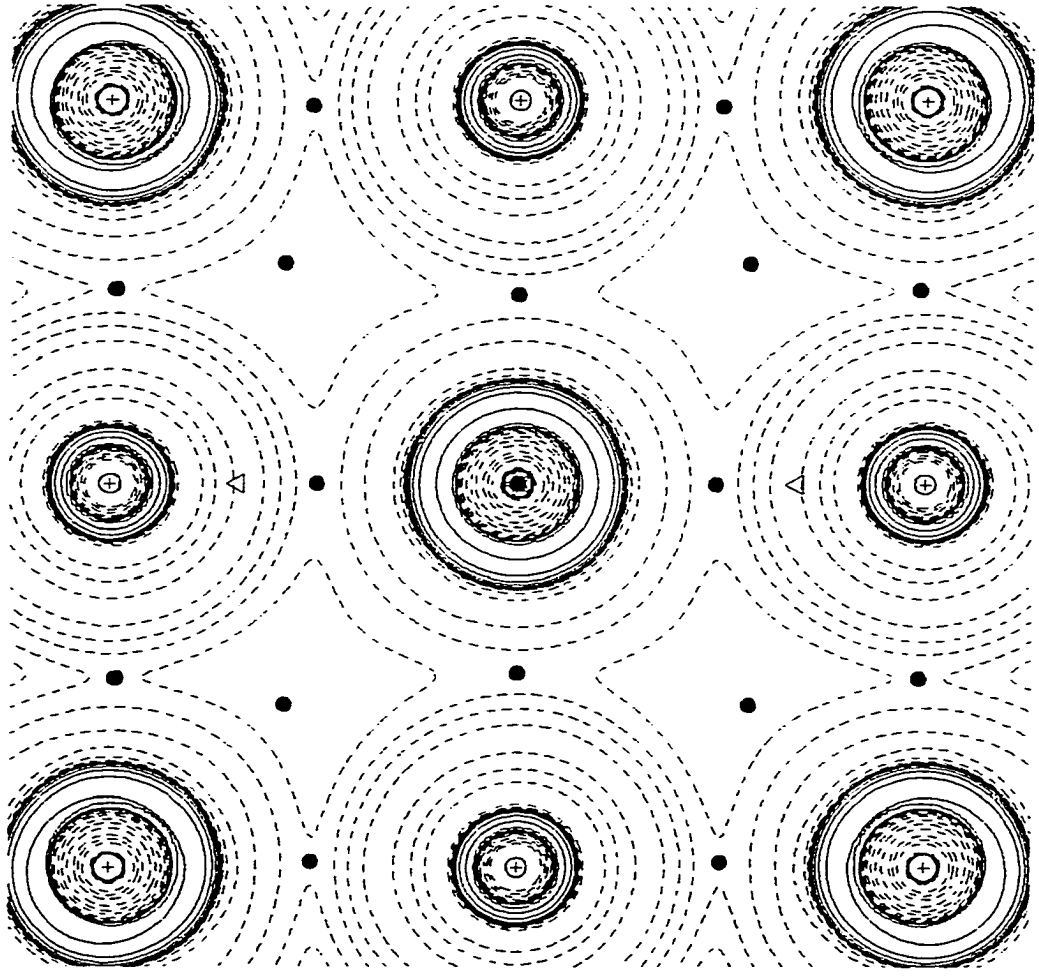

Figure 3-36. MgO surface with O in the center, Mg under the layer, 0 charge on the cluster, CO with C down. The plot is in the plane of the surface.

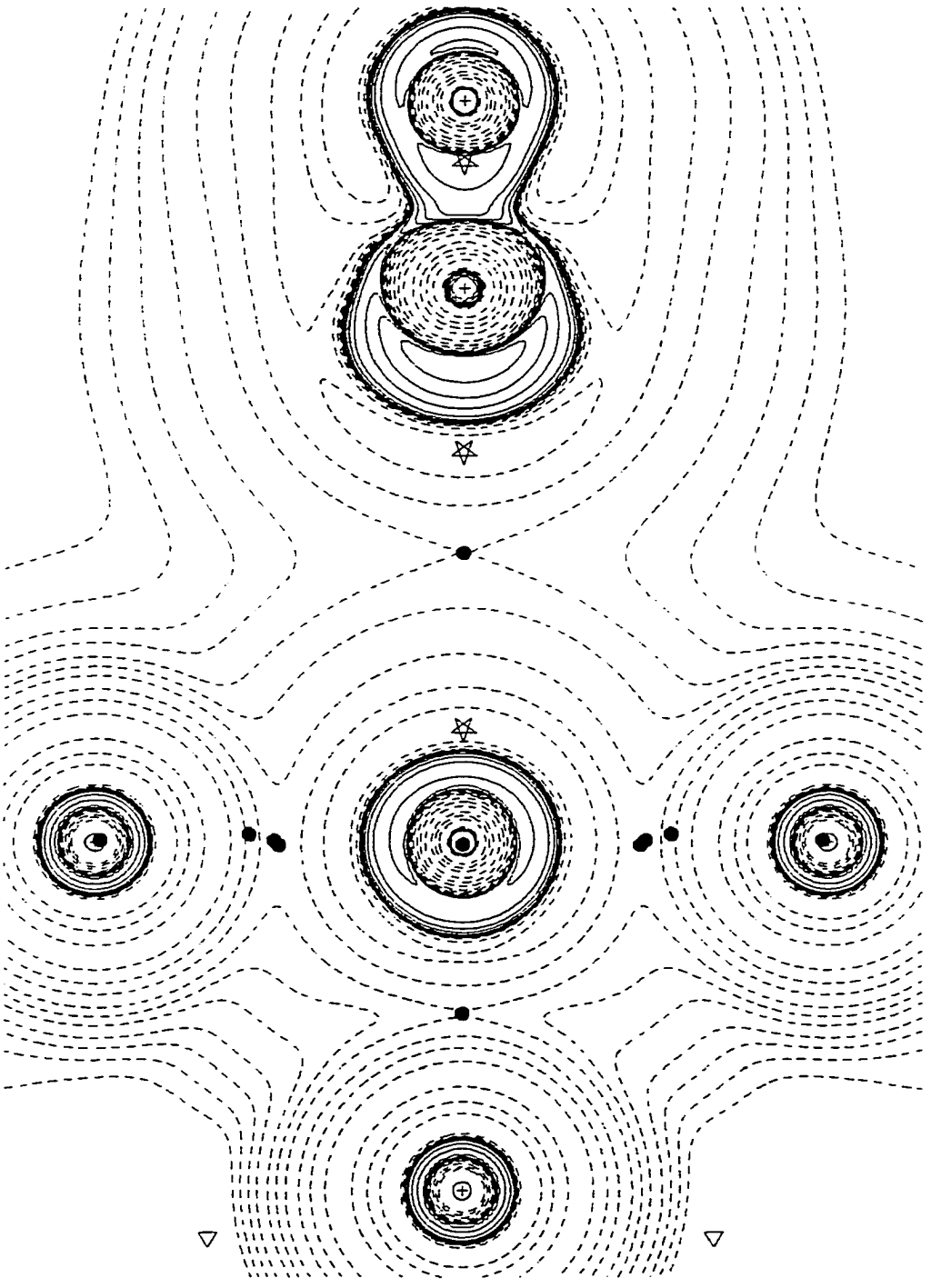

Figure 3-37. MgO surface with O in the center, Mg under the layer, 0 charge on the cluster, CO with C down. The plot is perpendicular to the plane of the surface.

3.5.6 Cluster with magnesium in the center and sulfur under the layer, with no CO, CO with carbon down, and CO with oxygen down.

This final series of plots places a sulfur atom beneath the central Mg. The radius of the S^{-2} ion is 1.84 Å and for O^{-2} is 1.32 Å[108]. The size of the sulfur ion will place a strain causing the magnesium in the center to rise above the surface plane defined by the oxygen atoms. The optimized position for the central magnesium atom was determined using GAUSSIAN 92 and the 3-21G* basis set. The magnesium atom was placed at this optimized position to determine the optimized distances for the CO adsorption. Surface plots and plots at 90° to the surface of the Laplacian of the charge density were produced for each of the CO orientations as well as the condition with no CO molecule. The figures, all having magnesium in the center with sulfur under the central magnesium and 0 charge on the cluster, are as follows:

Figure 3-38; no CO, surface plane.

Figure 3-39; no CO, plane parallel to the surface through the central magnesium.

Figure 3-40; no CO perpendicular to the surface.

Figure 3-41; CO with carbon down, surface plane.

Figure 3-42; CO with carbon down, plane parallel to the surface through the central magnesium.

Figure 3-43; CO with carbon down, perpendicular to the surface.

Figure 3-44; CO with oxygen down, surface plane.

Figure 3-45; CO with oxygen down, plane parallel to the surface through the central magnesium.

Figure 3-46; CO with oxygen down, perpendicular to the surface.

In Figures 3-38, 3-41, and 3-44, the contour plots for the surface plane, the plots are virtually identical. The presence of the sulfur atom under the layer changes the magnitudes of the bonding and nonbonding charge concentrations from previous orientations, they are broader and thinner than with other magnesium centered clusters, but within this set of plots, they are the same. Again this supports the claim that there is little electron transfer from the CO molecule to the surface for either orientation of the molecule. This is also seen in the series of plots in Figures 3-39, 3-42, and 3-45 which are parallel to the surface through the central magnesium ion. These plots are also almost identical to one another. Again this reinforces the conclusion of the small charge transfer for the adsorption of the CO molecule on the surface. However, there is a marked difference in the plots perpendicular to the surface that include the sulfur atom, Figures 3-40, 3-43, and 3-46. In Figures 3-40 and 3-46 the Laplacian of the electron density for the sulfur, the central magnesium, and the oxygen ions is transferable, even though in Figure 3-40 there is no CO molecule and in 3-46 there is a CO molecule

oriented with the oxygen down. In Figure 3-43, there is a CO molecule oriented with the carbon down and the electron density for the sulfur and the oxygens is changed significantly. Although it has been successfully shown that the CO molecule adsorption on the surface involves little charge transfer, when there is a low-coordinated atom beneath the surface and the CO molecule is oriented with the carbon end down, there is a charge withdrawal from the atom beneath the surface. This was seen in Figure 3-19 where the atom under the layer was oxygen, and now with sulfur, thus reinforcing the generality of the previous observation. Both atoms are in group VI-A of the periodic table, so will behave alike chemically, although the charge withdrawal from the sulfur is not as great as that from the oxygen. Future investigations should address this issue to determine the nature of this charge withdrawal, using other "impurity" elements and other adsorbants.

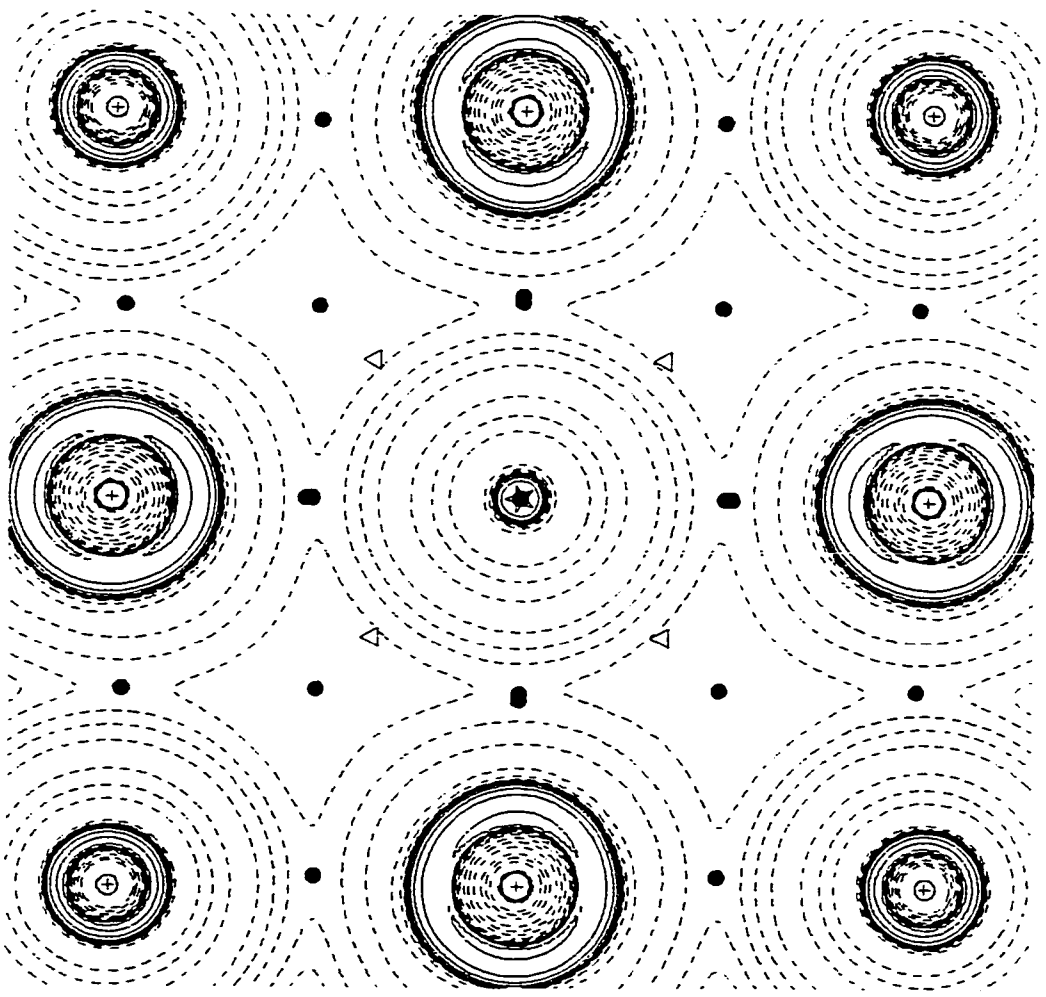

Figure 3-38. MgO surface with Mg in the center lifted above the plane of the surface oxygens, S under the layer, 0 charge on the cluster, no CO. The plot is in the plane of the surface oxygens.

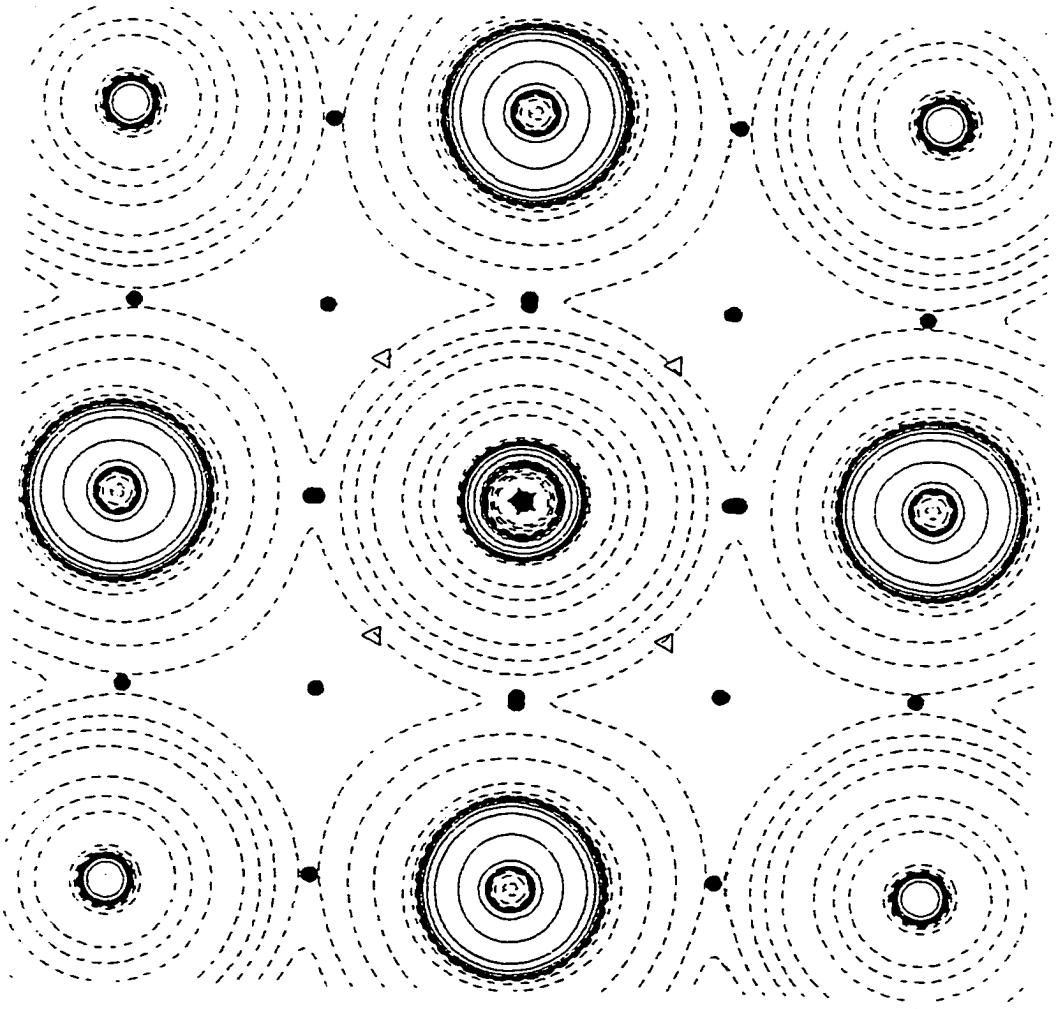

Figure 3-39. MgO surface with Mg in the center lifted above the plane of the surface oxygens, S under the layer, 0 charge on the cluster, no CO. The plot is in the plane parallel to the plane of the surface oxygens through the central Mg.

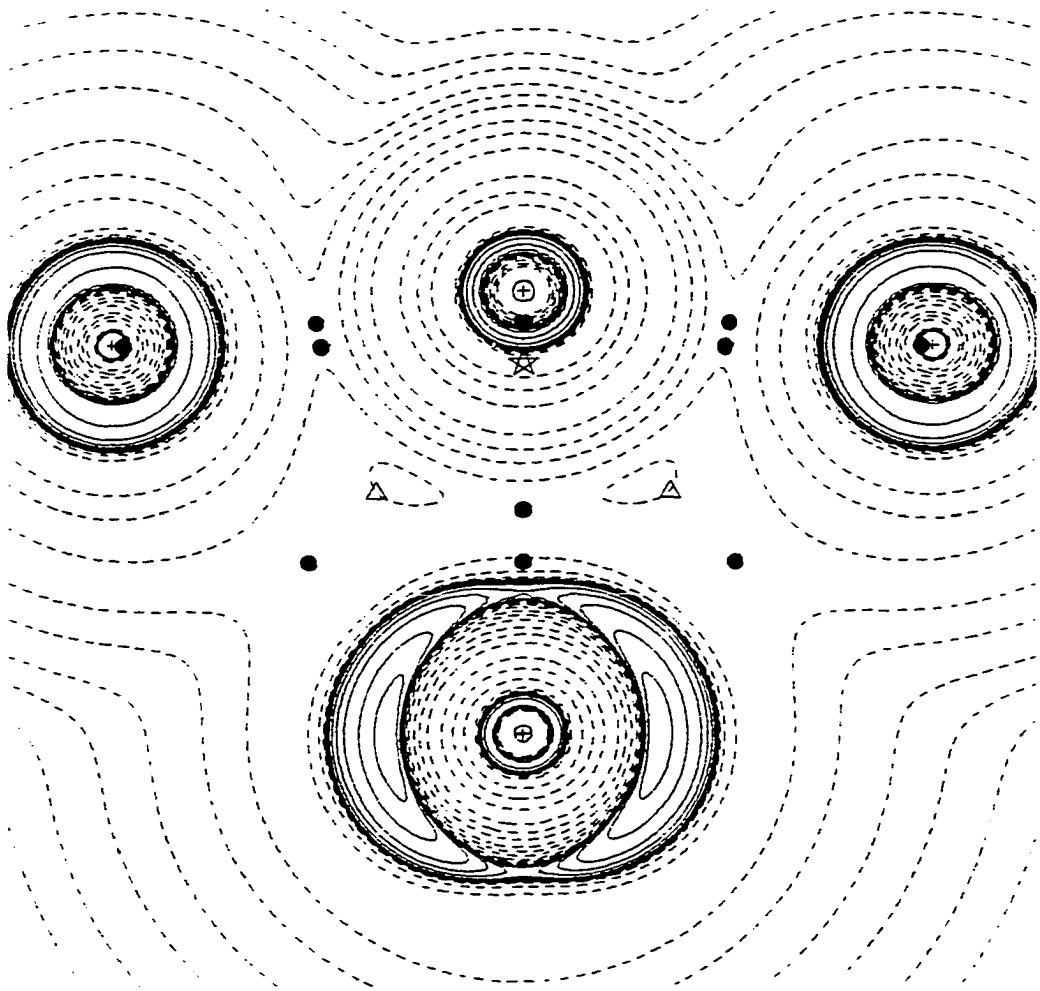

Figure 3-40. MgO surface with Mg in the center lifted above the plane of the surface oxygens, S under the layer, 0 charge on the cluster, no CO. The plot is perpendicular to the plane of the surface oxygens.

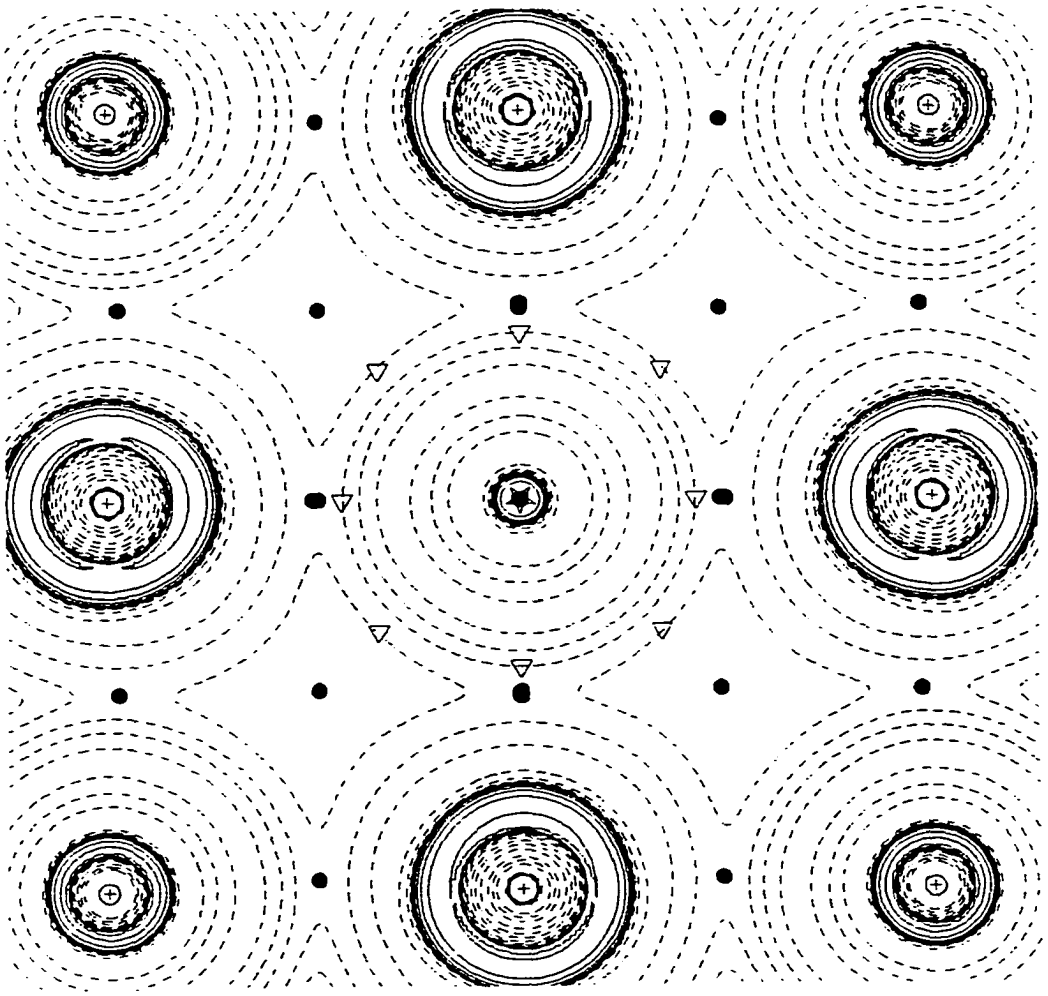

Figure 3-41. MgO surface with Mg in the center lifted above the plane of the surface oxygens, S under the layer, 0 charge on the cluster, CO with C down. The plot is in the plane of the surface oxygens.

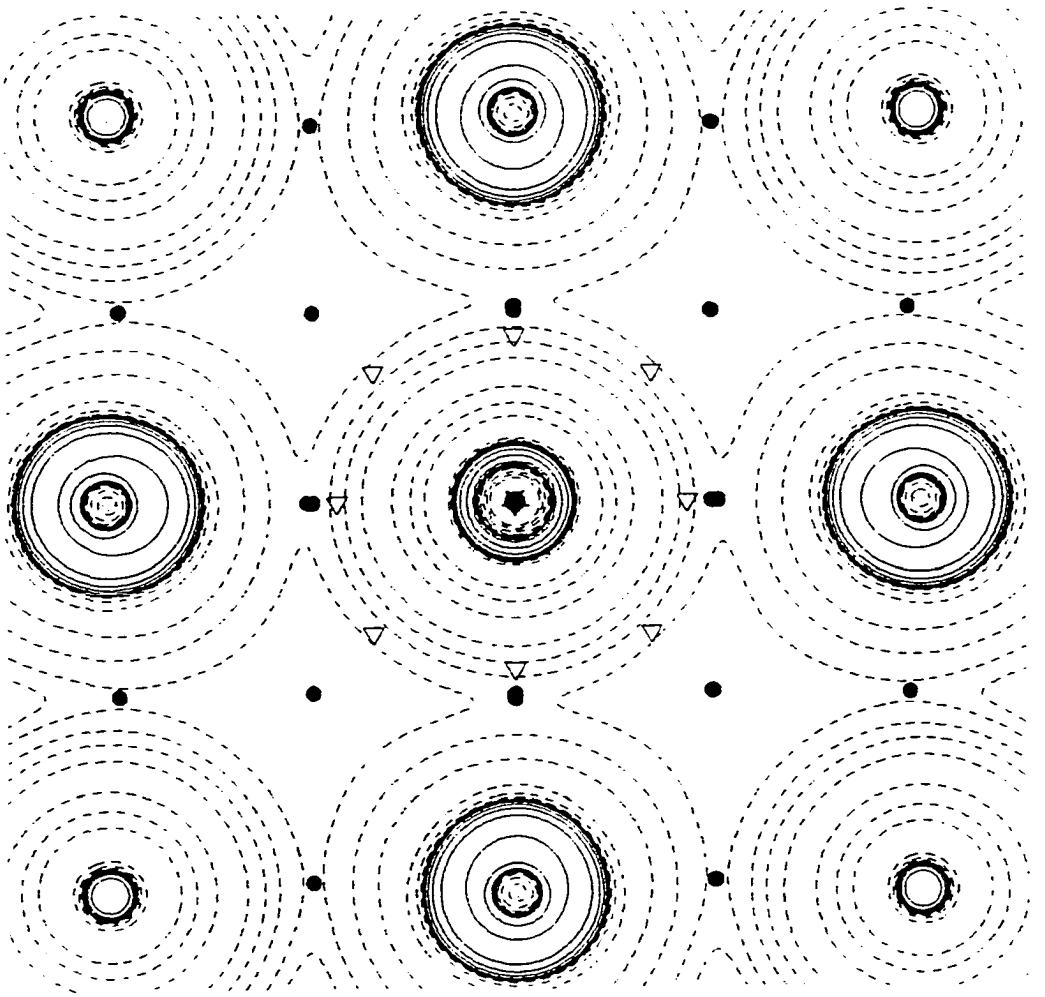

Figure 3-42. MgO surface with Mg in the center lifted above the plane of the surface oxygens, S under the layer, 0 charge on the cluster, CO with C down. The plot is in the plane parallel to the surface oxygens through the central Mg.

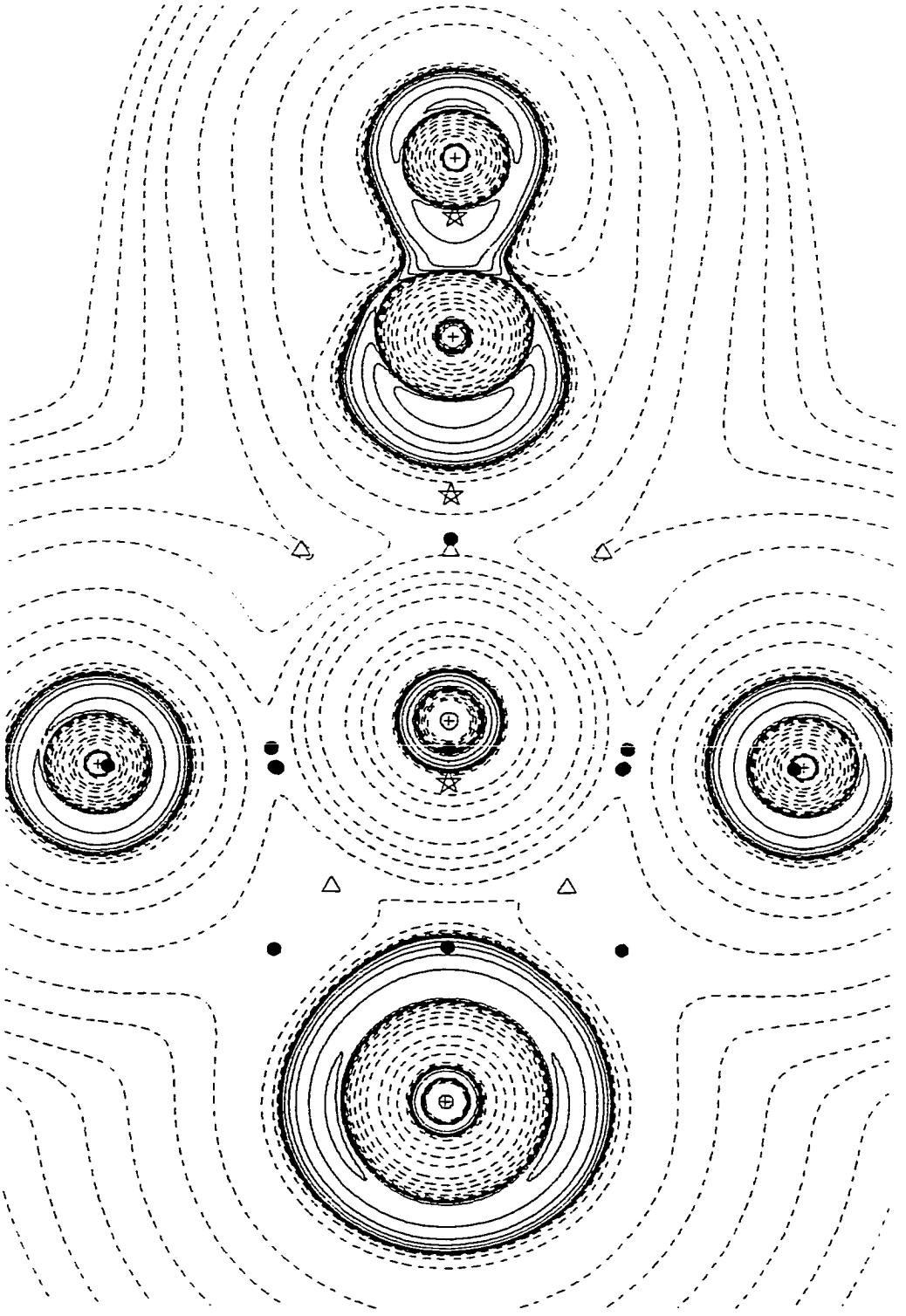

Figure 3-43. MgO surface with Mg in the center lifted above the plane of the surface oxygens, S under the layer, 0 charge on the cluster, CO with C down. The plot is perpendicular to the plane of the surface oxygens.

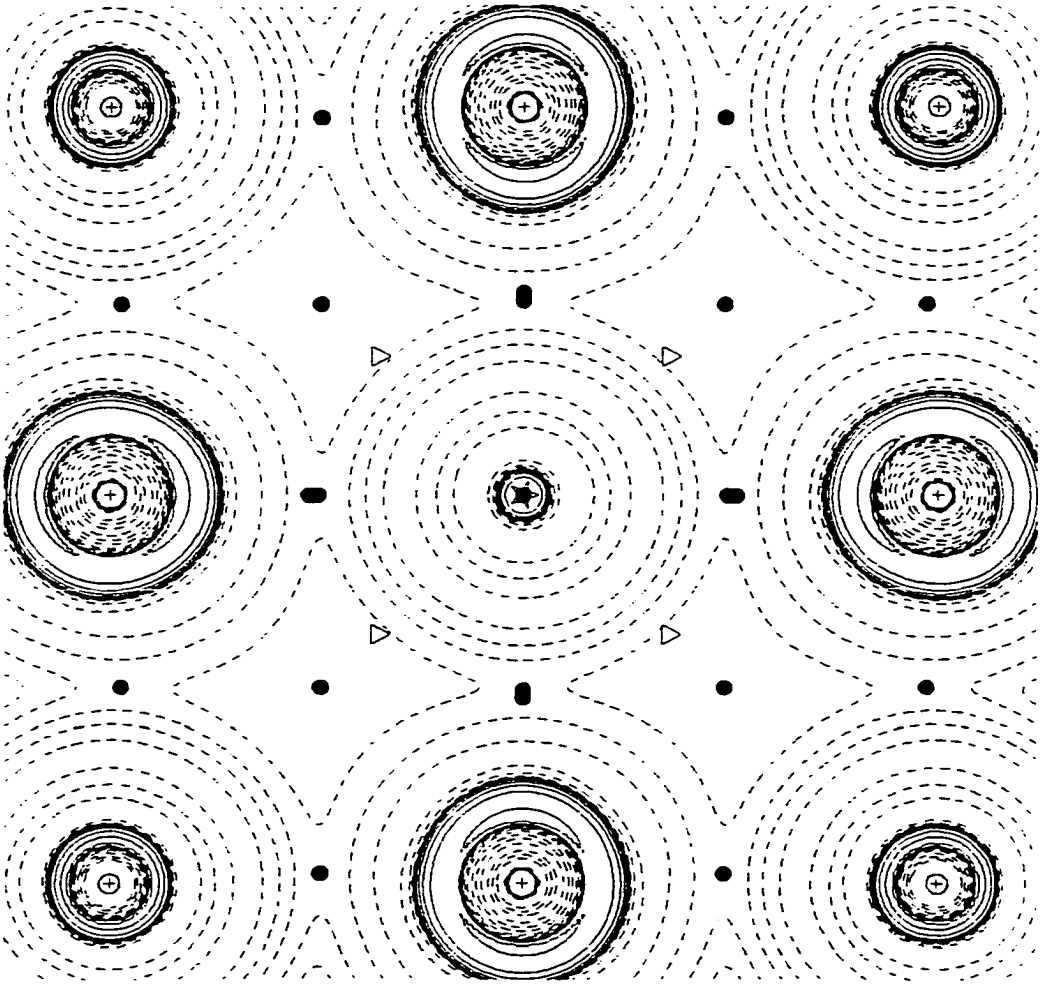

Figure 3-44. MgO surface with Mg in the center lifted above the plane of the surface oxygens, S under the layer, 0 charge on the cluster, CO with O down. The plot is in the plane of the surface oxygens.

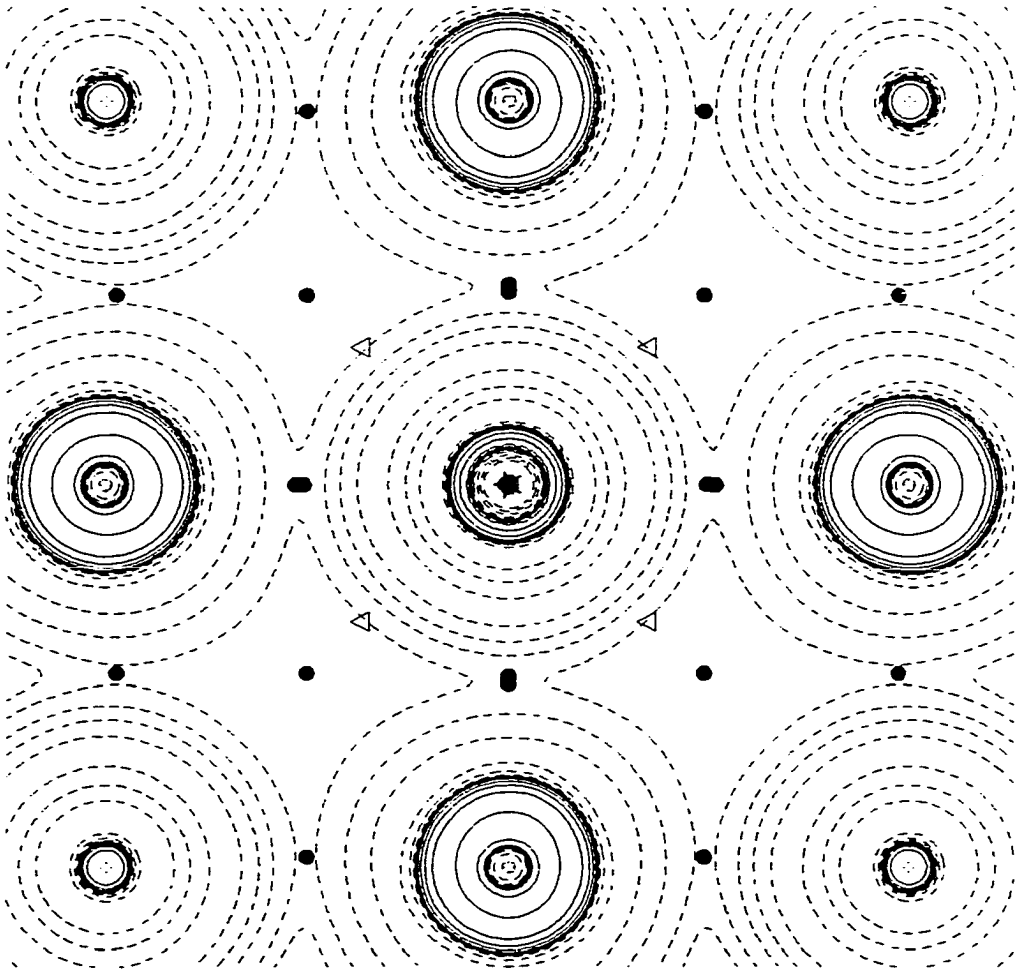

Figure 3-45. MgO surface with Mg in the center lifted above the plane of the surface oxygens, S under the layer, 0 charge on the cluster, CO with O down. The plot is in the plane parallel to the surface oxygens through the central Mg.

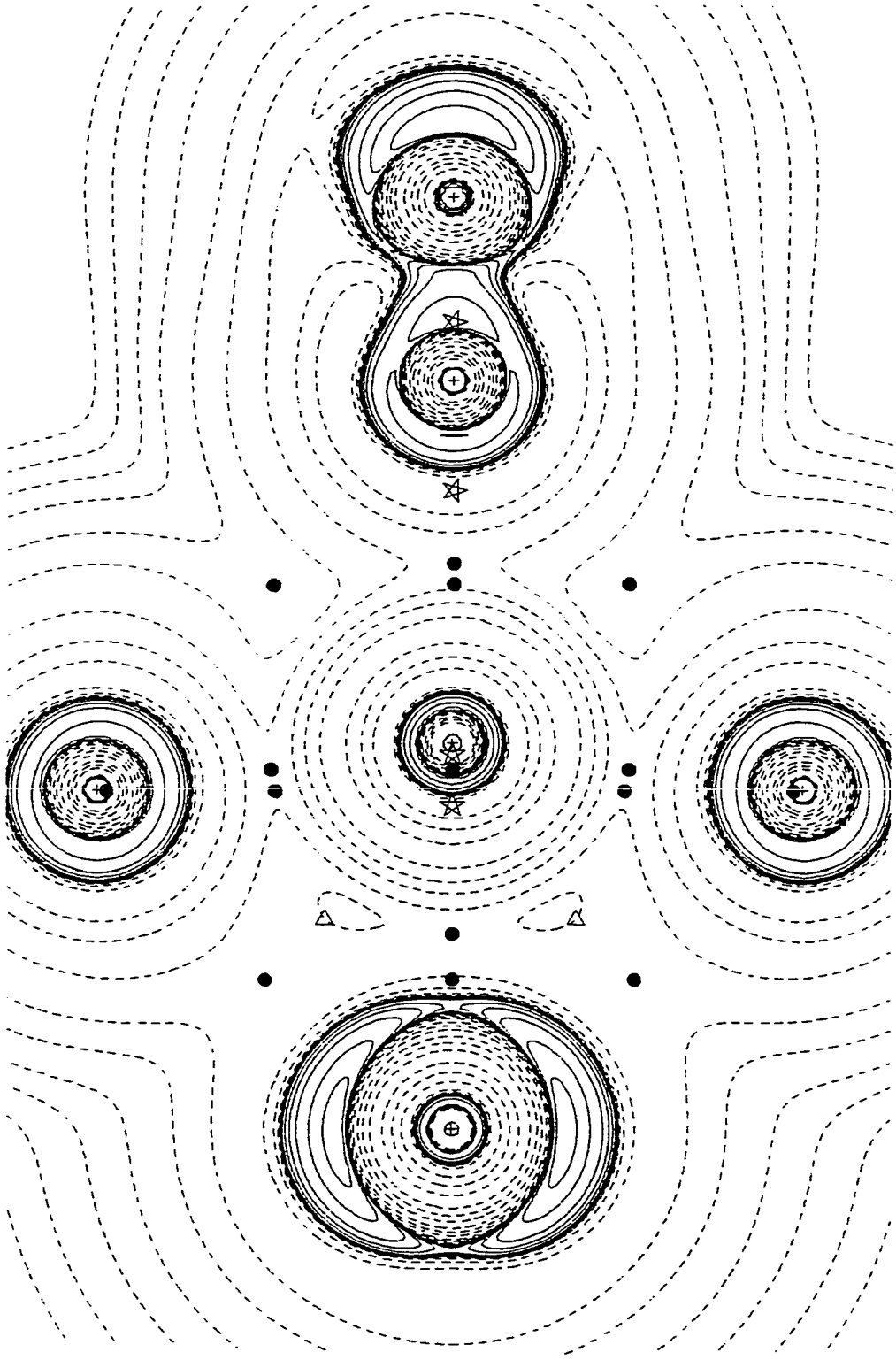

Figure 3-46. MgO surface with Mg in the center lifted above the plane of the surface oxygens, S under the layer, 0 charge on the cluster, CO with O down. The plot is perpendicular to the plane of the surface oxygens.

Chapter 4

Conclusions and Future Research

4.1 Conclusions from Chapters 2 and 3.

The original results from Chapters 2 and 3 are summarized as follows:

1. The different cluster models, 3x3x1, 3x3x2, and 5x5x1 had little effect on the optimized distance of the CO molecule from the surface, or the CO bond length.
2. The choice of basis set, STO-3G, LANL1DZ, and 3-21G* had little effect on the optimized distance of the CO molecule from the surface, or the CO bond length.
3. The 3-21G* basis set provides a better value for the dipole moment than the STO-3G basis set.
4. The choice of cluster model or basis set has little effect on binding energy with the exception where magnesium is the center atom, oxygen is below the layer and CO is oriented with carbon down. Here the binding energy was large compared to all other orientations. This appears to be related to the creation of a p(z) like hole in the sublayer oxygen. All calculated binding energies in Table 2-8 compare favorably with values produced experimentally and by other *ab initio* calculations.
5. The Laplacian of the electron charge density $-\nabla^2\rho$ provides information on the local charge concentrations of electron charge in the valence shell of an atom or molecule, duplicating the number, location, and size of

spatially localized electron pairs of the VSEPR model. The Laplacian also recovers the electronic shell model of an atom by producing a corresponding number of pairs of shells of charge concentration and depletion. It also efficiently points to unexpected reorganizations of the charge density that have significant chemical consequences. It is thus a valuable "data mining" tool.

4.2 Directions of Future Research.

Future research on the topic of adsorption of molecules on a metal oxide surface can take several different courses. Listed below are some of the possibilities for investigation in the future. This list is not exhaustive, as other topics and areas of interest will develop from the future research.

4.2.1 Surface defects and dislocations.

In this paper, the surface was considered "perfect". That is, there were no structural defects in the structure of the surface. Even in the 3x3x2 cluster model, the cluster was considered to be without defect. However, the study of the effect of defect sites on the adsorption of molecules is a topic of much interest and effort. Much of the chemistry at the surface of metal oxides is due to the presence of highly reactive defect sites[58]. There are two different types of defects that should be considered, dislocations and vacancies. Dislocations, such as edge, slip and screw

dislocations have received considerable attention[24,26,30,36,56]. There are two types of vacancies that are of possible consideration: 1) if the metal ion is missing, the vacancy is called a V center; 2) if the oxide ion is missing, the vacancy is called an F center. The effect of F and V centers on the reactivity of the adsorbing molecule is of interest[37,48,62,75,109,110]. In addition, an orientation of the MgO surface is a possibility. In this paper, the MgO(001) surface was considered. However it may prove interesting to study the MgO(111)surface and compare results from this surface with the MgO(001) surface and with the results of Hermansson, et. al.[111]

An example of this can be seen in the following. Figures 4-1, 4-2, 4-3, and 4-4 are the Laplacian plots for an MgO 3x3x1 cluster with 0 charge, which is expected for five Mg^{+2}, four O^{-2}, and one S^{-2} ions. The cluster is oriented so that there should be an oxygen in the center, but the central oxygen is replaced with a magnesium, and there is a sulfur atom under the central magnesium. The central magnesium is in the optimized position above the layer for this cluster configuration. From the contour plots it can be seen that the O/Mg substitution combined with the sulfur impurity modifies the central magnesium ion's VSCC to resemble that of a d-block transition metal. The magnesium has d-like valence shell charge concentrations as seen in the clover leaf pattern[112]. There is a pair of corresponding

d orbitals, d_{xz} and d_{yz}. The cause of this modification of the VSCC, as well as the chemical consequences are a subject for future research.

4.2.2 Dopants in the Surface.

The interaction of simple adsorbates and the surfaces of metal oxides has been extensively used as a test case of theoretical models of chemisorption on ionic surfaces[34]. The effect of impurities is of great importance in the study of adsorption on surfaces. Alkali-doped metal oxides have been successfully employed in the synthesis of ethane and other higher hydrocarbons from natural gas[28,29,113]. The presence of impurities, or dopants, in the surface or under the surface layer can have an effect on the surface properties such as adsorption energy and binding site preference[20,24,30,36,56,75]. Impurities such as Li, Na, and K cause increases in the number of O^- sites (as opposed to the usual O^{-2}) in the surface[114]. Ca and Fe as dopants have also been studied[24]. The effect of these and other impurities on the acidic or basic nature of the metal oxide surface can determine its catalytic activity towards an adsorbed species. It is important to establish some general rules to rationalize and predict the acidic/basic character of the different sites and different oxides.

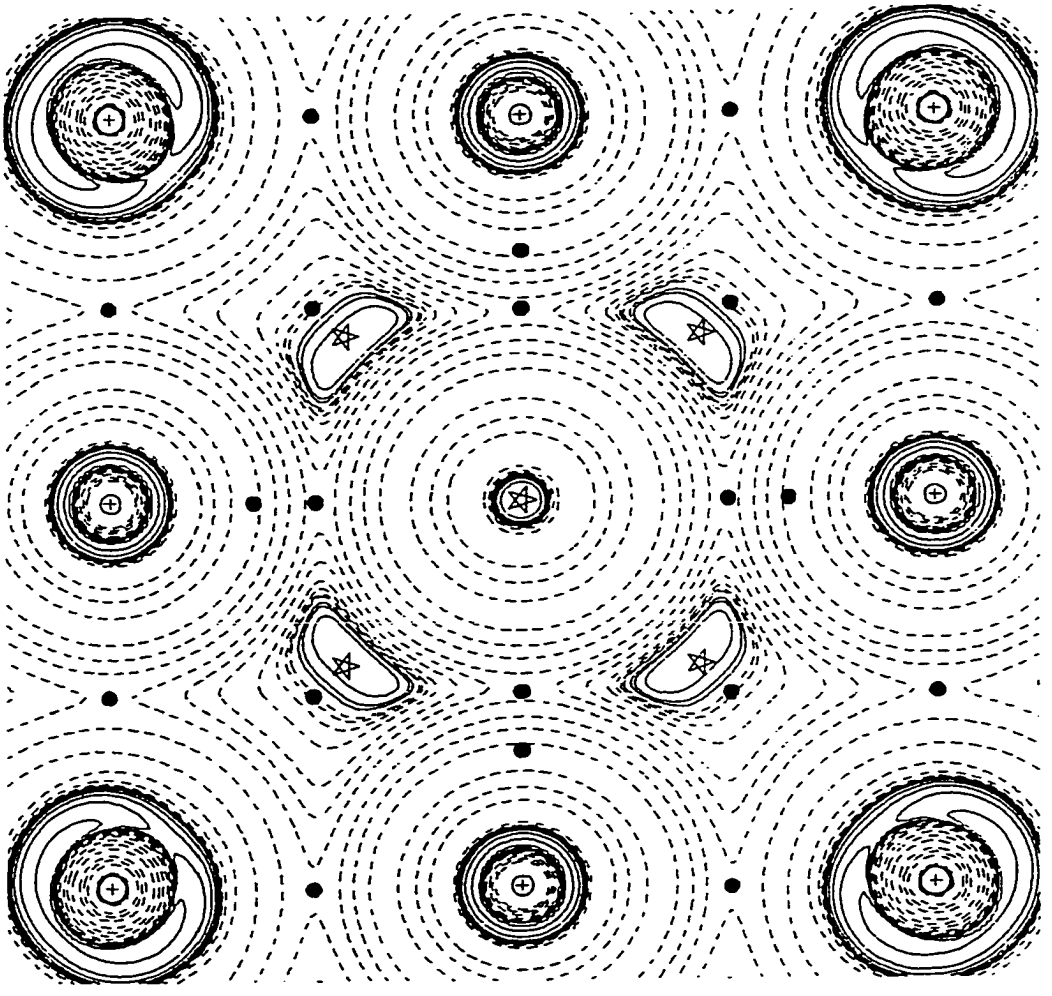

Figure 4-1. MgO surface with Mg in the center lifted above the plane of the surface oxygens, and adjacent to the center Mg, O in the corners, S under the central Mg. The plot is in the plane of the surface oxygens and shows the cloverleaf pattern of the Laplacian of the electron density around the central Mg. This suggests the Mg atom has d -like valence shell electrons.

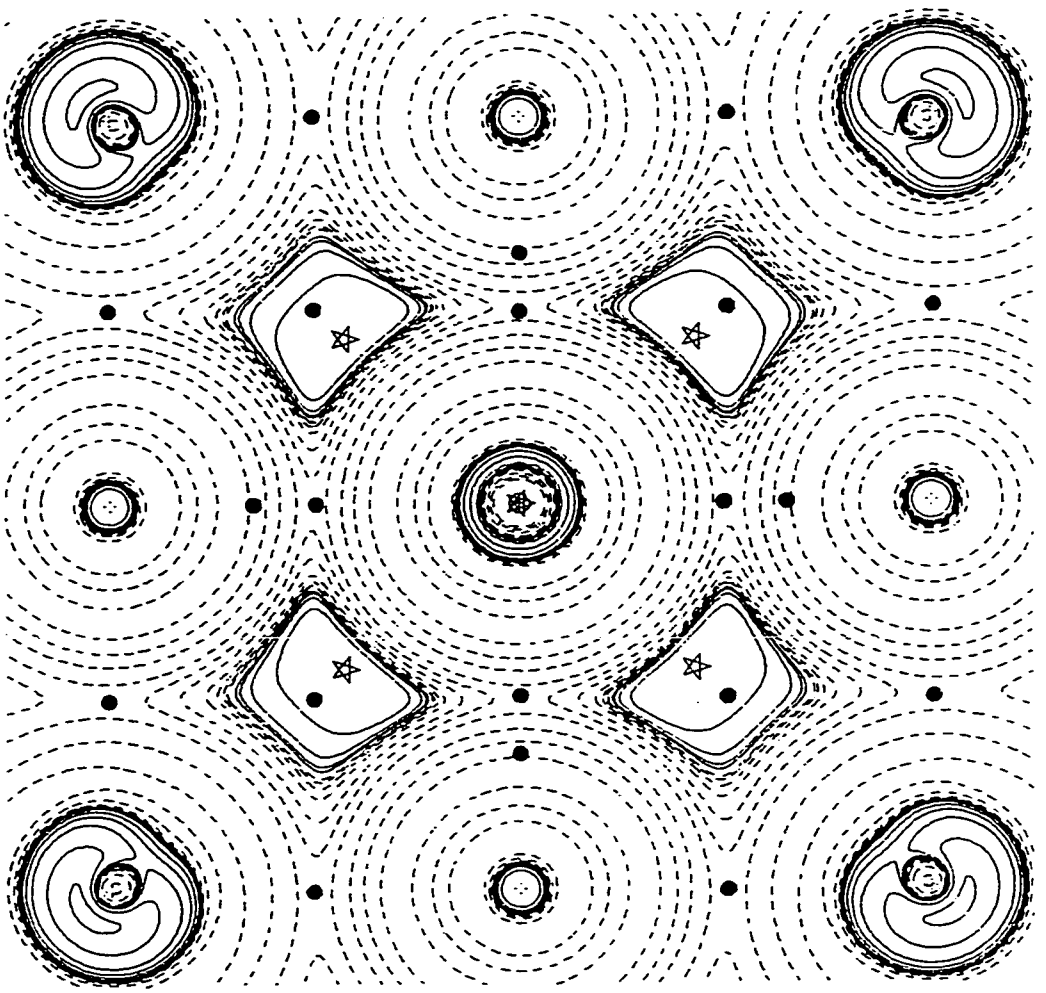

Figure 4-2. MgO surface with Mg in the center lifted above the plane of the surface oxygens, and adjacent to the center Mg, O in the corners, S under the central Mg showing the cloverleaf pattern around the central Mg. The plot is parallel to the plane of the surface oxygens through the central Mg.

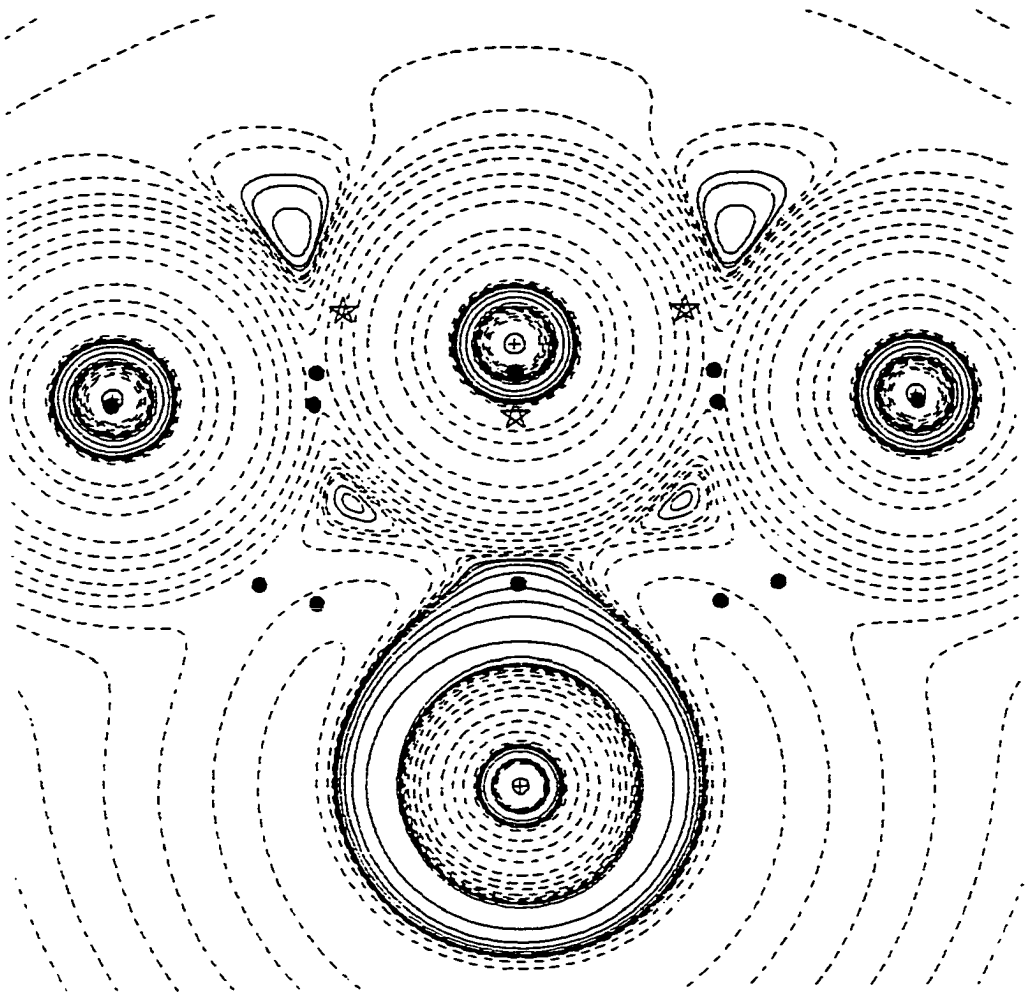

Figure 4-3. MgO surface with Mg in the center lifted above the plane of the surface oxygens, and adjacent to the center Mg, O in the corners, S under the central Mg. The plot is perpendicular to the surface through the three Mg atoms.

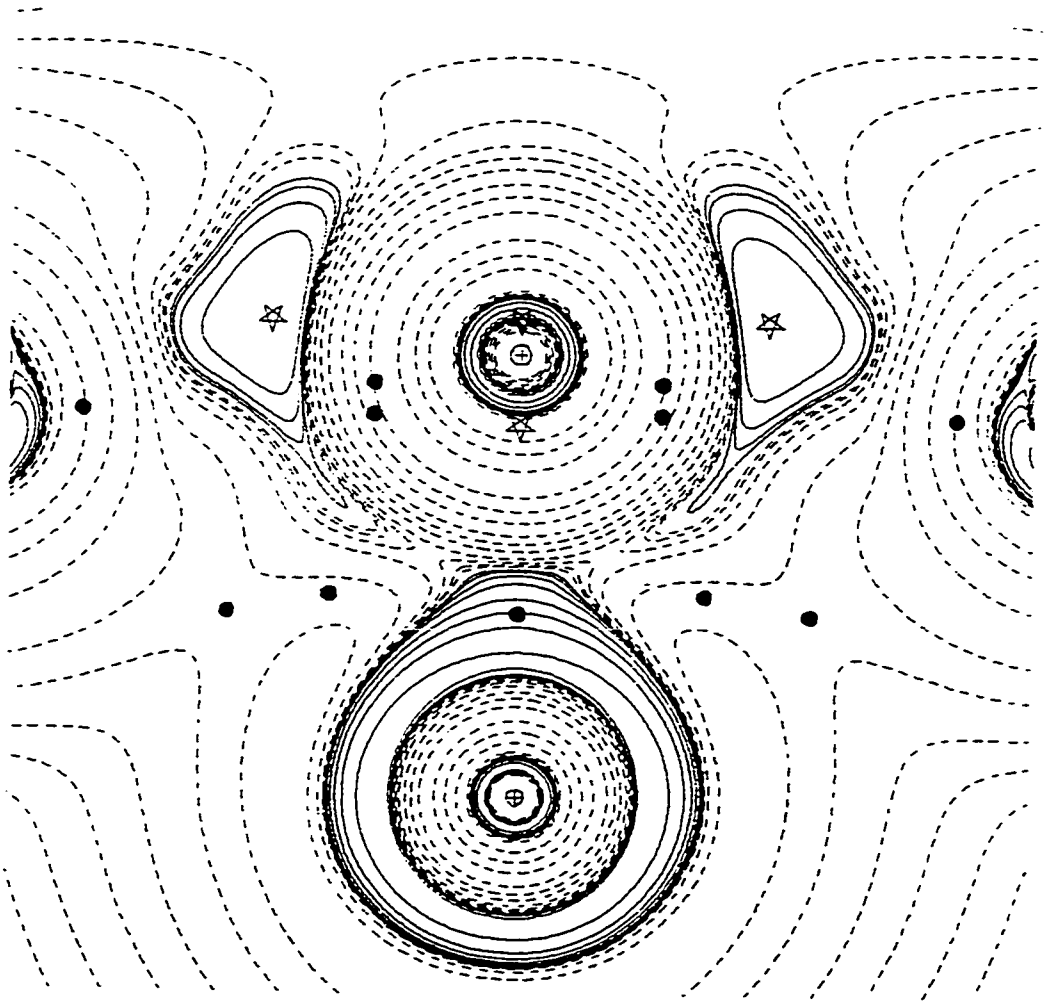

Figure 4-4. MgO surface with Mg in the center lifted above the plane of the surface oxygens, and adjacent to the center Mg, O in the corners, S under the central Mg. The plot is perpendicular to the surface through the central Mg and two corner O atoms.

4.2.3 Different metal-oxide surfaces.

The present study involved the MgO surface. However, there are other metal-oxide surfaces of interest, such as NiO[18,34,115], CaO[23], ZnO[46], Al_2O_3 and NiO[49], and KCl[62] which is not a metal-oxide surface but is chosen for its high ionicity and the vast literature on its defects and their optical and paramagnetic manifestations. As mentioned above, the different oxides have different acidic/basic characteristics which influence their effect on the adsorbed molecules.

4.2.4 Different molecules adsorbing on the surface.

There are many molecules that have proven interesting in the study of adsorption on metal-oxide surfaces. Some possible choices that are of interest are H_2[30,111,116], H_2O[24,25], H_2CO[22], and CO_2[48]. For example, H_2 adsorption on an oxide surface is an essential step in many catalytic processes[111]. The H_2 molecule is nonpolar, has a low polarizability, and a very strong H-H bond. This means H_2 will only adsorb on the most reactive oxide surfaces. There are others that could also prove useful in the study of surfaces.

4.2.5 Oxidative coupling of methane.

There has been a lot of interest in the study of the oxidative coupling of methane on Li doped surfaces[28,117] and Pb and Sn doped surfaces[29]. This research is of practical significance due to the use of natural gas (which has methane as the most abundant component) as a raw material in the synthesis of C_2-compounds which are more valuable chemicals. Due to the remote locations of most natural gas reserves, the transportation of methane can be more reasonable if it is first converted to more useful liquid hydrocarbons. Previous methods for methane conversion have proven cost prohibitive[118]. Developing a more cost effective catalytic conversion method is of great interest and technological significance. This would be an area for future research.

4.2.6 Electron density and the VSEPR model of molecular geometry.

Further investigations using the electron density and the Laplacian of the electron density and their correlation to the VSEPR model are warranted. Many researchers are using electron density differences, EDD, or charge density differences, in investigations of molecular properties and geometries[21,31-33,35]. The electron density difference is obtained by substracting the densities of the isolated

spherical atoms from the observed total electron density. Bader showed that subtracting the density of an atom that had one electron pointing in the direction of the bond to be formed, and axially averaging the others, versus subtracting spherical atoms (which is usually done) would produce completely different interpretations[120]. Bader also showed that using spherical atoms produces a greater density difference in the nonbonding region than the bonding region[106]. Gillespie has shown that there are problems associated in the interpretation of EDD plots. The EDD plot for tetrafluoroterephthalonitrile shows no density in the C-F bond regions. "The problem arises because the subtraction of the spherical densities of isolated atoms is an arbitrary procedure that cannot be theoretically justified."[25] Obviously there is a great oportunity for future research in this area.

4.2.7 The effect of cluster size on electronic and adsorption properties.

The effect of the size of the cluster and cluster topology on such properties as cluster stability, band gap, adsorption geometry and binding energy have recently been investigated[119]. The topological parameters considered were the number of dangling bonds of a cut-out cluster and the average dangling bond on each in-cluster atom. In the

present work, these were not considered. In future investigations these could be included to determine the effect, if any, they have on the calculated values.

APPENDIX A

Archive Entries for GAUSSIAN 92 Jobs

1. 5x5x1 with Mg in the center, nothing under the layer, CO with C down, 0 charge on the cluster, STO-3G basis set.

1|1|GINC-UNK|POPT|RHF|STO-3G|C1Mg13O13|PCUSER|21-Mar-1999|1|
|#RHF/STO-3G OPT SCFCONV=8 SCFCYC=99 OPTCYC=99 POP=REG
OUT=WFN TEST||5x5x1, CO opt, C down, STO-3G|
|0,1|Mg,0,0.,0.,0.|O,0,2.1,0.,0.|Mg,0,4.2,0.,0.|O,0,6.3,0.,
0.|Mg,0,8.4,0.,0.|O,0,0.,2.1,0.|Mg,0,2.1,2.1,0.|O,0,4.2,2.1,
0.|Mg,0,6.3,2.1,0.|O,0,8.4,2.1,0.|Mg,0,0.,4.2,0.|O,0,2.1,4.2
,0.|Mg,0,4.2,4.2,0.|O,0,6.3,4.2,0.|Mg,0,8.4,4.2,0.|O,0,0.,6.
3,0.|Mg,0,2.1,6.3,0.|O,0,4.2,6.3,0.|Mg,0,6.3,6.3,0.|O,0,8.4,
6.3,0.|Mg,0,0.,8.4,0.|O,0,2.1,8.4,0.|Mg,0,4.2,8.4,0.|O,0,6.3
,8.4,0.|Mg,0,8.4,8.4,0.|C,0,Cx,Cy,Cz|O,0,Ox,Oy,Oz||Cz=2.5334
6992|Oz=3.67883569|Cx=4.2|Cy=4.2|Ox=4.2|Oy=4.2||Version=486-
Windows-G92RevE.1|HF=-3560.0664484|RMSD=7.372e-009|RMSF=4.06
2e-002|Dipole=0.000007,0.0000076,0.1724848|PG=C04V[C4(O1C1Mg
1),2SGV(Mg2O2),2SGD(Mg4),X(O8)]||@

2. 5x5x1 with Mg in the center, nothing under the layer, CO with C down, 0 charge on the cluster, LANL1DZ basis set.

1|1|GINC-UNK|FOPT|RHF|LANL1DZ|C1Mg13O13|PCUSER|14-Oct-1997|1
||#RHF/LANL1DZ OPT SCFCYC=80 POP=REG OUT=WFN TEST||5x5x1, CO
opt, C down, LANL1DZ|
|0,1|Mg,0,0.,0.,0.|O,0,2.1,0.,0.|Mg,0,4.2,0.,0.|O,0,6.3,0.,
0.|Mg,0,8.4,0.,0.|O,0,0.,2.1,0.|Mg,0,2.1,2.1,0.|O,0,4.2,2.1,
0.|Mg,0,6.3,2.1,0.|O,0,8.4,2.1,0.|Mg,0,0.,4.2,0.|O,0,2.1,4.2
,0.|Mg,0,4.2,4.2,0.|O,0,6.3,4.2,0.|Mg,0,8.4,4.2,0.|O,0,0.,6.
3,0.|Mg,0,2.1,6.3,0.|O,0,4.2,6.3,0.|Mg,0,6.3,6.3,0.|O,0,8.4,
6.3,0.|Mg,0,0.,8.4,0.|O,0,2.1,8.4,0.|Mg,0,4.2,8.4,0.|O,0,6.3
,8.4,0.|Mg,0,8.4,8.4,0.|C,0,Cx,Cy,Cz|O,0,Ox,Oy,Oz||Cx=4.1999
342|Cy=4.20000861|Cz=2.59571647|Ox=4.19985078|Oy=4.20001951|
Oz=3.73015128||Version=486-Windows-G92RevE.1|HF=-1022.477332
9|RMSD=8.609e-009|RMSF=1.806e-002|Dipole=0.0000272,-0.000007
9,-0.0955888|PG=||@

3. 5x5x1 with Mg in the center, nothing under the layer, CO with C down, 0 charge on the cluster, 3-21G* basis set.

1|1|GINC-UNK|FOPT|RHF|3-21G*|C1Mg13O13|PCUSER|25-Oct-1997|1|
|#RHF/3-21G* OPT SCFCYC=80 POP=REG OUT=WFN TEST||5x5x1, CO
opt, C down, 3-21G*|
|0,1|Mg,0,0.,0.,0.|O,0,2.1,0.,0.|Mg,0,4.2,0.,0.|O,0,6.3,0.,
0.|Mg,0,8.4,0.,0.|O,0,0.,2.1,0.|Mg,0,2.1,2.1,0.|O,0,4.2,2.1,
0.|Mg,0,6.3,2.1,0.|O,0,8.4,2.1,0.|Mg,0,0.,4.2,0.|O,0,2.1,4.2
,0.|Mg,0,4.2,4.2,0.|O,0,6.3,4.2,0.|Mg,0,8.4,4.2,0.|O,0,0.,6.
3,0.|Mg,0,2.1,6.3,0.|O,0,4.2,6.3,0.|Mg,0,6.3,6.3,0.|O,0,8.4,
6.3,0.|Mg,0,0.,8.4,0.|O,0,2.1,8.4,0.|Mg,0,4.2,8.4,0.|O,0,6.3
,8.4,0.|Mg,0,8.4,8.4,0.|C,0,Cx,Cy,Cz|O,0,Ox,Oy,Oz||Cx=4.1999
4476|Cy=4.2000073|Cz=2.42889025|Ox=4.19987214|Oy=4.2000169|O
z=3.55450552||Version=486-Windows-G92RevE.1|HF=-3587.6020385
|RMSD=8.519e-009|RMSF=2.181e-002|Dipole=0.0000116,-0.000002,
0.0020869|PG=||@

4. 3x3x2 with Mg in the center, CO with C down, 0 charge on the cluster, STO-3G basis set.

1|1|GINC-UNK|SP|RHF|STO-3G|C1Mg9O10|PCUSER|15-Feb-1998|0||#R
HF/STO-3G POP=REG OUT=WFN TEST||3x3x2 Opt for CO, C down,
STO-3G|
|0,1|O,0,0.,0.,0.|Mg,0,2.1,0.,0.|O,0,4.2,0.,0.|Mg,0,0.,2.1,
0.|O,0,2.1,2.1,0.|Mg,0,4.2,2.1,0.|O,0,0.,4.2,0.|Mg,0,2.1,4.2
,0.|O,0,4.2,4.2,0.|Mg,0,0.,0.,2.1|O,0,2.1,0.,2.1|Mg,0,4.2,0.
,2.1|O,0,0.,2.1,2.1|Mg,0,2.1,2.1,2.1|O,0,4.2,2.1,2.1|Mg,0,0.
,4.2,2.1|O,0,2.1,4.2,2.1|Mg,0,4.2,4.2,2.1|C,0,2.1,2.1,4.6797
|O,0,2.1,2.1,5.8251||Version=486-Windows-G92RevE.1|State=1-A
1|HF=-2550.4865894|RMSD=1.717e-005|Dipole=0.,0.,4.2502659|PG
=C04V [C4(O1Mg1C1O1),2SGV(Mg2O2),2SGD(Mg2O2)]||@

5. 3x3x2 with Mg in the center, CO with C down, 0 charge on the cluster, LANL1DZ basis set.

1|1|GINC-UNK|SP|RHF|LANL1DZ|C1Mg9O10|PCUSER|12-Nov-1997|0||#
RHF/LANL1DZ POP=REG OUT=WFN TEST||3x3x2, Opt for CO, C down,
3-21G*|
|0,1|O,0,0.,0.,0.|Mg,0,2.1,0.,0.|Mg,0,0.,2.1,0.|Mg,0,0.,0.,
2.1|O,0,4.2,0.,0.|O,0,2.1,0.,2.1|Mg,0,4.2,0.,2.1|O,0,0.,2.1,
2.1|O,0,2.1,2.1,0.|Mg,0,2.1,2.1,2.1|Mg,0,4.2,2.1,0.|O,0,0.,4
.2,0.|Mg,0,0.,4.2,2.1|Mg,0,2.1,4.2,0.|O,0,2.1,4.2,2.1|O,0,4.
2,4.2,0.|Mg,0,4.2,4.2,2.1|O,0,4.2,2.1,2.1|C,0,2.1,2.1,4.8924
8622|O,0,2.1,2.1,6.02775295||Version=486-Windows-G92RevE.1|S
tate=1-A1|HF=-794.5316994|RMSD=4.373e-005|Dipole=0.,0.,5.692
0582|PG=C04V[C4(O1Mg1C1O1),2SGV(Mg2O2),2SGD(Mg2O2)]||@

6. 3x3x2 with Mg in the center, CO with C down, 0 charge on the cluster, 3-21G* basis set.

1|1|GINC-UNK|POPT|RHF|3-21G*|C1Mg9O10|PCUSER|21-Mar-1999|1||
#RHF/3-21G* OPT POP=REG OUT=WFN SCFCONV=8 OPTCYC=99
SCFCYC=99 TEST||3x3x2 Opt for CO, 3-21G*, C down
||0,1|O,0,0.,0.,0.|Mg,0,2.1,0.,0.|Mg,0,0.,2.1,0.|Mg,0,0.,0.,
2.1|O,0,4.2,0.,0.|O,0,2.1,0.,2.1|Mg,0,4.2,0.,2.1|O,0,0.,2.1,
2.1|O,0,2.1,2.1,0.|Mg,0,2.1,2.1,2.1|Mg,0,4.2,2.1,0.|O,0,0.,4
.2,0.|Mg,0,0.,4.2,2.1|Mg,0,2.1,4.2,0.|O,0,2.1,4.2,2.1|O,0,4.
2,4.2,0.|Mg,0,4.2,4.2,2.1|O,0,4.2,2.1,2.1|C,0,Cx,Cy,Cz|O,0,O
x,Oy,Oz||Cz=4.58574906|Oz=5.71182892|Cx=2.1|Cy=2.1|Ox=2.1|Oy
=2.1||Version=486-Windows-G92RevE.1|State=1-A1|HF=-2570.0666
671|RMSD=8.579e-009|RMSF=2.990e-002|Dipole=0.,0.,5.2617772|P
G=C04V[C4(O1Mg1C1O1),2SGV(Mg2O2),2SGD(Mg2O2)]||@

7. 3x3x1 with Mg in the center, 0 charge on the cluster, CO with C down, STO-3G basis set.

1|1|GINC-UNK|SP|RHF|STO-3G|C1Mg5O5|PCUSER|08-Feb-1998|0||#RH
F/STO-3G POP=REG OUT=WFN TEST||MgO Opt for CO, C down,
3x3x1||0,1|Mg,0,0.,0.,0.|O,0,2.1,0.,0.|O,0,0.,2.1,0.|Mg,0,4.
2,0.,0.|Mg,0,2.1,2.1,0.|O,0,4.2,2.1,0.|Mg,0,0.,4.2,0.|O,0,2.
1,4.2,0.|Mg,0,4.2,4.2,0.|C,0,2.1,2.1,2.5508|O,0,2.1,2.1,3.69
648||Version=486-Windows-G92RevE.1|State=1-A1|HF=-1391.93191
58|RMSD=6.591e-005|Dipole=0.,0.,0.1592209|PG=C04V [C4(O1
C1Mg1),2SGV(O2),2SGD(Mg2)]||@

8. 3x3x1 with Mg in the center, 0 charge on the cluster, CO with C down, LANL1DZ basis set.

1|1|GINC-UNK|SP|RHF|LANL1DZ|C1Mg5O5|PCUSER|07-Mar-1998|0||#R
HF/LANL1DZ POP=REG OUT=WFN TEST||MgO, 3x3x1, CO, LANL1DZ
||0,1|Mg,0,0.,0.,0.|O,0,2.1,0.,0.|Mg,0,4.2,0.,0.|O,0,0.,2.1,
0.|Mg,0,2.1,2.1,0.|O,0,4.2,2.1,0.|Mg,0,0.,4.2,0.|O,0,2.1,4.2
,0.|Mg,0,4.2,4.2,0.|C,0,2.1,2.1,2.67769|O,0,2.1,2.1,3.81337|
|Version=486-Windows-G92RevE.1|State=1-A1|HF=-416.276342|RMS
D=2.644e-005|Dipole=0.,0.,-0.171382|PG=C04V[C4(O1C1Mg1),2SGV
(O2),2SGD(Mg2)]||@

9. 3x3x1 with Mg in the center, nothing under the layer, 0 charge on the cluster, CO with C down, 3-21G* basis set.

1|1|GINC-UNK|SP|RHF|3-21G*|C1Mg5O5|PCUSER|10-Mar-1998|0||#RH
F/3-21G* POP=REG OUT=WFN TEST||MgO CO, 3x3x1 layer, C down
3-21G*|
|0,1|Mg,0,0.,0.,0.|O,0,2.1,0.,0.|Mg,0,4.2,0.,0.|O,0,0.,2.1,
0.|Mg,0,2.1,2.1,0.|O,0,4.2,2.1,0.|Mg,0,0.,4.2,0.|O,0,2.1,4.2
,0.|Mg,0,4.2,4.2,0.|C,0,2.1,2.1,2.478098|O,0,2.1,2.1,3.60449
1||Version=486-Windows-G92RevE.1|State=1-A1|HF=-1402.7192746
|RMSD=2.023e-005|Dipole=0.,0.,-0.0349321|PG=C04V[C4(O1C1Mg1)
,2SGV(O2),2SGD(Mg2)]||@

10. CO with STO-3G

1|1|GINC-UNK|FOPT|RHF|STO-3G|C1O1|PCUSER|05-Apr-1999|1||#RHF
/STO-3G OPT OPTCYC=99 SCFCONV=8 SCFCYC=99 POP=REG OUT=WFN
TEST||Opt for CO separation, STO-3G basis set|
|0,1|C,0,0.,0.,0.|O,0,Ox,Oy,Oz||Oz=1.14551362|Ox=0.|Oy=0.||V
ersion=486-Windows-G92RevE.1|State=1-SG|HF=-111.2254495|RMSD
=6.595e-011|RMSF=5.640e-005|Dipole=0.,0.,0.0488989|PG=C*V[C*
(C1O1)]||@

11. CO with LANL1DZ

1|1|GINC-UNK|FOPT|RHF|LANL1DZ|C1O1|PCUSER|05-Apr-1999|1||#RH
F/LANL1DZ OPT OPTCYC=99 SCFCONV=8 SCFCYC=99 POP=REG OUT=WFN
TEST||Opt for CO separation, LANL1DZ basis set|
|0,1|C,0,0.,0.,0.|O,0,Ox,Oy,Oz||Oz=1.13793916|Ox=0.|Oy=0.||V
ersion=486-Windows-G92RevE.1|State=1-SG|HF=-112.6850704|RMSD
=7.509e-009|RMSF=5.791e-006|Dipole=0.,0.,-0.1878874|PG=C*V[C
*(C1O1)]||@

12. CO with 3-21G* basis set.

1|1|GINC-UNK|FOPT|RHF|3-21G*|C1O1|PCUSER|05-Apr-1999|1||#RHF
/3-21G* OPT OPTCYC=99 SCFCONV=8 SCFCYC=99 POP=REG OUT=WFN
TEST||Opt for CO separation, 3-21G* basis set|
|0,1|C,0,0.,0.,0.|O,0,Ox,Oy,Oz||Oz=1.12895962|Ox=0.|Oy=0.||V
ersion=486-Windows-G92RevE.1|State=1-SG|HF=-112.093299|RMSD=
2.034e-009|RMSF=1.548e-005|Dipole=0.,0.,-0.1563025|PG=C*V[C*
(C1O1)]||@

13. 3x3x1 with Mg in the center, nothing under the layer, 0 charge on the cluster, no CO, STO-3G Basis set.

1|1|GINC-UNK|SP|RHF|STO-3G|Mg5O4|PCUSER|02-Jan-1999|0||#RHF/
STO-3G SCFCYC=99 SCFCONV=8 POP=REG OUT=WFN TEST||MgO, 3x3x1
layer, STO-3G Basis set, No CO|
|0,1|Mg,0,0.,0.,0.|O,0,2.1,0.,0.|Mg,0,4.2,0.,0.|O,0,0.,2.1,0
.|Mg,0,2.1,2.1,0.|O,0,4.2,2.1,0.|Mg,0,0.,4.2,0.|O,0,2.1,4.2,
0.|Mg,0,4.2,4.2,0.||Version=486-Windows-G92RevE.1|State=1-A1
G|HF=-1280.7021438|RMSD=9.638e-009|Dipole=0.,0.,0.|PG=D04H[O
(Mg1),2C2'(O1.O1),2C2"(Mg1.Mg1)]||@

14. 3x3x1 with Mg in the center, nothing under the layer, 0 charge on the cluster, no CO, LANL1DZ Basis set.

1|1|GINC-UNK|SP|RHF|LANL1DZ|Mg5O4|PCUSER|02-Jan-1999|0||#RHF
/LANL1DZ SCFCYC=99 SCFCONV=8 POP=REG OUT=WFN TEST||MgO,
3x3x1 layer, LANL1DZ Basis set, No CO|
|0,1|Mg,0,0.,0.,0.|O,0,2.1,0.,0.|Mg,0,4.2,0.,0.|O,0,0.,2.1,0
.|Mg,0,2.1,2.1,0.|O,0,4.2,2.1,0.|Mg,0,0.,4.2,0.|O,0,2.1,4.2,
0.|Mg,0,4.2,4.2,0.||Version=486-Windows-G92RevE.1|State=1-A1
G|HF=-303.5861729|RMSD=1.865e-009|Dipole=0.,0.,0.|PG=D04H
[O(Mg1),2C2'(O1.O1),2C2"(Mg1.Mg1)]||@

15. 3x3x1 with Mg in the center, nothing under the layer, 0 charge on the cluster, no CO, 3-21G* Basis set.

```
1|1|GINC-UNK|SP|RHF|3-21G*|Mg5O4|PCUSER|02-Jan-1999|0||#RHF/
3-21G* SCFCYC=99 SCFCONV=8 POP=REG OUT=WFN TEST||MgO, 3x3x1
layer, 3-21G*Basis set, No CO|
|0,1|Mg,0,0.,0.,0.|O,0,2.1,0.,0.|Mg,0,4.2,0.,0.|O,0,0.,2.1,0
.|Mg,0,2.1,2.1,0.|O,0,4.2,2.1,0.|Mg,0,0.,4.2,0.|O,0,2.1,4.2,
0.|Mg,0,4.2,4.2,0.||Version=486-Windows-G92RevE.1|State=1-A1
G|HF=-1290.6133559|RMSD=4.789e-009|Dipole=0.,0.,0.|PG=D04H[O
(Mg1),2C2'(O1.O1),2C2"(Mg1.Mg1)]||@
```

16. 3x3x1 with Mg in the center, nothing under the layer, +2 charge on the cluster, no CO, STO-3G basis set.

```
1|1|GINC-UNK|SP|RHF|STO-3G|Mg5O4(2+)|PCUSER|22-May-1999|0||#
RHF/STO-3G POP=REG SCFCONV=8 SCFCYC=99 OUT=WFN TEST||3x3x1
Mg in the center, No CO, STO-3G basis set +2 Charge on
the cluster|
|2,1|Mg,0,0.,0.,0.|O,0,2.1,0.,0.|O,0,0.,2.1,0.|Mg,0,4.2,0.,0
.|Mg,0,2.1,2.1,0.|O,0,4.2,2.1,0.|Mg,0,0.,4.2,0.|O,0,2.1,4.2,
0.|Mg,0,4.2,4.2,0.||Version=486-Windows-G92RevE.1|State=1-A1
G|HF=-1280.7391072|RMSD=8.897e-009|Dipole=0.,0.,0.|PG=D04H[O
(Mg1),2C2'(O1.O1),2C2"(Mg1.Mg1)]||@
```

17. 3x3x1 with Mg in the center, nothing under the layer, +2 charge on the cluster, no CO, LANL1DZ basis set.

```
1|1|GINC-UNK|SP|RHF|LANL1DZ|Mg5O4(2+)|PCUSER|27-May-1999|0||
#RHF/LANL1DZ POP=REG OUT=WFN TEST SCFCONV=8||MgO 3x3x1 with
+2 charge on the cluster, No CO, LANL1DZ basis set|
|2,1|Mg,0,0.,0.,0.|O,0,2.1,0.,0.|O,0,0.,2.1,0.|Mg,0,4.2,0.,0
.|Mg,0,2.1,2.1,0.|O,0,4.2,2.1,0.|Mg,0,0.,4.2,0.|O,0,2.1,4.2,
0.|Mg,0,4.2,4.2,0.||Version=486-Windows-G92RevE.1|State=1-A1
G|HF=-303.2143423|RMSD=7.997e-009|Dipole=0.,0.,0.|PG=D04H[O(
Mg1),2C2'(O1.O1),2C2"(Mg1.Mg1)]||@
```

18. 3x3x1 with Mg in the center, nothing under the layer, +2 charge on the cluster, no CO, 3-21G* basis set.

```
1|1|GINC-UNK|SP|RHF|3-21G*|Mg5O4(2+)|PCUSER|27-May-1999|0||#
RHF/3-21G* POP=REG OUT=WFN TEST SCFCONV=8||MgO 3x3x1 with +2
charge on the cluster, No CO, 3-21G* basis set|
|2,1|Mg,0,0.,0.,0.|O,0,2.1,0.,0.|O,0,0.,2.1,0.|Mg,0,4.2,0.,0
.|Mg,0,2.1,2.1,0.|O,0,4.2,2.1,0.|Mg,0,0.,4.2,0.|O,0,2.1,4.2,
0.|Mg,0,4.2,4.2,0.||Version=486-Windows-G92RevE.1|State=1-A1
G|HF=-1290.2433849|RMSD=9.997e-009|Dipole=0.,0.,0.|PG=D04H[O
(Mg1),2C2'(O1.O1),2C2"(Mg1.Mg1)]||@
```

19. 3x3x1 with Mg in the center, O under the layer, 0 charge on the cluster, no CO, STO-3G basis set.

1|1|GINC-UNK|SP|RHF|STO-3G|Mg5O5|PCUSER|05-Jul-1999|0||#RHF/STO-3G SCFCONV=8 SCFCYC=99 POP=REG OUT=WFN TEST||3x3x1, Mg in the center, O under the layer, STO-3G basis set||0,1|Mg,0,0.,0.,0.|O,0,2.1,0.,0.|Mg,0,4.2,0.,0.|O,0,0.,2.1,0.|O,0,4.2,2.1,0.|Mg,0,0.,4.2,0.|O,0,2.1,4.2,0.|Mg,0,4.2,4.2,0.|O,0,2.1,2.1,-2.1|Mg,0,2.1,2.1,0.||Version=486-Windows-G92RevE.1|State=1-A1|HF=-1354.3689015|RMSD=2.740e-009|Dipole=0.,0.,0.82431|PG=C04V [C4(O1Mg1),2SGV(O2),2SGD(Mg2)]||@

20. 3x3x1 with Mg in the center, O under the layer, 0 charge on the cluster, no CO, LANL1DZ basis set.

1|1|GINC-UNK|SP|RHF|LANL1DZ|Mg5O5|PCUSER|05-Jul-1999|0||#RHF/LANL1DZ SCFCYC=99 SCFCONV=8 POP=REG OUT=WFN TEST||3x3x1, Mg in the center, O under the layer, no CO, LANL1DZ basis set||0,1|Mg,0,0.,0.,0.|O,0,2.1,0.,0.|Mg,0,4.2,0.,0.|O,0,0.,2.1,0.|Mg,0,2.1,2.1,0.|O,0,4.2,2.1,0.|Mg,0,0.,4.2,0.|O,0,2.1,4.2,0.|Mg,0,4.2,4.2,0.|O,0,2.1,2.1,-2.1||Version=486-Windows-G92RevE.1|State=1-A1|HF=-378.1805719|RMSD=3.475e-009|Dipole=0.,0.,3.7899721|PG=C04V [C4(O1Mg1),2SGV(O2),2SGD(Mg2)]||@

21. 3x3x1 with Mg in the center, O under the layer, 0 charge on the cluster, no CO, 3-21G* basis set.

1|1|GINC-UNK|SP|RHF|3-21G*|Mg5O5|PCUSER|05-Jul-1999|0||#RHF/3-21G* SCFCONV=8 SCFCYC=99 POP=REG OUT=WFN TEST||MgO 3x3x1 with O under the layer, No CO 3-21G* basis set||0,1|Mg,0,0.,0.,0.|O,0,2.1,0.,0.|O,0,0.,2.1,0.|Mg,0,4.2,0.,0.|Mg,0,2.1,2.1,0.|O,0,4.2,2.1,0.|Mg,0,0.,4.2,0.|O,0,2.1,4.2,0.|Mg,0,4.2,4.2,0.|O,0,2.1,2.1,-2.1||Version=486-Windows-G92RevE.1|State=1-A1|HF=-1364.8057892|RMSD=4.877e-009|Dipole=0.,0.,3.1953517|PG=C04V [C4(O1Mg1),2SGV(O2),2SGD(Mg2)]||@

22. 3x3x1 with Mg in the center, nothing under the layer, +2 charge on the cluster, CO with C down, STO-3G basis set.

1|1|GINC-UNK|POPT|RHF|STO-3G|C1Mg5O5(2+)|PCUSER|23-May-1999|1||#RHF/STO-3G OPT POP=REG OPTCYC=200 SCFCONV=8 SCFCYC=200 OUT=WFN TEST||3x3x1 Mg in the center, opt for CO, STO-3G basis set +2 Charge on the cluster||2,1|Mg,0,0.,0.,0.|O,0,2.1,0.,0.|O,0,0.,2.1,0.|Mg,0,4.2,0.,0.|Mg,0,2.1,2.1,0.|O,0,4.2,2.1,0.|Mg,0,0.,4.2,0.|O,0,2.1,4.2,0.|Mg,0,4.2,4.2,0.|C,0,Cx,Cy,Cz|O,0,Ox,Oy,Oz||Cz=2.50161158|Oz=3.64427184|Cx=2.1|Cy=2.1|Ox=2.1|Oy=2.1||Version=486-Windows-G92RevE.1|State=1-A1|HF=-1391.9739662|RMSD=3.280e-009|RMSF=5.906e-002|Dipole=0.,0.,-1.2381237|PG=C04V[C4(O1C1Mg1),2SGV(O2),2SGD(Mg2)]||@

23. 3x3x1 with Mg in the center, nothing under the layer, +2 charge on the cluster, CO with C down, LANL1DZ basis set.

1|1|GINC-UNK|POPT|RHF|LANL1DZ|C1Mg5O5(2+)|PCUSER|26-May-1999|1||#RHF/LANL1DZ OPT POP=REG OPTCYC=200 SCFCONV=8 SCFCYC=200 OUT=WFN TEST||3x3x1 Mg center, opt for CO, LANL1DZ,+2 Charge||2,1|Mg,0,0.,0.,0.|O,0,2.1,0.,0.|O,0,0.,2.1,0.|Mg,0,4.2,0.,0.|Mg,0,2.1,2.1,0.|O,0,4.2,2.1,0.|Mg,0,0.,4.2,0.|O,0,2.1,4.2,0.|Mg,0,4.2,4.2,0.|C,0,Cx,Cy,Cz|O,0,Ox,Oy,Oz||Cz=2.640238|Oz=3.77040868|Cx=2.1|Cy=2.1|Ox=2.1|Oy=2.1||Version=486-Windows-G92RevE.1|State=1-A1|HF=-415.9051264|RMSD=6.778e-009|RMSF=2.839e-002|Dipole=0.,0.,-1.5535187|PG=C04V[C4(O1C1Mg1),2SGV(O2),2SGD(Mg2)]||@

24. 3x3x1 with Mg in the center, nothing under the layer, +2 charge on the cluster, CO with C down, 3-21G* basis set.

1|1|GINC-UNK|POPT|RHF|3-21G*|C1Mg5O5(2+)|PCUSER|25-May-1999|1||#RHF/3-21G* OPT POP=REG OPTCYC=200 SCFCONV=8 SCFCYC=200 OUT=WFN TEST||3x3x1 Mg in the center, opt for CO, 3-21G* basis set +2 Charge on the cluster
||2,1|Mg,0,0.,0.,0.|O,0,2.1,0.,0.|O,0,0.,2.1,0.|Mg,0,4.2,0.,0.|Mg,0,2.1,2.1,0.|O,0,4.2,2.1,0.|Mg,0,0.,4.2,0.|O,0,2.1,4.2,0.|Mg,0,4.2,4.2,0.|C,0,Cx,Cy,Cz|O,0,Ox,Oy,Oz||Cz=2.4679809|Oz=3.5904292|Cx=2.1|Cy=2.1|Ox=2.1|Oy=2.1||Version=486-Windows-G92RevE.1|State=1-A1|HF=-1402.3522837|RMSD=2.878e-009|RMSF=3.282e-002|Dipole=0.,0.,-1.3761919|PG=C04V[C4(O1C1Mg1),2SGV(O2),2SGD(Mg2)]||@

25. 3x3x1 with Mg in the center, O under the layer, 0 charge on the cluster, CO with C down, STO-3G basis set.

1|1|GINC-UNK|SP|RHF|STO-3G|C1Mg5O6|PCUSER|06-Jul-1999|0||#RHF/STO-3G SCFCONV=8 SCFCYC=400 POP=REG OUT=WFN TEST||MgO, single layer, 3x3x1, Mg in the center, O under the layer, STO-3G basis set, CO at opt, C down|
|0,1|Mg,0,0.,0.,0.|O,0,2.1,0.,0.|Mg,0,4.2,0.,0.|O,0,0.,2.1,0.|O,0,4.2,2.1,0.|Mg,0,0.,4.2,0.|O,0,2.1,4.2,0.|Mg,0,4.2,4.2,0.|O,0,2.1,2.1,-2.1|Mg,0,2.1,2.1,0.|C,0,2.1,2.1,2.519405|O,0,2.1,2.1,3.664939||Version=486-Windows-G92RevE.1|State=1-A1|HF=-1465.5992863|RMSD=6.395e-009|Dipole=0.,0.,0.9898595|PG=C04V [C4(O1C1Mg1O1),2SGV(O2),2SGD(Mg2)]||@

26. 3x3x1 with Mg in the center, O under the layer, 0 charge on the cluster, CO with C down, LANL1DZ basis set.

1|1|GINC-UNK|SP|RHF|LANL1DZ|C1Mg5O6|PCUSER|06-Jul-1999|0||#R HF/LANL1DZ SCFCYC=400 SCFCONV=8 POP=REG OUT=WFN TEST||MgO, 3x3x1 layer, LANL1DZ Basis set, No CO, O under the layer, CO at opt, C down|
|0,1|Mg,0,0.,0.,0.|O,0,2.1,0.,0.|Mg,0,4.2,0.,0.|O,0,0.,2.1,0 .|Mg,0,2.1,2.1,0.|O,0,4.2,2.1,0.|Mg,0,0.,4.2,0.|O,0,2.1,4.2, 0.|Mg,0,4.2,4.2,0.|O,0,2.1,2.1,-2.1|C,0,2.1,2.1,2.6169506|O, 0,2.1,2.1,3.7542876||Version=486-Windows-G92RevE.1|State=1-A 1|HF=-490.8669228|RMSD=3.523e-010|Dipole=0.,0.,3.5715588|PG= C04V [C4(O1C1Mg1O1),2SGV(O2),2SGD(Mg2)]||@

27. 3x3x1 with Mg in the center, O under the layer, 0 charge on the cluster, CO with C down, 3-21G* basis set.

1|1|GINC-UNK|SP|RHF|3-21G*|C1Mg5O6|PCUSER|08-Jul-1999|0||#RH F/3-21G* POP=REG OUT=WFN SCFCONV=8 SCFCYC=400 TEST||3x3x1 Mg in the center, with O under the layer, CO at opt, C down 3-21G* basis set|
|0,1|Mg,0,0.,0.,0.|O,0,2.1,0.,0.|O,0,0.,2.1,0.|Mg,0,4.2,0.,0 .|Mg,0,2.1,2.1,0.|O,0,4.2,2.1,0.|Mg,0,0.,4.2,0.|O,0,2.1,4.2, 0.|Mg,0,4.2,4.2,0.|O,0,2.1,2.1,-2.1|C,0,2.1,2.1,2.44481298|O ,0,2.1,2.1,3.57251475||Version=486-Windows-G92RevE.1|State=1 -A1|HF=-1476.9815908|RMSD=9.014e-009|Dipole=0.,0.,0.4087114| PG=C04V [C4(O1C1Mg1O1),2SGV(O2),2SGD(Mg2)]||@

28. 3x3x1 with Mg in the center, nothing under the layer, 0 charge on the cluster, CO with O down, STO-3G basis set.

1|1|GINC-UNK|POPT|RHF|STO-3G|C1Mg5O5|PCUSER|24-Dec-1998|1||# RHF/STO-3G OPT OPTCYC=99 SCFCONV=8 SCFCYC=99 POP=REG OUT=WFN TEST||3x3x1 Mg in the center, nothing under, O down, STO-3G basis set|
|0,1|Mg,0,0.,0.,0.|O,0,2.1,0.,0.|O,0,0.,2.1,0.|Mg,0,4.2,0.,0 .|Mg,0,2.1,2.1,0.|O,0,4.2,2.1,0.|Mg,0,0.,4.2,0.|O,0,2.1,4.2, 0.|Mg,0,4.2,4.2,0.|O,0,Ox,Oy,Oz|C,0,Cx,Cy,Cz||Oz=2.2293|Cz=3 .3758|Ox=2.1|Oy=2.1|Cx=2.1|Cy=2.1||Version=486-Windows-G92Re vE.1|State=1-A1|HF=-1391.9348672|RMSD=8.739e-009|RMSF=4.585e -002|Dipole=0.,0.,0.1532438|PG=C04V[C4(C1O1Mg1),2SGV(O2),2SG D(Mg2)]||@

29. 3x3x1 with Mg in the center, nothing under the layer, 0 charge on the cluster, CO with O down, LANL1DZ basis set.

1|1|GINC-UNK|POPT|RHF|LANL1DZ|C1Mg5O5|PCUSER|08-Apr-1998|1||
#RHF/LANL1DZ OPT SCFCONV=8 OPTCYC=99 SCFCYC=99 POP=REG
OUT=WFN TEST||3x3x1 Mg in the Center, nothing under, OPT for
CO O down, LANL1DZ basis set|
|0,1|Mg,0,0.,0.,0.|O,0,2.1,0.,0.|O,0,0.,2.1,0.|Mg,0,4.2,0.,0
.|Mg,0,2.1,2.1,0.|O,0,4.2,2.1,0.|Mg,0,0.,4.2,0.|O,0,2.1,4.2,
0.|Mg,0,4.2,4.2,0.|O,0,Ox,Oy,Oz|C,0,Cx,Cy,Cz||Oz=2.65120412|
Cz=3.78607794|Ox=2.1|Oy=2.1|Cx=2.1|Cy=2.1||Version=486-Windo
ws-G92RevE.1|State=1-A1|HF=-416.2730378|RMSD=7.052e-009|RMSF
=2.571e-002|Dipole=0.,0.,0.2610524|PG=C04V[C4(C1O1Mg1),2SGV(
O2),2SGD(Mg2)]||@

30. 3x3x1 with Mg in the center, nothing under the layer, 0 charge on the cluster, CO with O down, 3-21G* basis set.

1|1|GINC-UNK|POPT|RHF|3-21G*|C1Mg5O5|PCUSER|24-Dec-1998|1||#
RHF/3-21G* OPT OPTCYC=99 SCFCONV=8 SCFCYC=99 POP=REG OUT=WFN
TEST||3x3x1 Mg in the center, nothing under, O down, 3-21G*
basis set|
|0,1|Mg,0,0.,0.,0.|O,0,2.1,0.,0.|O,0,0.,2.1,0.|Mg,0,4.2,0.,0
.|Mg,0,2.1,2.1,0.|O,0,4.2,2.1,0.|Mg,0,0.,4.2,0.|O,0,2.1,4.2,
0.|Mg,0,4.2,4.2,0.|O,0,Ox,Oy,Oz|C,0,Cx,Cy,Cz||Oz=2.40170504|
Cz=3.5341368|Ox=2.1|Oy=2.1|Cx=2.1|Cy=2.1||Version=486-Windows-G92RevE.1|State=1-A1|HF=-1402.7181404|RMSD=6.946e-009|RMSF
=3.024e-002|Dipole=0.,0.,0.403253|PG=C04V[C4(C1O1Mg1),2SGV(O
2),2SGD(Mg2)]||@

31. 3x3x1 with Mg in the center, nothing under the layer, +2 charge on the cluster, CO with O down, STO-3G basis set.

1|1|GINC-UNK|POPT|RHF|STO-3G|C1Mg5O5(2+)|PCUSER|27-May-1999|
1||#RHF/STO-3G OPT OPTCYC=200 SCFCYC=200 SCFCONV=8 POP=REG
OUT=WFN TEST||MgO, 3x3x1 layer, Mg in center, nothing under,
Opt for CO, O down, STO-3G basis set, +2 charge on the
cluster|
|2,1|Mg,0,0.,0.,0.|O,0,2.1,0.,0.|Mg,0,4.2,0.,0.|O,0,0.,2.1,0
.|Mg,0,2.1,2.1,0.|O,0,4.2,2.1,0.|Mg,0,0.,4.2,0.|O,0,2.1,4.2,
0.|Mg,0,4.2,4.2,0.|O,0,Ox,Oy,Oz|C,0,Cx,Cy,Cz||Oz=2.17399123|
Cz=3.3249236|Cx=2.1|Cy=2.1|Ox=2.1|Oy=2.1||Version=486-Windows-G92RevE.1|State=1-A1|HF=-1391.9765998|RMSD=6.499e-009|RMSF
=5.909e-002|Dipole=0.,0.,-0.9895014|PG=C04V[C4(C1O1Mg1),2SGV
(O2),2SGD(Mg2)]||@

32. 3x3x1 with Mg in the center, nothing under the layer, +2 charge on the cluster, CO with O down, LANL1DZ basis set.

1|1|GINC-UNK|POPT|RHF|LANL1DZ|C1Mg5O5(2+)|PCUSER|28-May-1999|1||#RHF/LANL1DZ OPT OPTCYC=200 SCFCYC=200 SCFCONV=8 POP=REG OUT=WFN TEST||MgO, 3x3x1 layer, Mg in center, nothing under, Opt for CO, O down, LANL1DZ basis set, +2 charge on the cluster|
|2,1|Mg,0,0.,0.,0.|O,0,2.1,0.,0.|Mg,0,4.2,0.,0.|O,0,0.,2.1,0.|Mg,0,2.1,2.1,0.|O,0,4.2,2.1,0.|Mg,0,0.,4.2,0.|O,0,2.1,4.2,0.|Mg,0,4.2,4.2,0.|O,0,Ox,Oy,Oz|C,0,Cx,Cy,Cz||Oz=2.50542238|Cz=3.64592625|Cx=2.1|Cy=2.1|Ox=2.1|Oy=2.1||Version=486-Windows-G92RevE.1|State=1-A1|HF=-415.9065043|RMSD=9.184e-009|RMSF=2.894e-002|Dipole=0.,0.,-0.9509037|PG=C04V[C4(C1O1Mg1),2SGV(O2),2SGD(Mg2)]||@

33. 3x3x1 with Mg in the center, nothing under the layer, +2 charge on the cluster, CO with O down, 3-21G* basis set.

1|1|GINC-UNK|POPT|RHF|3-21G*|C1Mg5O5(2+)|PCUSER|28-May-1999|1||#RHF/3-21G* OPT OPTCYC=200 SCFCYC=200 SCFCONV=8 POP=REG OUT=WFN TEST||MgO, 3x3x1 layer, Mg in center, nothing under, Opt for CO, O down, 3-21G* basis set, +2 charge on the cluster|
|2,1|Mg,0,0.,0.,0.|O,0,2.1,0.,0.|Mg,0,4.2,0.,0.|O,0,0.,2.1,0.|Mg,0,2.1,2.1,0.|O,0,4.2,2.1,0.|Mg,0,0.,4.2,0.|O,0,2.1,4.2,0.|Mg,0,4.2,4.2,0.|O,0,Ox,Oy,Oz|C,0,Cx,Cy,Cz||Oz=2.36520809|Cz=3.50313766|Cx=2.1|Cy=2.1|Ox=2.1|Oy=2.1||Version=486-Windows-G92RevE.1|State=1-A1|HF=-1402.3555239|RMSD=3.336e-009|RMSF=3.336e-002|Dipole=0.,0.,-0.774127|PG=C04V[C4(C1O1Mg1),2SGV(O2),2SGD(Mg2)]||@

34. 3x3x1 with Mg in the center, O under the layer, 0 charge on the cluster, CO with O down, STO-3G basis set.

1|1|GINC-UNK|SP|RHF|STO-3G|C1Mg5O6|PCUSER|06-Jul-1999|0||#RHF/STO-3G SCFCONV=8 SCFCYC=400 POP=REG OUT=WFN TEST||MgO, single layer, 3x3x1, Mg in the center, O under the layer, STO-3G basis set, CO at opt, O down, 0 charge on the cluster||0,1|Mg,0,0.,0.,0.|O,0,2.1,0.,0.|Mg,0,4.2,0.,0.|O,0,0.,2.1,0.|O,0,4.2,2.1,0.|Mg,0,0.,4.2,0.|O,0,2.1,4.2,0.|Mg,0,4.2,4.2,0.|O,0,2.1,2.1,-2.1|Mg,0,2.1,2.1,0.|O,0,2.1,2.1,2.24151168|C,0,2.1,2.1,3.3877337||Version=486-Windows-G92RevE.1|State=1-A1|HF=-1465.6021805|RMSD=4.930e-009|Dipole=0.,0.,0.971845|PG=C04V [C4(C1O1Mg1O1),2SGV(O2),2SGD(Mg2)]||@

35. 3x3x1 with Mg in the center, O under the layer, 0 charge on the cluster, CO with O down, LANL1DZ basis set.

1|1|GINC-UNK|SP|RHF|LANL1DZ|C1Mg5O6|PCUSER|08-Jul-1999|0||#R
HF/LANL1DZ POP=REG OUT=WFN SCFCYC=400 SCFCONV=8 TEST||MgO,
3x3x1 layer, LANL1DZ Basis set, O under the layer, CO at
opt, O down, 0 charge on the cluster|
|0,1|Mg,0,0.,0.,0.|O,0,2.1,0.,0.|Mg,0,4.2,0.,0.|O,0,0.,2.1,0
.|Mg,0,2.1,2.1,0.|O,0,4.2,2.1,0.|Mg,0,0.,4.2,0.|O,0,2.1,4.2,
0.|Mg,0,4.2,4.2,0.|O,0,2.1,2.1,-2.1|O,0,2.1,2.1,3.10514392|C
,0,2.1,2.1,4.24046092||Version=486-Windows-G92RevE.1|State=1
-A1|HF=-490.9287491|RMSD=3.142e-009|Dipole=0.,0.,1.0425996|P
G=C04V [C4(C1O1Mg1O1),2SGV(O2),2SGD(Mg2)]||@

36. 3x3x1 with Mg in the center, O under the layer, 0 charge on the cluster, CO with O down, 3-21G* basis set.

1|1|GINC-UNK|SP|RHF|3-21G*|C1Mg5O6|PCUSER|09-Jul-1999|0||#RH
F/3-21G* POP=REG OUT=WFN SCFCONV=8 SCFCYC=400 TEST||MgO,
single layer, 3x3x1, Mg in the center, O under the layer,
3-21G* basis set, CO at opt, O down, 0 charge on the cluster
||0,1|Mg,0,0.,0.,0.|O,0,2.1,0.,0.|Mg,0,4.2,0.,0.|O,0,0.,2.1,
0.|O,0,4.2,2.1,0.|Mg,0,0.,4.2,0.|O,0,2.1,4.2,0.|Mg,0,4.2,4.2
,0.|O,0,2.1,2.1,-2.1|Mg,0,2.1,2.1,0.|O,0,2.1,2.1,2.41202926|
C,0,2.1,2.1,3.54306116||Version=486-Windows-G92RevE.1|State=
1-A1|HF=-1476.909191|RMSD=7.406e-009|Dipole=0.,0.,3.5970417|
PG=C04V[C4(C1O1Mg1O1),2SGV(O2),2SGD(Mg2)]||@

37. 3x3x1 with O in center, nothing under the layer, 0 charge on the cluster, no CO, STO-3G basis set.

1|1|GINC-UNK|SP|RHF|STO-3G|Mg4O5|PCUSER|24-Dec-1998|0||#RHF/
STO-3G SCFCONV=8 POP=REG OUT=WFN TEST||3x3x1, O in center,
No Mg under, STO-3G, 0 charge, no CO|
|0,1|O,0,0.,0.,0.|Mg,0,2.1,0.,0.|Mg,0,0.,2.1,0.|O,0,4.2,0.,0
.|Mg,0,4.2,2.1,0.|O,0,0.,4.2,0.|Mg,0,2.1,4.2,0.|O,0,4.2,4.2,
0.|O,0,2.1,2.1,0.||Version=486-Windows-G92RevE.1|State=1-A1G
|HF=-1157.3018118|RMSD=8.222e-009|Dipole=0.0000084,0.0000056
,0.|PG=D04H[O(O1),2C2'(Mg1.Mg1),2C2"(O1.O1)]||@

38. 3x3x1 with O in center, nothing under the layer, 0 charge on the cluster, no CO, LANL1DZ basis set.

1|1|GINC-UNK|SP|RHF|LANL1DZ|Mg4O5|PCUSER|29-Dec-1998|0||#RHF
/LANL1DZ SCFCONV=8 SCFCYC=200 POP=REG OUT=WFN TEST||3x3x1, O
in center, No Mg under, LANL1DZ basis set, 0 charge, no CO|
|0,1|O,0,0.,0.,0.|Mg,0,2.1,0.,0.|Mg,0,0.,2.1,0.|O,0,4.2,0.,0
.|Mg,0,4.2,2.1,0.|O,0,0.,4.2,0.|Mg,0,2.1,4.2,0.|O,0,4.2,4.2,
0.|O,0,2.1,2.1,0.||Version=486-Windows-G92RevE.1|HF=-377.395
2533|RMSD=6.802e-009|Dipole=0.,0.,0.|PG=D04H[O(O1),2C2'(Mg1.
Mg1),2C2"(O1.O1)]||@

39. 3x3x1 with O in center, nothing under the layer, 0 charge on the cluster, no CO, 3-21G* basis set.

1|1|GINC-UNK|SP|RHF|3-21G*|Mg4O5|PCUSER|28-Dec-1998|0||#RHF/3-21G* SCF CONV=8 SCFCYC=200 POP=REG OUT=WFN TEST||3x3x1, O in center, No Mg under,3-21G*, 0 charge, no CO|
|0,1|O,0,0.,0.,0.|Mg,0,2.1,0.,0.|Mg,0,0.,2.1,0.|O,0,4.2,0.,0.|Mg,0,4.2,2.1,0.|O,0,0.,4.2,0.|Mg,0,2.1,4.2,0.|O,0,4.2,4.2,0.|O,0,2.1,2.1,0.||Version=486-Windows-G92RevE.1|HF=-1166.3169592|RMSD=6.993e-009|Dipole=-0.0000001,-0.0000112,0.|PG=D04H[O(O1),2C2'(Mg1.Mg1),2C2"(O1.O1)]||@

40. 3x3x1 with O in the center, nothing under the layer, -2 charge on the cluster, no CO, STO-3G basis set.

1|1|GINC-UNK|SP|RHF|STO-3G|Mg4O5(2-)|PCUSER|22-May-1999|0||#RHF/STO-3G POP=REG SCFCONV=8 SCFCYC=99 OUT=WFN TEST||3x3x1, O in the Center, -2 charge on the cluster, nothing under, no CO, STO-3G basis set|
|-2,1|O,0,0.,0.,0.|Mg,0,2.1,0.,0.|Mg,0,0.,2.1,0.|O,0,4.2,0.,0.|O,0,2.1,2.1,0.|Mg,0,4.2,2.1,0.|O,0,0.,4.2,0.|Mg,0,2.1,4.2,0.|O,0,4.2,4.2,0.||Version=486-Windows-G92RevE.1|State=1-A1G|HF=-1157.0015601|RMSD=3.420e-009|Dipole=0.,0.,0.|PG=D04H[O(O1),2C2'(Mg1.Mg1),2C2"(O1.O1)]||@

41. 3x3x1 with O in the center, nothing under the layer, -2 charge on the cluster, no CO, LANL1DZ basis set.

1|1|GINC-UNK|SP|RHF|LANL1DZ|Mg4O5(2-)|PCUSER|27-May-1999|0||#RHF/LANL1DZ POP=REG SCFCONV=8 SCFCYC=300 OUT=WFN TEST|
|3x3x1, O in the center, No CO, No Mg under, LANL1DZ basis set, -2 charge|
|-2,1|O,0,0.,0.,0.|Mg,0,2.1,0.,0.|O,0,4.2,0.,0.|Mg,0,0.,2.1,0.|Mg,0,4.2,2.1,0.|O,0,0.,4.2,0.|Mg,0,2.1,4.2,0.|O,0,4.2,4.2,0.|O,0,2.1,2.1,0.||Version=486-Windows-G92RevE.1|State=1-A1G|HF=-377.6322763|RMSD=6.302e-009|Dipole=0.,0.,0.|PG=D04H[O(O1),2C2'(Mg1.Mg1),2C2"(O1.O1)]||@

42. 3x3x1 with O in the center, nothing under the layer, -2 charge on the cluster, no CO, 3-21G* basis set.

1|1|GINC-UNK|SP|RHF|3-21G*|Mg4O5(2-)|PCUSER|28-May-1999|0||#RHF/3-21G* POP=REG SCFCONV=8 SCFCYC=300 OUT=WFN TEST||3x3x1, O in the center, No CO, No Mg under, 3-21G* basis set, -2 charge||-2,1|O,0,0.,0.,0.|Mg,0,2.1,0.,0.|O,0,4.2,0.,0.|Mg,0,0.,2.1,0.|Mg,0,4.2,2.1,0.|O,0,0.,4.2,0.|Mg,0,2.1,4.2,0.|O,0,4.2,4.2,0.|O,0,2.1,2.1,0.||Version=486-Windows-G92RevE.1|State=1-A1G|HF=-1166.515798|RMSD=5.328e-009|Dipole=0.,0.,0.|PG=D04H[O(O1),2C2'(Mg1.Mg1),2C2"(O1.O1)]||@

43. 3x3x1 with O in the center, Mg under the layer, 0 charge on the cluster, no CO, STO-3G basis set.

1|1|GINC-UNK|SP|RHF|STO-3G|Mg5O5|PCUSER|13-Jul-1999|0||#RHF/STO-3G POP=REG OUT=WFN SCFCYC=400 SCFCONV=8 TEST||3x3x1 STO-3G Basis set, O in the center, Mg under the layer, No CO||0,1|O,0,0.,0.,0.|Mg,0,2.1,0.,0.|O,0,4.2,0.,0.|Mg,0,0.,2.1,0.|Mg,0,4.2,2.1,0.|O,0,0.,4.2,0.|Mg,0,2.1,4.2,0.|O,0,4.2,4.2,0.|O,0,2.1,2.1,0.|Mg,0,2.1,2.1,-2.1||Version=486-Windows-G92RevE.1|State=1-A1|HF=-1354.4862908|RMSD=9.362e-009|Dipole=0.,0.,-3.7634036|PG=C04V[C4(O1Mg1),2SGV(Mg2),2SGD(O2)]||@

44. 3x3x1 with O in the center, Mg under the layer, 0 charge on the cluster, no CO, LANL1DZ basis set.

1|1|GINC-UNK|SP|RHF|LANL1DZ|Mg5O5|PCUSER|05-Jul-1999|0||#RHF/LANL1DZ SCFCONV=8 SCFCYC=99 POP=REG OUT=WFN TEST||3x3x1, O in the Center,Mg under the layer, No CO LANL1DZ basis set||0,1|O,0,0.,0.,0.|Mg,0,2.1,0.,0.|Mg,0,0.,2.1,0.|O,0,4.2,0.,0.|O,0,2.1,2.1,0.|Mg,0,4.2,2.1,0.|O,0,0.,4.2,0.|Mg,0,2.1,4.2,0.|O,0,4.2,4.2,0.|Mg,0,2.1,2.1,-2.1||Version=486-Windows-G92RevE.1|HF=-378.2932644|RMSD=8.059e-009|Dipole=0.,0.,-3.528886|PG=C04V [C4(O1Mg1),2SGV(Mg2),2SGD(O2)]||@

45. 3x3x1 with O in the center, Mg under the layer, 0 charge on the cluster, no CO, 3-21G* basis set.

1|1|GINC-UNK|SP|RHF|3-21G*|Mg5O5|PCUSER|05-Jul-1999|0||#RHF/3-21G* SCFCONV=8 SCFCYC=99 POP=REG OUT=WFN TEST||3x3x1 with O in the center, Mg under No CO, 3-21G* basis set||0,1|O,0,0.,0.,0.|Mg,0,2.1,0.,0.|Mg,0,0.,2.1,0.|O,0,4.2,0.,0.|O,0,2.1,2.1,0.|Mg,0,4.2,2.1,0.|O,0,0.,4.2,0.|Mg,0,2.1,4.2,0.|O,0,4.2,4.2,0.|Mg,0,2.1,2.1,-2.1||Version=486-Windows-G92RevE.1|State=1-A1|HF=-1364.9731346|RMSD=4.180e-009|Dipole=0.,0.,-3.1016868|PG=C04V [C4(O1Mg1),2SGV(Mg2),2SGD(O2)]||@

46. 3x3x1 with O in the center, nothing under the layer, 0 charge on the cluster, CO with C down, STO-3G basis set.

1|1|GINC-UNK|POPT|RHF|STO-3G|C1Mg4O6|PCUSER|24-Dec-1998|1||#RHF/STO-3G OPT OPTCYC=99 SCFCONV=8 SCFCYC=99 POP=REG OUT=WFN TEST||3x3x1, O in center, Opt for CO, C down, STO-3G||0,1|O,0,0.,0.,0.|Mg,0,2.1,0.,0.|O,0,4.2,0.,0.|Mg,0,0.,2.1,0.|Mg,0,4.2,2.1,0.|O,0,0.,4.2,0.|Mg,0,2.1,4.2,0.|O,0,4.2,4.2,0.|O,0,2.1,2.1,0.|C,0,Cx,Cy,Cz|O,0,Ox,Oy,Oz||Cz=1.30447025|Oz=2.47008846|Cx=2.1|Cy=2.1|Ox=2.1|Oy=2.1||Version=486-Windows-G92RevE.1|State=1-A1|HF=-1268.5846081|RMSD=4.475e-009|RMSF=5.991e-002|Dipole=0.,0.,0.5644191|PG=C04V[C4(O1C1O1),2SGV(Mg2),2SGD(O2)]||@

47. 3x3x1 with O in the center, nothing under the layer, 0 charge on the cluster, CO with C down, LANL1DZ basis set.

1|1|GINC-UNK|POPT|RHF|LANL1DZ|C1Mg4O6|PCUSER|26-Dec-1998|1||
#RHF/LANL1DZ OPT OPTCYC=99 SCFCONV=8 SCFCYC=99 POP=REG
OUT=WFN TEST||3x3x1, O in center, Opt for CO, CO with C
down, LANL1DZ|
|0,1|O,0,0.,0.,0.|Mg,0,2.1,0.,0.|O,0,4.2,0.,0.|Mg,0,0.,2.1,0
.|Mg,0,4.2,2.1,0.|O,0,0.,4.2,0.|Mg,0,2.1,4.2,0.|O,0,4.2,4.2,
0.|O,0,2.1,2.1,0.|C,0,Cx,Cy,Cz|O,0,Ox,Oy,Oz||Cz=1.29745132|O
z=2.42175983|Cx=2.1|Cy=2.1|Ox=2.1|Oy=2.1||Version=486-Window
s-G92RevE.1|State=1-A1|HF=-490.0393311|RMSD=4.004e-009|RMSF=
4.819e-002|Dipole=0.,0.,0.7000626|PG=C04V[C4(O1C1O1),2SGV(Mg
2),2SGD(O2)]||@

48. 3x3x1 with O in the center, nothing under the layer, 0 charge on the cluster, CO with C down, 3-21G* basis set.

1|1|GINC-UNK|POPT|RHF|3-21G*|C1Mg4O6|PCUSER|24-Dec-1998|1||#
RHF/3-21G* OPT OPTCYC=99 SCFCONV=8 SCFCYC=99 POP=REG OUT=WFN
TEST||3x3x1, O in center, Opt for CO, C down, 3-21G*|
|0,1|O,0,0.,0.,0.|Mg,0,2.1,0.,0.|O,0,4.2,0.,0.|Mg,0,0.,2.1,0
.|Mg,0,4.2,2.1,0.|O,0,0.,4.2,0.|Mg,0,2.1,4.2,0.|O,0,4.2,4.2,
0.|O,0,2.1,2.1,0.|C,0,Cx,Cy,Cz|O,0,Ox,Oy,Oz||Cz=1.28371944|O
z=2.40819364|Cx=2.1|Cy=2.1|Ox=2.1|Oy=2.1||Version=486-Window
s-G92RevE.1|State=1-A1|HF=-1278.4266715|RMSD=4.761e-009|RMSF
=4.803e-002|Dipole=0.,0.,0.5065488|PG=C04V[C4(O1C1O1),2SGV(M
g2),2SGD(O2)]||@

49. 3x3x1 with O in the center, CO with C down, -2 charge on the cluster, STO-3G basis set.

1|1|GINC-UNK|POPT|RHF|STO-3G|C1Mg4O6(2-)|PCUSER|26-May-1999|
1||#RHF/STO-3G OPT POP=REG OPTCYC=300 SCFCONV=8 SCFCYC=300
OUT=WFN TEST||3x3x1, O Center,-2 charge, Opt for CO, C down,
||-2,1|O,0,0.,0.,0.|Mg,0,2.1,0.,0.|Mg,0,0.,2.1,0.|O,0,4.2,0.
,0.|O,0,2.1,2.1,0.|Mg,0,4.2,2.1,0.|O,0,0.,4.2,0.|Mg,0,2.1,4.
2,0.|O,0,4.2,4.2,0.|C,0,Cx,Cy,Cz|O,0,Ox,Oy,Oz||Cz=1.44310511
|Oz=2.76249799|Cx=2.1|Cy=2.1|Ox=2.1|Oy=2.1||Version=486-Wind
ows-G92RevE.1|HF=-1268.1241176|RMSD=2.961e-009|RMSF=5.087e-0
02|Dipole=0.,0.,-2.1262592|PG=C04V[C4(O1C1O1),2SGV(Mg2),2SGD
(O2)]||@

50. 3x3x1 with O in the center, nothing under the layer, -2 charge on the cluster, CO with C down, LANL1DZ basis set.

1|1|GINC-UNK|POPT|RHF|LANL1DZ|C1Mg4O6(2-)|PCUSER|29-May-1999|1||#RHF/LANL1DZ OPT POP=REG OPTCYC=300 SCFCONV=8 SCFCYC=300 OUT=WFN TEST||3x3x1, O in the Center, -2 charge on the cluster Opt for CO, C down, LANL1DZ basis set|
|-2,1|O,0,0.,0.,0.|Mg,0,2.1,0.,0.|Mg,0,0.,2.1,0.|O,0,4.2,0.,0.|O,0,2.1,2.1,0.|Mg,0,4.2,2.1,0.|O,0,0.,4.2,0.|Mg,0,2.1,4.2,0.|O,0,4.2,4.2,0.|C,0,Cx,Cy,Cz|O,0,Ox,Oy,Oz||Cz=3.80401021|Oz=4.94726544|Cx=2.1|Cy=2.1|Ox=2.1|Oy=2.1||Version=486-Windows-G92RevE.1|State=1-A1|HF=-490.3210687|RMSD=2.677e-009|RMSF=2.181e-002|Dipole=0.,0.,1.9542964|PG=C04V[C4(O1C1O1),2SGV(Mg2),2SGD(O2)]||@

51. 3x3x1 with O in the center, nothing under the layer, -2 charge on the cluster, CO with C down, 3-21G* basis set.

1|1|GINC-UNK|POPT|RHF|3-21G*|C1Mg4O6(2-)|PCUSER|28-May-1999|1||#RHF/3-21G* OPT POP=REG OPTCYC=300 SCFCONV=8 SCFCYC=300 OUT=WFN TEST||3x3x1, O in the Center, -2 charge on the cluster Opt for CO, C down, 3-21G* basis set|
|-2,1|O,0,0.,0.,0.|Mg,0,2.1,0.,0.|Mg,0,0.,2.1,0.|O,0,4.2,0.,0.|O,0,2.1,2.1,0.|Mg,0,4.2,2.1,0.|O,0,0.,4.2,0.|Mg,0,2.1,4.2,0.|O,0,4.2,4.2,0.|C,0,Cx,Cy,Cz|O,0,Ox,Oy,Oz||Cz=3.21069801|Oz=4.34439209|Cx=2.1|Cy=2.1|Ox=2.1|Oy=2.1||Version=486-Windows-G92RevE.1|State=1-A1|HF=-1278.6164769|RMSD=7.787e-009|RMSF=2.755e-002|Dipole=0.,0.,1.6991187|PG=C04V[C4(O1C1O1),2SGV(Mg2),2SGD(O2)]||@

52. 3x3x1 with O in the center, Mg under the layer, 0 charge on the cluster, CO with C down, STO-3G basis set.

1|1|GINC-UNK|SP|RHF|STO-3G|C1Mg5O6|PCUSER|12-Jul-1999|0||#RHF/STO-3G POP=REG OUT=WFN SCFCYC=400 SCFCONV=8 TEST||MgO, 3x3x1 layer,STO-3G Basis set, O in the center, Mg under the layer, CO at opt with C down, 0 charge|
|0,1|O,0,0.,0.,0.|Mg,0,2.1,0.,0.|O,0,4.2,0.,0.|Mg,0,0.,2.1,0.|Mg,0,4.2,2.1,0.|O,0,0.,4.2,0.|Mg,0,2.1,4.2,0.|O,0,4.2,4.2,0.|O,0,2.1,2.1,0.|Mg,0,2.1,2.1,-2.1|C,0,2.1,2.1,3.34134372|O,0,2.1,2.1,4.48627348||Version=486-Windows-G92RevE.1|State=1-A1|HF=-1465.7134502|RMSD=9.305e-009|Dipole=0.,0.,-3.6624327|PG=C04V[C4(O1C1O1Mg1),2SGV(Mg2),2SGD(O2)]||@

53. 3x3x1 with O in the center, Mg under the layer, 0 charge on the cluster, CO with C down, LANL1DZ basis set.

1|1|GINC-UNK|SP|RHF|LANL1DZ|C1Mg5O6|PCUSER|09-Jul-1999|0||#RHF/LANL1DZ POP=REG OUT=WFN SCFCONV=8 SCFCYC=400 TEST||3x3x1 with O in the center, Mg under CO at opt, C down, LANL1DZ basis set, 0 charge|
|0,1|O,0,0.,0.,0.|Mg,0,2.1,0.,0.|Mg,0,0.,2.1,0.|O,0,4.2,0.,0.|O,0,2.1,2.1,0.|Mg,0,4.2,2.1,0.|O,0,0.,4.2,0.|Mg,0,2.1,4.2,0.|O,0,4.2,4.2,0.|Mg,0,2.1,2.1,-2.1|C,0,2.1,2.1,3.83544689|O,0,2.1,2.1,4.97104037||Version=486-Windows-G92RevE.1|State=1-A1|HF=-490.9812224|RMSD=4.075e-009|Dipole=0.,0.,-3.6497554|PG=C04V [C4(O1C1O1Mg1),2SGV(Mg2),2SGD(O2)]||@

54. 3x3x1 with O in the center, Mg under the layer, 0 charge on the cluster, CO with C down, 3-21G* basis set.

1|1|GINC-UNK|SP|RHF|3-21G*|C1Mg5O6|PCUSER|08-Jul-1999|0||#RHF/3-21G* POP=REG OUT=WFN SCFCONV=8 SCFCYC=400 TEST||MgO with CO, 3x3x1 with O in the center, Mg under CO at opt, C down, 3-21G* basis set|
|0,1|O,0,0.,0.,0.|Mg,0,2.1,0.,0.|Mg,0,0.,2.1,0.|O,0,4.2,0.,0.|O,0,2.1,2.1,0.|Mg,0,4.2,2.1,0.|O,0,0.,4.2,0.|Mg,0,2.1,4.2,0.|O,0,4.2,4.2,0.|Mg,0,2.1,2.1,-2.1|C,0,2.1,2.1,3.34063789|O,0,2.1,2.1,4.46712095||Version=486-Windows-G92RevE.1|State=1-A1|HF=-1477.0747705|RMSD=6.743e-009|Dipole=0.,0.,-3.1462844|PG=C04V [C4(O1C1O1Mg1),2SGV(Mg2),2SGD(O2)]||@

55. 3x3x1 with O in the center, nothing under the layer, -2 charge on the cluster, CO with O down, STO-3G basis set.

1|1|GINC-UNK|SP|RHF|STO-3G|C1Mg4O6(2-)|PCUSER|18-Jun-1999|0||#RHF/STO-3G POP=REG SCFCONV=8 OUT=WFN TEST||3x3x1, O in the Center, -2 charge on the cluster, Optimization done, CO with O down, STO-3G basis set|
|-2,1|O,0,0.,0.,0.|Mg,0,2.1,0.,0.|Mg,0,0.,2.1,0.|O,0,4.2,0.,0.|O,0,2.1,2.1,0.|Mg,0,4.2,2.1,0.|O,0,0.,4.2,0.|Mg,0,2.1,4.2,0.|O,0,4.2,4.2,0.|O,0,2.1,2.1,19.4484|C,0,2.1,2.1,20.5937||Version=486-Windows-G92RevE.1|State=1-A1|HF=-1268.2270077|RMSD=8.203e-009|Dipole=0.,0.,10.2855303|PG=C04V[C4(O1O1C1),2SGV(Mg2),2SGD(O2)]||@

56. 3x3x1 with Mg inthe center, S under the layer, 0 charge on the cluster, no CO, 3-21G* basis set, opt for Mg position

1|1|GINC-UNK|POPT|RHF|3-21G*|Mg5O4S1|PCUSER|05-Apr-1999|1||#
RHF/3-21G* OPT SCFCYC=200 SCFCONV=8 OPTCYC=200 POP=REG
OUT=WFN TEST||MgO CO, 3x3x1, 3-21G* Basis set, S under, Opt
for Mg position|
|0,1|Mg,0,0.,0.,0.|O,0,2.1,0.,0.|Mg,0,4.2,0.,0.|O,0,0.,2.1,0
.|O,0,4.2,2.1,0.|Mg,0,0.,4.2,0.|O,0,2.1,4.2,0.|Mg,0,4.2,4.2,
0.|S,0,2.1,2.1,-2.1|Mg,0,Mgx,Mgy,Mgz||Mgz=0.28745746|Mgx=2.1
|Mgy=2.1||Version=486-Windows-G92RevE.1|State=1-A1|HF=-1686.
1390667|RMSD=3.929e-009|RMSF=3.962e-002|Dipole=0.,0.,1.7847
604|PG=C04V [C4(Mg1S1),2SGV(O2),2SGD(Mg2)]||@

57. 3x3x1 with Mg in the center, S under the layer, Mg relaxed, 0 charge on the cluster, CO with C down, 3-21G* basis set.

1|1|GINC-UNK|POPT|RHF|3-21G*|C1Mg5O5S1|PCUSER|23-Mar-1998|1|
|#RHF/3-21G* OPT SCFCYC=99 SCFCONV=8 OPTCYC=99 POP=REG
OUT=WFN TEST| |MgO,3x3x1 layer, 3-21G* Basis set, opt for CO
Mg in the Center,sulfur under the layer|
|0,1|Mg,0,0.,0.,0.|O,0,2.1,0.,0.|Mg,0,4.2,0.,0.|O,0,0.,2.1,
0.|O,0,4.2,2.1,0.|Mg,0,0.,4.2,0.|O,0,2.1,4.2,0.|Mg,0,4.2,4.2
,0.|S,0,2.1,2.1,-2.1|Mg,0,2.1,2.1,0.2864|C,0,Cx,Cy,Cz|O,0,Ox
,Oy,Oz||Cx=2.1|Cy=2.1|Cz=2.679743|Ox=2.1|Oy=2.1|Oz=3.804909|
|Version=486-Windows-G92RevE.1|HF=-1798.2409502|RMSD=1.946e-
009|RMSF=3.894e-002|Dipole=0.,0.,3.0091354|PG=C04V[C4(O1C1Mg
1S1),2SGV(O2),2SGD(Mg2)]||@

58. 3x3x1 with Mg in the center, S under the layer, 0 charge on the cluster, CO with O down, Mg relaxed, 3-21G* basis set.

1|1|GINC-UNK|SP|RHF|3-21G*|C1Mg5O5S1|PCUSER|18-Oct-1999|0||#
RHF/3-21G* POP=REG OUT=WFN SCFCONV=8 SCFCYC=400 TEST||MgO
and CO molecule, O down, sulfur under the layer, Mg relaxed,
3-21G* basis set|
|0,1|Mg,0,0.,0.,0.|O,0,2.1,0.,0.|O,0,0.,2.1,0.|Mg,0,4.2,0.,0
.|Mg,0,2.1,2.1,0.28746|O,0,4.2,2.1,0.|Mg,0,0.,4.2,0.|O,0,2.1
,4.2,0.|Mg,0,4.2,4.2,0.|S,0,2.1,2.1,-2.1|O,0,2.1,2.1,2.52654
|C,0,2.1,2.1,3.66157||Version=486-Windows-G92RevE.1|State=1-
A1|HF=-1798.2489649|RMSD=4.580e-009|Dipole=0.,0.,2.3453913|P
G=C04V [C4(C1O1Mg1S1),2SGV(O2),2SGD(Mg2)]||@

APPENDIX B

Wavefunction file for the CO Molecule

```
 Opt for CO separation, 3-21G* basis set
GAUSSIAN              7 MOL ORBITALS     30 PRIMITIVES
2 NUCLEI
  C    1    (CENTRE  1)   0.00000000  0.00000000 -1.21909962
CHARGE =  6.0
  O    2    (CENTRE  2)   0.00000000  0.00000000  0.91432471
CHARGE =  8.0
CENTRE ASSIGNMENTS    1  1  1  1  1  1  1  1  1  1  1  1  1
1  1  2  2  2  2  2
CENTRE ASSIGNMENTS    2  2  2  2  2  2  2  2  2  2
TYPE ASSIGNMENTS      1  1  1  1  1  2  2  3  3  4  4  1  2
3  4  1  1  1  1  1
TYPE ASSIGNMENTS      2  2  3  3  4  4  1  2  3  4
EXPONENTS  0.1722560D+03 0.2591090D+02 0.5533350D+01
0.3664980D+01 0.7705450D+00
EXPONENTS  0.3664980D+01 0.7705450D+00 0.3664980D+01
0.7705450D+00 0.3664980D+01
EXPONENTS  0.7705450D+00 0.1958570D+00 0.1958570D+00
0.1958570D+00 0.1958570D+00
EXPONENTS  0.3220370D+03 0.4843080D+02 0.1042060D+02
0.7402940D+01 0.1576200D+01
EXPONENTS  0.7402940D+01 0.1576200D+01 0.7402940D+01
0.1576200D+01 0.7402940D+01
EXPONENTS  0.1576200D+01 0.3736840D+00 0.3736840D+00
0.3736840D+00 0.3736840D+00
MO  1       MO 0.0         OCC NO =    2.0000000  ORB. ENERGY
= -20.5789584
  0.13602657D-02  0.19085091D-02  0.11708964D-02
-0.95296457D-03  0.90869005D-03
 -0.18838618D-17 -0.97613589D-18 -0.12651780D-17
-0.65556066D-18  0.41821091D-02
  0.21669885D-02  0.43757560D-02  0.42002698D-16
0.56832619D-19  0.28626915D-02
  0.31569900D+01  0.45237625D+01  0.28772407D+01
-0.12805920D+00  0.12123077D+00
  0.29997778D-14  0.15147862D-14 -0.11941066D-16
-0.60298340D-17 -0.19305481D-01
 -0.97486143D-02 -0.17688277D-01 -0.30845575D-15
0.46271556D-18  0.58561715D-02
MO  2       MO 0.0         OCC NO =    2.0000000  ORB. ENERGY
= -11.3177169
  0.20641965D+01  0.28961531D+01  0.17768295D+01
-0.65854841D-01  0.62795239D-01
  0.14126429D-16  0.73197057D-17  0.72097836D-17
0.37357987D-17  0.12387362D-01
  0.64185966D-02 -0.48331758D-02 -0.20696991D-16
-0.14216355D-16 -0.11541736D-03
 -0.66581565D-03 -0.95407075D-03 -0.60681594D-03
-0.27038465D-03  0.25596706D-03
 -0.13391107D-14 -0.67620558D-15 -0.92514314D-15
-0.46716596D-15  0.49960487D-02
  0.25228354D-02 -0.68302644D-03  0.14116451D-15
```

```
0.97544421D-16  0.30952493D-02
MO  3        MO 0.0         OCC NO =    2.0000000  ORB. ENERGY
=  -1.5476455
 -0.25548182D+00 -0.35845155D+00 -0.21991492D+00
-0.10601545D+00  0.10108999D+00
  0.27411691D-15  0.14203555D-15  0.31511720D-15
0.16328014D-15  0.31673896D+00
  0.16412046D+00  0.88384876D-02 -0.20627740D-16
-0.27032036D-16 -0.92153542D-02
 -0.69635006D+00 -0.99782459D+00 -0.63464462D+00
-0.27475664D+00  0.26010593D+00
  0.10342643D-15  0.52226845D-16  0.35086600D-15
0.17717545D-15 -0.66892210D+00
 -0.33778301D+00  0.22709384D+00 -0.68428797D-16
-0.33135115D-16 -0.60385105D-01
MO  4        MO 0.0         OCC NO =    2.0000000  ORB. ENERGY
=  -0.7853501
  0.28148268D+00  0.39493185D+00  0.24229608D+00
0.14304177D+00 -0.13639608D+00
 -0.39474114D-15 -0.20453782D-15  0.25939960D-16
0.13440968D-16 -0.21180809D+00
 -0.10974981D+00 -0.53052348D-01  0.20697923D-16
0.38704339D-16  0.92869050D-02
 -0.40691033D+00 -0.58307618D+00 -0.37085292D+00
-0.15676620D+00  0.14840704D+00
 -0.12592786D-14 -0.63589307D-15  0.15296300D-14
0.77241135D-15  0.17195165D+01
  0.86829763D+00  0.17195222D+00 -0.68700994D-16
-0.70129265D-16  0.15152914D+00
MO  5        MO 0.0         OCC NO =    2.0000000  ORB. ENERGY
=  -0.6347647
  0.14470287D-15  0.20302410D-15  0.12455806D-15
0.52186755D-16 -0.49762169D-16
  0.42911052D+00  0.22234655D+00  0.39805894D-01
0.20625697D-01  0.16321206D-15
  0.84569445D-16 -0.48641132D-16  0.36892466D-01
0.34222829D-02  0.14176066D-16
 -0.25669861D-15 -0.36783250D-15 -0.23395186D-15
-0.53323720D-16  0.50480366D-16
  0.18902447D+01  0.95450955D+00  0.17534615D+00
0.88543870D-01  0.39138014D-15
  0.19763372D-15  0.90471633D-16  0.20158784D+00
0.18700041D-01  0.45382076D-16
MO  6        MO 0.0         OCC NO =    2.0000000  ORB. ENERGY
=  -0.6347647
 -0.14137318D-15 -0.19835241D-15 -0.12169191D-15
-0.67509985D-16  0.64373485D-16
 -0.39805894D-01 -0.20625697D-01  0.42911052D+00
0.22234655D+00 -0.75122223D-16
 -0.38925094D-16  0.41082177D-16 -0.34222829D-02
0.36892466D-01 -0.13174304D-16
  0.12685584D-15  0.18177622D-15  0.11561481D-15
```

```
0.35876077D-16 -0.33963076D-16
 -0.17534615D+00 -0.88543870D-01  0.18902447D+01
0.95450955D+00 -0.28121790D-15
 -0.14200552D-15 -0.50877100D-16 -0.18700041D-01
0.20158784D+00 -0.32086802D-16
MO  7       MO 0.0         OCC NO =    2.0000000  ORB. ENERGY
=  -0.5432441
 -0.31575482D+00 -0.44301707D+00 -0.27179702D+00
-0.10048407D+00  0.95815599D-01
 -0.52470478D-15 -0.27187938D-15 -0.81495266D-16
-0.42227330D-16 -0.65649246D+00
 -0.34016606D+00  0.16278247D+00  0.77620063D-16
-0.21391358D-16 -0.32242942D-01
  0.40410586D-01  0.57905755D-01  0.36829696D-01
0.20111495D-01 -0.19039100D-01
  0.19255604D-15  0.97234282D-16 -0.76554440D-15
-0.38657400D-15  0.94158320D+00
  0.47546763D+00 -0.31896335D-01  0.48324462D-16
0.25169469D-16  0.10079271D+00
END DATA
 THE  HF ENERGY =   -112.093298981330 THE VIRIAL(-V/T)=
2.00339675
```

REFERENCES

1. Robinson, W. R.; Odom, J. D.; Holtzclaw, H. F; Essentials of General Chemistry; Houghton Mifflin Co., New York, **1997**.

2. Hehre, W. J.; Radom, L.; Schleyer, P. v.R.; Pople, J. A. Ab initio Molecular Orbital Theory; Wiley, New York, **1986**.

3. Sargent, A. L. Electronic Structure and Bonding in Transition Metal Inorganic and Organometallic Complexes: New Basis Sets, Linear Semibridging Carbonyls and Thiocarbonyls, and Oxidative Addition of Molecular Hydrogen to Square-Planar Iridium Complexes. Ph.D. Thesis, Texas A&M University, College Station, TX, **1991**.

4. Nobel Foundation web address www.nobel.se

5. Bernholc, J. Physics Today, **1999**, Sept., 30.

6. Eberhart, M. E. Scientific American **1999**, Oct., 66.

7. Lehman, W. J. Atomic and Molecular Structure: The Development of Our Concepts; Wiley, New York, 1972.

8. Schrödinger, E. Ann. Physik **1926**, 79, 361.

9. Born, M; Oppenheimer, J. R. Ann. Physik **1927**, 84, 457.

10. Levine, I. N. Quantum Chemistry; Prentice-Hall: New York, **1991**.

11. Hinchliffe, A. Computational Quantum Chemistry; Wiley, New York, **1988**.

12. Eisberg, R; Resnick, R. Quantum Physics of Atoms, Molecules, Solids, Nuclei, and Particles; John Wiley and Sons, New York, **1974**.

13. Slater, J. C. Phys. Rev. **1929**, 34, 1293.

14. Slater, J. C. Phys. Rev. **1930**, 35, 509.

15. Flurry, R. L. Jr.; Molecular Orbital Theories of Bonding in Organic Molecules; Marcel Dekker, Inc., New York, **1968**.

16. Slater, J. C. Phys. Rev. **1932**, 42, 33.

17. Frisch, M. J.; Trucks, G. W.; Head-Gordon, M.; Gill, P. M. W.; Wong, M. W.; Foresman, J. B.; Johnson, B. G.; Schlegel, H. B.; Robb, M. A.; Replogle, E. S.; Gomperts, R.; Andres, J. L.; Raghavachari, K.; Binkley, J. S.; Gonzalez, C.; Martin, R. L.; Fox, D. J.; Defrees, D. J.; Baker, J.; Stewart, J. J. P.; Pople, J. A. Gaussian 92, Revision E.1, Gaussian, Inc., Pittsburgh PA, **1992**.

18. Pacchioni, G.; Cogliandro, G. Surface Science **1991**, 255, 344.

19. Neyman, K. M.; Ruzankin, S. P.; Rösch, N. Chem. Phys. Lett. **1995**, 246, 546.

20. Colbourn, E. A.; Mackrodt, W. C.; Surface Sci. **1984**, 143, 391.

21. Neyman, K. M.; Rösch, N. Chem. Phys. **1992**, 168, 267.

22. Pope, S. A.; Hillier, I. H.; Guest, M. F.; Colbourn, E. A.; Kendrick, J. Surface Sci. **1984**, 139, 299.

23. Utamapanya, S.; Ortiz, J. V.; Kladunde, K. J. J. Am. Chem. Soc. **1989**, 111, 799.

24. Almeida, A. L.; Martins, J. B. L.; Taft, C. A.; Longo, E.; Lester, W. A. Jr. J. Chem. Phys. **1998**, 109, 3671.

25. Seamehorn, C. A.; Hess, A. C.; McCarthy, M. C. J. Chem. Phys., **1993**, 99, 2786.

26. Seamehorn, C. A.; Harrison, N. M.; McCarthy, M. C. J. Chem. Phys., **1994**, 101, 1547.

27. Tashiro, T.; Ito, J.; Sim, R.; Miyazawa, K.; Hamada, E.; Toi, K.; Kobayashi, H.; Ito, T. J. Chem. Phys., **1995**, 99, 6115.

28. Dai, G. H.; Yan, Q. J.; Wang, Y.; Liu, Q. S. Chem. Phys. **1991**, 155, 275.

29. Argawal, S. K.; Migone, R. A.; Marcelin, G. J. Catal. **1990**, 123, 228.

30. Colbourn, E. A.; Mackrodt, W. C. Surface Sci. **1982**, 117, 571.

31. Dovesi, R.; Orlando, R.; Ricca, F.; Roetti, C. Surface Sci. **1987**, 186, 267.

32. Nygren, M. A.; Pettersson, Lars G. M.; Barandiarán, Z.; Seijo, L. J. Chem. Phys. 1994, 100, 2010.

33. Causá, M.; Kotomin, E.; Pisani, C.; Roetti, C. J. Phys. C: Solid State Phys. 1987, 20, 4991.

34. Nygren, M. A.; Pettersson, Lars G. M. J. Chem. Phys. 1996, 105, 9339.

35. Causá, M.; Dovesi, R.; Pisani, C.; Roetti, C. Surface Sci. 1986, 175, 551.

36. Colbourn, E. A.; Kendrick, J.; Mackrodt, W. C. Surface Sci. 1983, 126, 550.

37. Ferrari, A. M.; Pacchioni, G. J. Chem. Phys., 1997, 107, 2066.

38. Pelmenshikov, A. G.; Morosi, G.; Gamba, A.; Coluccia, S. J. Phys. Chem. 1998, 102, 2226.

39. Pelmenshikov, A. G.; Morosi, G.; Gamba, A.; Coluccia, S. J. Phys. Chem. 1995, 99, 15018.

40. Heidberg, J.; Kandel, M.; Meine, D.; Wildt, U. Surface Sci. 1995, 331, 1467.

41. Jug, K.; Geudtner, G. J. Chem. Phys. 1996, 105, 5285.

42. Wu, R.; Zhang, Q. Chem. Phys. Lett. 1999, 306, 205.

43. Hoang, P. N. M.; Picaud, S.; Girardet, C. Surface Sci. 1996, 360, 261.

44. Neyman, K. M.; Rösch, N. Surface Sci. 1993, 297, 223.

45. Neyman, K. M.; Rösch, N. J. Mol. Struct. 1993, 293, 303.

46. Vulliermet, N.; Wesolowski, T.; Weber, J. Collect. Czech. Chem. Commun., 1998, 63, 1447.

47. Goldman, A. S.; Krogh-Jepersen, K. J. Am. Chem. Soc., 1996, 118, 12159.

48. Pacchioni, G.; Ferrari, A. M.; Márquez, A.; Illas, F. J. Computational Chem. 1997, 18, 617.

49. Klinkman, J.; Cappus, D.; Homann, K.; Risse, T.; Sandell, A.; Porwol, T.; Freund, H.-J.; Fink, K.; Staemmler, V. J. Electron Spec. and Rel. Phenomena, 1996, 77, 155.

50. Foresman, J. B.; Frisch, Æ. Exploring Chemistry with Electronic Structure Methods: A Guide to Using Gaussian; Gaussian, Inc., Pittsburg, PA., **1993**.

51. Binkley, J. S.; Pople, J. A.; Hehre, W. J. J. Am Chem. Soc. **1980**, 102, 939.

52. Gordon, M. S.; Binkley, J. A.; Pople, J. A.; Pietro, W. J.; Hehre, W. J. ibid. **1982**, 104, 2797.

53. Pietro, W. J.; Francl, W. W.; Hehre, W. J.; DeFrees, D. J.; Pople, J. A.; Binkley, J. S. J. Am. Chem. Soc. **1982**, 104, 5039.

54. Dunning, T. H.; Hay, P. J. Modern Theoretical Chemistry vol. 3; H. F. Schaefer III, ed., Plenum Press, New York, **1977**.

55. Gaussian Basis Sets for Molecular Calculations, S. Huzinaga, ed., Elsevier, Amsterdam, **1984**.

56. Mackrodt, W. C.; Stewart, R. F. J. Phys. **1977**, C10, 143.

57. Kinninburg, C. G. J. Phys. **1975**, C8, 2382.

58. Heinrich, V. E.; Cox, P. The Surface Science of Metal Oxides, Cambridge University Press, Cambridge, **1994**.

59. Kittel, C. Introduction to Solid State Physics, 6th ed., Wiley, New York, **1986**.

60. Gevirzman, R.; Kozirovski, Y.; Folman, N. Trans. Faraday Soc. **1969**, 65, 2206.

61. Escalona-Platero, E.; Scarano, D.; Spoto, G.; Zecchina, A. Faraday Discuss. Chem. Soc. **1985**, 80, 183.

62. Zecchina, A.; Scarano, D. Surface Sci. **1986**, 166, 347.

63. Minot, C.; Van Hove, M. A.; Biberian, J. Surface Sci. **1996**, 346, 283.

64. Neyman, K. M.; Ruzankin, S. P.; Rösch, N. Chem. Phys. Lett. **1995**, 246, 546.

65. Bromberg, J. P. Physical Chemistry, 2nd ed., Allyn and Bacon, Boston, **1984**.

66. Methods of Electronic Structure Theory, H. F. Schaefer, ed., Plenum, New York, **1977**.

67. Boys, S. F.; Bernardi, F. Molecular Physics, **1970**, 19, 533.

68. Furuyana, S.; Fujii, H.; Kawamura, M.; Morimoto, T. J. Phys. Chem. **1978**, 82, 1028.

69. Henry, C. R.; Chapon, C.; Durienz, C. J. Chem. Phys. **1991**, 95, 700

70. He, J.-W.; Estrada, C. A.; Cornielle, J. S.; Wu, M. -C.; Goodman, D. W. Surface Sci. **1992**, 261, 164.

71. Wichtendahl, R,; Rodriquez-Rodrigo, M.; Hartel, U.; Kuhlenbeck, K.; Freund, H.-J. Surface Sci. **1999**, 423, 90.

72. Lakhlifi, A.; Girardet, C. Surface Sci. **1991**, 241, 400.

73. Lakhlifi, A.; Girardet, C. J. Chem. Phys. **1991**, 94, 688.

74. Aray, Y,; Bader, R. F. W. Surface Sci. **1996**, 351, 233.

75. Aray, Y.; Rosillo, F.; Murgich, J.; J. Am. Chem. Soc. **1994**, 116, 10639.

76. Bader, R. F. W.; MacDougall, P. J.; Lau, C. D. H. J. Am. Chem. Soc., **1984**, 106, 1594.

77. MacDougall, P. J.; Hall, M. B.; Bader, R. F. W.; Cheeseman, J. R. Can. J. Chem., **1989**, 67, 1842.

78. Bader, R. F. W. Chem. Rev., **1991**, 91, 893.

79. Bader, R. F. W.; Essen, H. J. Chem. Phys., **1984**, 80, 1943.

80. Bader, R. F. W.; Ngoyen-Dang, T. T.; Tal, Y. Rep. Prog. Phys., **1981**, 44, 895.

81. Bader, R. F. W.; Popelier, P. L. A.; Chang, C. J. J. Mol. Struct. (Theochem), **1992**, 255, 145.

82. Bader, R. F. W. Atoms in Molecules: A Quantum Theory, Clarendon Press, Oxford, UK, **1990**.

83. Bader, R. F. W. Molecules in Physics, Chemistry and Biology, Vol. III, Kluwer, Dordrecht, **1989**.

84. Bader, R. F. W.; Gillespie, R. J.; MacDougall, P. J. J. Am. Chem. Soc., **1988**, 110, 7329.

85. Gillespie, R. J. Can. J. Chem., 1992, 70, 742.

86. Aray, Y.; Rodriguez, J. Surf. Sci., 1998, 405, L532.

87. Wang, J.; Shi, Z.; Boyd, R. J.; Gonzalez, C. J. Phys. Chem., 1994, 98, 6988.

88. Pacchioni, G.; Neyman, K. M.; Rösch, N. J. Elec. Spec. and Rel. Phenomena 1994, 69, 13.

89. Wang, J.; Smith, V. H. Jr. Chem. Phys. Lett., 1994, 220, 331.

90. Waber, J. T.; Cromer, D. T. J. Chem. Phys., 1965, 42, 4116.

91. Sierraalta, A.; Ruette, F. Int. J. Quantum Chem., 1996, 60, 1015.

92. Shi, Z.; Boyd, R. J. J. Chem. Phys., 1988, 88, 4375.

93. Sagar, R. P.; Ku, A. C. T.; Smith, V. H. Jr. J. Chem. Phys., 1988, 88, 4367.

94. Aray, Y.; Rodriguez, J.; López-Boada, R. J. Phys. Chem., 1997, 101, 2178.

95. Tsirelson, V. G.; Zou, P. F.; Tang, T.-H., Bader, R. F. W. Acta. Crystal. A., 1995, 51, 143.

96. Hunter, G. Can. J. Chem., 1996, 74, 1008.

97. Koritsánszky, T.; Flaig, R.; Zobel, D.; Krane, H.-G.; Morgenroth, W.; Luger, P. Science, 1998, 279, 356.

98. Tsirelson, V. G.; Avilov, A. S.; Abramov, Y. A.; Belokovena, E. L.; Kitaneh, R.; Feil, D. Acta. Cryst., 1998, B54, 8.

99. Bader, R. F. W.; MacDougall, P. J. J. Am. Chem. Soc., 1985, 107, 6788.

100. Carrol, M. T.; Chang, C.; Bader, R. F. W. Mol. Phys., 1988, 63, 387.

101. Aray, Y.; Rodriguez, J. Can. J. Chem., 1996, 74, 1014.

102. Aray, Y.; Rodriguez, J.; Murgich, J.; Ruette, F. J. Phys. Chem., 1993, 97, 8393.

103. Davis, H. F. Introduction to Vector Analysis, 2nd ed., Allyn and Bacon, Inc., Boston, 1967.

104. Hohn, F. E. Elementary Matrix Algebra, 3rd ed., The MacMillan Company, New York, **1972**.

105. MacDougall, P. J. The Laplacian of the Electronic Charge Distribution. Ph.D. Thesis, McMaster University, Hamilton, Ont. **1989**.

106. Bader, R. F. W.; Beddall, P. J. J. Chem. Phys. **1972**, 56, 3320.

107. Fang, D.-C.; Tang, T.-H. AIM98PC, The Modified Version of AIMPAC, R. F. W. Bader's Laboratory, McMaster University, Ontario, Canada, **1998**.

108. West, R. C. Handbook of Chemistry and Physics, 60th ed.; CRC Press, Inc., Boca Raton, Florida, **1980**.

109. Illas, F.; Pacchioni, G. J. Chem. Phys. **1998**, 108, 7835.

110. Ferrari, A. M.; Pacchioni, G. J. Phys. Chem., **1995**, 99, 17010.

111. Hermansson, K.; Baudin, M.; Ensing, B.; Alfredsson, M.; Wojcik, M. J. Chem. Phys., **1998**, 109, 7515.

112. MacDougall, P. J.; Hall, M. B. Trans. Am. Cryst. Assoc. **1990**, 26, 105.

113. Martin, G. A.; Bernal, S.; Perrichon, V.; Mirodatos, C. Catal. Today **1992**, 13, 487.

114. Lin, C. H.; Ito, T.; Wang, T. X.; Lunsford, J. H. J. Am. Chem. Soc. **1987**, 109, 4808.

115. Zecchina, A.; Coliccia, S.; Morterra, C. Applied Spect. Rev. **1985**, 21, 259.

116. Sawabe, K.; Koga, N.; Morokuma, K.; Iwasawa, Y. J. Chem. Phys., **1994**, 101, 4819.

117. Johnson, M. A.; Stefanovich, E. V.; Truong, T. N. J. Phys. Chem., **1997**, 101, 3196.

118. Crabtree, R. H. Cem. Rev. **1995**, 95, 987.

119. Lu, X.; Xu, X.; Wang, N.; Zhang, Q. Int. J. Quantum Chem. **1999**, 73, 377.

120. Bader, R. F. W.; Chandra, A. K. Can. J. Chem. **1968**, 46, 953.